DEVELOPMENT OF BIFUNCTIONAL CATALYSTS CONTAINING HYDRIDE-RELAY LIGANDS FOR CO_2 HYDROGENATION

A Thesis

Presented to

The Faculty of the Department of Chemistry

Sam Houston State University

In Partial Fulfillment

of the Requirements for the Degree of

Master of Science

by

Nilakshi Devi

May, 2019

DEVELOPMENT OF BIFUNCTIONAL CATALYSTS CONTAINING HYDRIDE-RELAY LIGANDS FOR CO_2 HYDROGENATION

by

Nilakshi Devi

_____

APPROVED:

_____
Christopher M. Zall, PhD
Thesis Director

_____
Richard E. Norman, PhD
Committee Member

_____
Darren L. Williams, PhD
Committee Member

_____
John B. Pascarella, PhD
Dean, College of Science and Engineering Technology

DEDICATION

I dedicate the time and research efforts of this thesis to my Ma, Deuta and little brother. I would also like to dedicate my thesis to the friends I've made here in USA, who have become my second family away from home.

ABSTRACT

Devi, Nilakshi , *Development of bifunctional catalysts containing hydride-relay ligands for CO_2 hydrogenation*. Master of Science (Chemistry), May, 2019, Sam Houston State University, Huntsville, Texas.

The research described in this thesis focuses on the synthesis of bifunctional catalysts for hydrogenation of CO_2. These catalysts contain redox active phenanthridinium and benzimidazolium groups capable of mediating hydride transfer incorporated within a transition metal phosphine complex. These redox active groups, called "hydride relays," are NADH-type organic hydride donors that can reversibly accept or donate hydride ions and transfer them to substrates, like CO_2. A series of bifunctional ligands, L^{PhenH}, L^{Phen+}, L^{BI+} and $L^{PhenBI+}$, were synthesized in which the targeted hydride relays are tethered to a phosphine donor via an ethylene linker so that they can be combined with transition metal ions that have complementary proton acceptor abilities. Ni(II) complexes proved to be too sterically hindered to bind these ligands when used with polydentate phosphine ligands. However, $[Ni(L^{PhenBI+})Br_3]$, a Ni(II) species containing bromide ligands, was synthesized. A crystal structure was obtained for $[Ni(L^{PhenBI+})Br_3]$: monoclinic, $P2_{1/c}$, a = 18.3574(13), b = 15.8651(8), c = 20.1961(12) Å, β = 106.102 (7)°, R = 0.0709, and R_W = 0.1150. Pd(II) complexes using redox active ligands in conjunction with ancillary polydentate phosphine ligands like PP_2 $[PhP(CH_2CH_2PPh_2)_2]$, and PN^HP $[HN(CH_2CH_2PPh_2)_2]$ were synthesized. Crystal structures were obtained for the complexes containing phenanthridinium relays, $[Pd(PP_2)(L^{PhenH})][BF_4]_2\bullet(CH_3CN)_{3.25}$ and $[Pd(PP_2)(L^{Phen+})][BF_4]_3\bullet(CH_3CN)_3$. For $[Pd(PP_2)(L^{PhenH})][BF_4]_2\bullet(CH_3CN)_{3.25}$: monoclinic, $P2_{1/n}$, a = 11.2927(4), b = 41.743(1), c = 12.9751(4) Å, β = 90.251(3)°, R = 0.0772, and R_W = 0.1483 and for

$[Pd(PP_2)(L^{Phen+})][BF_4]_3 \bullet (CH_3CN)_3$: monoclinic, $P2_{1/c}$, a = 21.822(2), b = 13.632(1), c = 22.575(2) Å, β = 91.116(8)°, R = 0.0632, and R_W = 0.1349. Pd^0 complexes were also synthesized. A crystal structure was obtained for the complex $[Pd^0(PP_2)(L^{PhenH})]$: triclinic, $P\text{-}1$, a = 11.5406(6), b = 12.6451(6), c = 18.3167(7) Å, α = 79.558(4)°, β = 80.469(4)°, γ = 78.061(4)°, R = 0.0680, and R_W = 0.1176. These complexes were also characterized using ^1H and ^{31}P NMR spectroscopy. These studies show that the hydride relays can be successfully incorporated in close proximity to the transition metal of tetraphosphine complexes.

KEY WORDS: Hydrogenation, Redox active, Hydride relays, Heteroleptic.

ACKNOWLEDGEMENTS

There are no proper words to convey my deepest gratitude and respect for my thesis advisor Dr. Christopher Zall. His indispensable guidance and support helped me immensely with completing this research. His mentorship for the past three years will never be forgotten.

I am thankful to my committee members: Dr. Richard Norman and Dr. Darren Williams for their assistance in completing this thesis. I am appreciative of the time they dedicated towards the betterment of my writing. I would also like to take this opportunity to thank the faculty members of the chemistry department for contributing to my success at SHSU and to Mrs. Rachell Haines for her day-to-day help.

My sincere thanks to Dr. Hiranya Nath for his selfless help and encouragement to join this program at SHSU and guiding me throughout these years.

I am grateful to my parents and family members for the strength and support they provided me with despite being thousands of miles away.

Furthermore, I offer my sincere thanks to the lab members in Dr. Zall's research group. They positively contributed to the friendly atmosphere in the lab which made completing my lab work an even greater experience. Lastly, a thank you to all my special friends at SHSU for their immense help and affection throughout this entire time. Looking back, I realize that their constant support and motivation has made this journey even more memorable and enjoyable—and for that I am most grateful.

TABLE OF CONTENTS

Page

LIST OF TABLES

LIST OF FIGURES

CHAPTER I

INTRODUCTION

1.1 Importance of CO_2 Hydrogenation

The development of renewable, carbon-neutral alternatives to fossil fuels is of great interest. These fuels can be produced by the conversion of CO_2 to energy rich molecules like methanol and formic acid using renewably generated H_2. Molecular catalysts for CO_2 hydrogenation typically activate H_2 to form H^+ and H^- ions that are transferred to the substrate. This work describes the synthesis of new catalysts designed to facilitate H_2 activation and CO_2 reduction through metal-ligand cooperativity. These new catalysts contain reactive functional groups, or "hydride relays," tethered to a phosphine donor so that they can bind to a transition metal center in a bifunctional complex. The hydride-relays are analogous to the biological hydride donor "NADH" and can reduce unsaturated substrates like ketones and aldehydes, when tethered to a metal center in conjunction with other polydentate ancillary phosphine ligands.

The increasing global demand for energy has led to the extensive use of fossil fuels like coal, petroleum oil, and natural gas. Also, the combustion of fossil fuels or any carbon-based materials used in cooking, transportation, heating, and other activities leads to an increase in CO_2 levels in the atmosphere. Nature efficiently recycles CO_2 produced from photosynthesis and converts it to carbohydrates, cellulose, and lipids. However, the rate that CO_2 is released from the burning of fossil fuels and other human activities is surpassing the rate that nature recycles CO_2. This excess CO_2 concentration is thus contributing to the rise in global temperatures.[1,2]

Following nature's example, CO_2 can be captured from the atmosphere and converted to fuels. Hydrogenation of carbon dioxide to produce carbon-based fuels and feedstocks like formic acid (HCOOH) and methanol (CH_3OH) requires efficient catalysts but generates energy-rich liquids that can be used as fuels or as a chemical feedstock.[1,3] Therefore, to reduce the atmospheric CO_2 concentration, chemical utilization of CO_2 to chemicals and fuels is becoming necessary.

1.2 Catalysis

CO_2, being a very stable molecule, ($\Delta G°_f = -396$ kJ mol^{-1}) requires a large energy input for its reduction.[4] The reaction involving the hydrogenation of CO_2 producing formic acid is entropically disfavored compared to $CO_{2(g)}$ and $H_{2(g)}$. Figure 1 shows the direct hydrogenation of CO_2 with H_2 (Eq 1) which is thermodynamically unfavorable but can be made favorable in the presence of a base (Eq 2).[5] The Gibbs free energy, $\Delta G°_{rxn}$ is calculated to be -9.5 kJ/mol in the presence of NH_3. This reaction even becomes more favorable with an even stronger base.[4]

Eq 1 $CO_{2(g)} + H_{2(g)} \longrightarrow HCOOH_{(l)}$ $\Delta G°_{rxn} = +32.8$ kJmol^{-1}

Eq 2 $CO_{2(g)} + H_{2(g)} + Base \longrightarrow HBase^+ + HCO_2^-$ $\Delta G°_{rxn} < 0$

Figure 1. Hydrogenation of CO_2 to formate. [4,6] ($\Delta G°_{rxn}$ is the Gibbs free energy)

In addition to the thermodynamic requirements, hydrogenation of CO_2 requires the use of an efficient catalyst for the reaction to take place at observable rates. Most homogeneous catalysts used for this reaction are transition metal-phosphine complexes typically containing expensive metals such as ruthenium[7] and iridium.[8] The major goals when developing catalysts for CO_2 hydrogenation are: (a) to improve the activity of the metal catalysts, (b) to improve the reaction conditions, and (c) to use cheaper metals that

can work as active catalysts. The catalytic activity of the metal complexes is compared using the turnover number (TON) and turnover frequency (TOF), where TON is mol product per mol catalyst and TOF is mol product per mol catalyst per unit time. Catalysts with high TON and TOF are considered more catalytically active. In addition, most reactions take place at elevated temperature and pressure, and catalysts operating at lower temperature and pressure are more efficient.

1.3 Catalysts used for CO_2 hydrogenation

Transition metal catalysts containing phosphine ligands have been widely used for CO_2 hydrogenation catalysis. Inoue *et al*.[9] demonstrated the earliest examples of CO_2 hydrogenation to formic acid using phosphine-based ligands like triphenylphosphine (PPh_3) and bis(diphenylphosphino)ethane (dppe) bound to a variety of late transition metals including Ru, Ir and Rh. The reaction was carried out in the presence of benzene as solvent and a base, triethylamine, at room temperature. In 1992, Graf and Leitner[10] developed various Rh-phosphine complexes that could work as catalysts at room temperatures with low H_2/CO_2 concentration and gave a TON up to 3400. The nature of solvents used during catalysis has been found to affect the performance of the catalysts. Noyori and co-workers[11,12] used Ru catalysts in supercritical CO_2 ($scCO_2$) that gave a TON of 7200. Ezhova et al.[13] found that hydrogenation catalysis was observed with higher rates in polar solvents like DMSO and methanol using Wilkinson's catalyst, $[Rh(PPh_3)_3Cl]$. Recently, the development of catalysts based on first-row transition metals has been explored by many researchers.[4] Linehan and co-workers[5] have reported the use of a $Co(dmpe)_2H$ complex in the presence of a strong base called Verkade's base which gave a TOF of 3400 and 74000 h^{-1} at a pressure of 1 and 20 atm of CO_2/H_2,

respectively. However, a major drawback of this system was the use of the strong base to regenerate the catalyst.

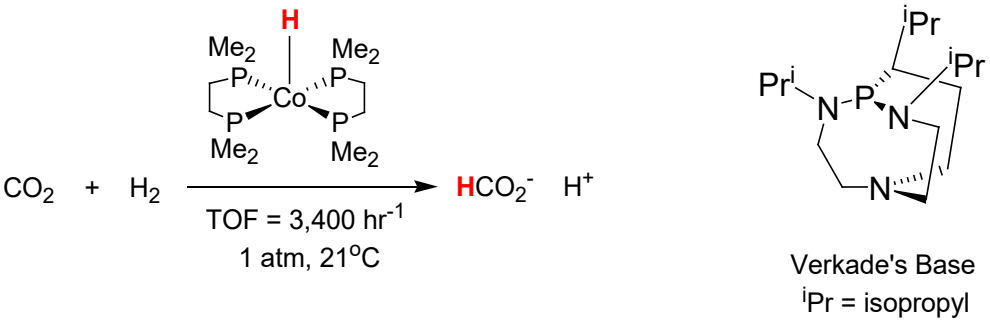

Figure 2. CO_2 hydrogenation using $Co(dmpe)_2H$ complex using Verkade's base.[5]

Another strategy has been to improve catalytic activity using pincer (meridionally coordinaing tridentate) ligands. Pincer ligands are multidentate ligands that can strongly bind to the metal center to prevent dissociation of the ligand from the metal, therefore allowing the catalysts to be used at higher temperatures. Use of iridium based complexes like $IrH_3(P_1)$ (P_1= 2,6-bis(di-isopropylphosphinomethyl)-pyridine) has been reported by Nozaki and co-workers[8] giving a TOF of 150000 h^{-1} at 200°C. This led to further research using these pincer ligands for CO_2 hydrogenation. Iron-PNP pincer complexes (PNP = $HN\{CH_2CH_2(PR_2)\}_2$); R = ^{i}Pr / Cy (^{i}Pr = isopropyl, Cy = cyclohexyl) containing secondary and tertiary amines were investigated by Bernskoetter and co-workers[14] which gave very high turnovers in the presence of a Lewis acid co-catalyst.

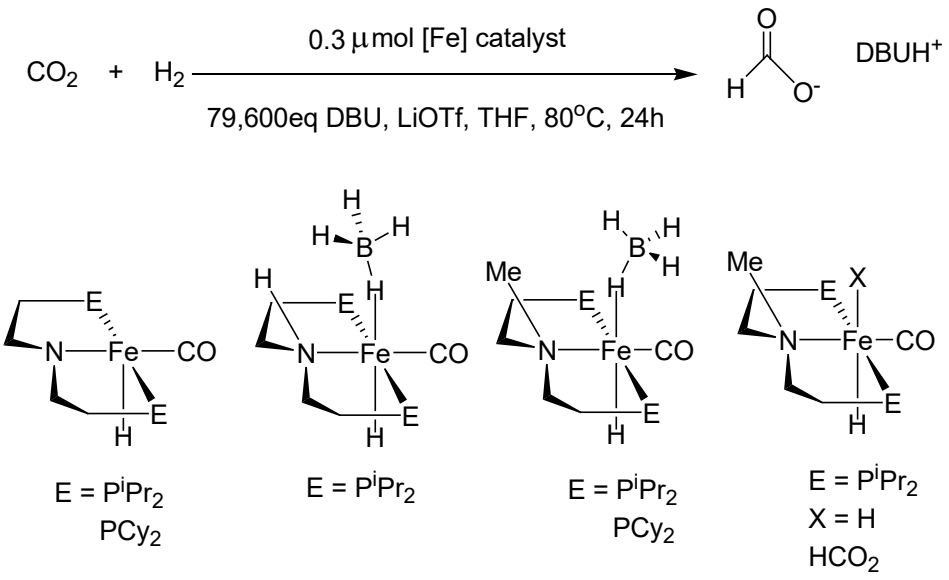

Figure 3. Iron-PNP pincer catalysts used for CO_2 hydrogenation.[14]

1.4 Bio-inspired ligands used for CO_2 hydrogenation

Multi-electron reduction processes are known to occur in biological systems. In these biological reduction processes hydride movement is facilitated by the nucleotide substituted nicotinamide NADH which transfers hydride to an enzyme activated substrate. NADH is therefore known as nature's hydride carrier. The substrates are activated by binding to a metal ion present in the enzymes. Two such enzymes are alcohol dehydrogenase and acetohydroxy acid isomeroreductase.[15,16]

Inspired by these reduction processes in biology, synthetic analogues of NADH are known and have been used as organic reductants. One of the first analogues of NADH was 1-benzyldihydronicotinamide (BNAH) (shown in Figure 4). Some well-defined hydride donor groups are dihydroquinolinidinamide (QAH), derivatives of Hantszch ester dihydropyridine (HEH) and 2,3-dihydrobenzo[d]imidazolines (BIH).[15] These groups

have the ability to transfer hydride to unsaturated organic substrates like imines, pyridines, aldehydes, and ketones.

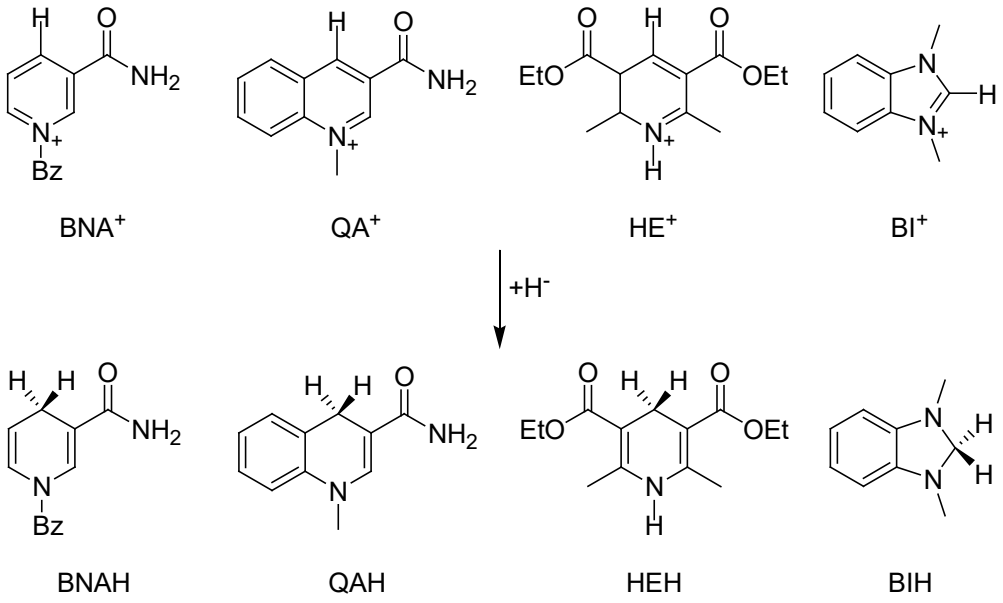

Figure 4. Some common organic hydride donors.[15]

In a few cases, organic hydride donors have been incorporated into metal complexes, where they have been shown to facilitate hydride transfer. In 1975, a BNAH derivative was used by Ohno and co-workers[17] for reduction of organic substrates catalyzed by Mg^{2+} ion. A variety of these complexes have been described by Tanaka and coworkers[18,19] over the past decade. They have used ruthenium and palladium complexes containing acridine groups that could work as hydride donors. Koizumi and Tanaka[20] have also demonstrated the use of these complexes for the reduction of unsaturated substrates. The complex $[Ru(bpy)_2(1\text{-apa})_2](PF_6)_2$ (1-apa = 1-aza-2-(2-pyridyl)) in its reduced form, $[Ru(bpy)_2(1\text{-apa-}H_2)]^{2+}$ was shown to reduce acetone to iso-propanol under ambient conditions. Catalytic studies for the reduction of CO_2 to formate ion using

1-aza-(2-pyridyl)-(dihydro)acridine)ruthenium complex has been observed by Ohtsu and Tanaka.[21]

Yang and List[22] have used Hantzsch ester (HEH) as an NADH analogue in the presence of a Cu catalyst for the hydrogenation of α-ketoesters. Colbran and Mcskimming[15] reported the use of Rh(I) complexes of an *N*-heterocyclic carbene ligand with a nicotinamide cation that could be reduced to the corresponding neutral dihydronicotinamide substituted complex. They were also found to reduce a variety of organic substrates. Colbran and coworkers[23] have shown the use of a benzimidazole-based system, $[C_PM(L^{BI})Cl](PF_6)_2$ (where M= Rh, Ir) for the reduction of imines by formate ion.

While incorporation of organic hydride donors into transition metal complexes has been shown to facilitate hydride transfer in some reactions, as described above, it has not been used for hydrogenation, in which hydride transfer must be coupled to proton transfer for net transfer of H_2. Most of the above studies have used the hydride donors as pure H^- transfer agents. H_2 has not been used as a reductant, as the transfer of both H^+ and H^- are required for H_2 chemistry. Also, the acridinium group used in most of these systems is too weak of a hydride donor to efficiently reduce CO_2. An exception was reported by Tanaka,[21] where a ruthenium-bipyridyl complex containing an acridinium relay was used for the reduction of CO_2 to formate in which hydride transfer was promoted by a base.

1.5 New Catalyst Design

In this study, bifunctional catalysts containing organic hydride donor groups called “hydride relays” have been synthesized. The relays are organic hydride donors,

like those shown in Figure 4, which are designed to reversibly accept or donate H^- ions during catalysis, and, unlike previous systems, these are tethered to a phosphine donor. These ligands have been incorporated into metal complexes that also contain more traditional chelating phosphine ligands, similar to those used in CO_2 hydrogenation. The goal is to use these complexes as catalysts for hydrogenation of renewable feedstock for small molecules like CO_2. The proposed catalytic cycle for the hydrogenation of CO_2 using a Pd-benzimidazolium with a pincer-type ancillary ligand (PP_2: bis(diphenylphosphinoethyl)phenylphosphine) as catalyst is shown in Figure 5. During catalysis, H_2 activation will reduce the hydride relay, forming an organic hydride donor, while the metal will be protonated, forming an acidic metal hydride (Figure 5: Step A). CO_2 will then be reduced by hydride transfer from the relay, forming formate ($HCOO^-$) (Figure 5: Step B) while the hydride on the metal center will be deprotonated by an external base, regenerating the original metal catalyst (Figure 5: Step C).

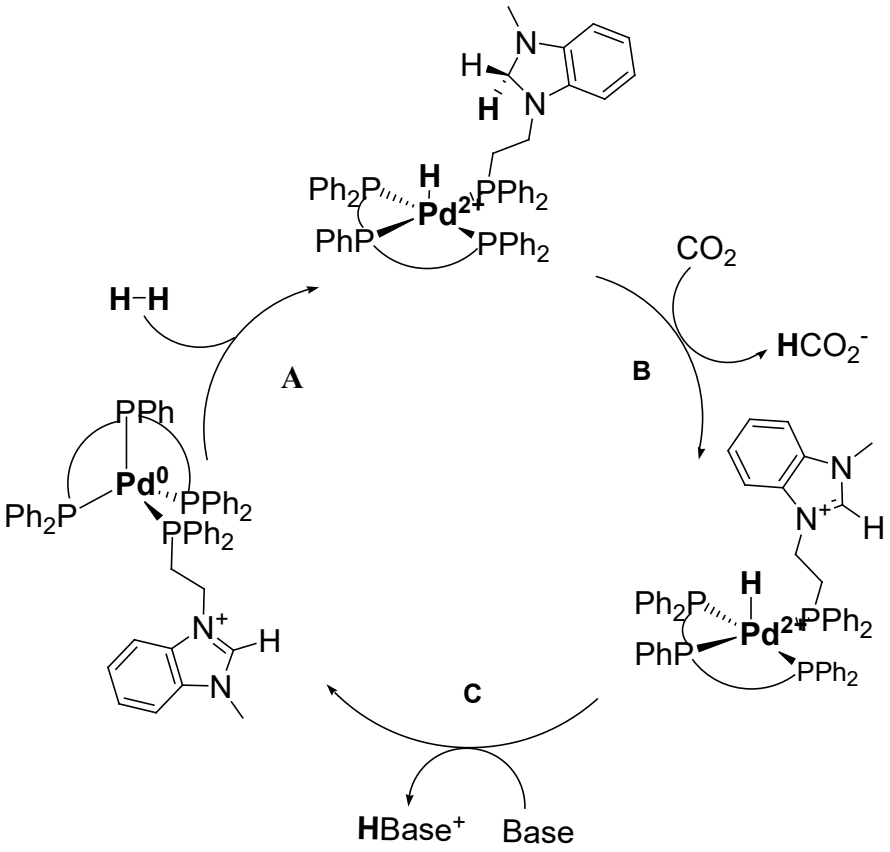

Figure 5. Proposed catalytic cycle for CO_2 hydrogenation.

The basic steps of the catalytic cycle can be summarized as:

Step A: Activation of H_2 to form an acidic M-H and a reduced hydride relay.

Step B: Hydride transfer from the relay to substrate.

Step C: Abstraction of the proton by a base and regeneration of the metal catalyst.

The challenge is to design catalysts that meet the structural and reactivity requirements. Hydride relays must be attached to a metal center so that they can work cooperatively with the metal to activate H_2 and then transfer hydride to the substrates. For this purpose, the newly designed ligands will be combined with late transition metal centers that are capable of forming acidic metal hydrides. Different hydride relays have a specific hydricity ($\Delta G^{o}_{H^-}$) value, which is a measure of the free energy required to

remove a hydride ion (H^-). Organic hydride donors will be used based on their hydricity values. The hydride donor/acceptor ability of the relay works synergistically with the proton donor/acceptor ability of the low-valent transition metal.

By estimating the thermodynamic parameters in each step (A through C) in the catalytic cycle in Figure 6, the relay and metal hydride can be chosen rationally for the hydrogenation of CO_2. These parameters include the hydride donor ability of the relay (benzimidazolium in Figure 6), the acidity of the metal-hydride, the proton and hydride-acceptor abilities of the substrate (CO_2 in Figure 6), and the proton affinity of the base. The hydricity values of most of the organic hydride donors can be calculated from data reported in the literature.[24,25] The free energy for the hydride transfer step in Step B (Eq 3) is the sum of the free energies associated with the hydride donor ability of the benzimidazolium relay ($\Delta G^{o}_{H^-}$) (Eq 4) and the hydride acceptor ability of CO_2 (Eq 5), as summarized in Eq 6.

Step B:

Eq 3	$L^{BIH} + CO_2 \longrightarrow L^{BI+} + HCO_2^-$	$\Delta G°$ (kcal/mol)	
Eq 4	$L^{BIH} \longrightarrow L^{BI+} + H^-$	$\Delta G°_{H^-}$	
Eq 5	$H^- + CO_2 \longrightarrow HCO_2^-$	-44	
Eq 6	$\Delta G° = \Delta G°_{H^-} - 44$		

Figure 6. Hydride transfer from relay to CO_2 (L^{BI} = benzimidazolium relay).

The free energy for the formation of formate from CO_2 and H^- (Eq 5) has been determined[26,27] to be -44 kcal/mol in MeCN solvent and hence the relay must have a $\Delta G^{o}_{H^-}$ value of ≤44 kcal/mol to transfer hydride to CO_2. The hydricity of a strongly donating group like benzimidazolium was determined to be 45±3 kcal/mol in MeCN

solvent which is ideal for a substrate like CO_2.[26] The choice of the metal ion can be targeted based on the pK_a of its metal hydride. Because the benzimidazolium relay is a strong hydride donor, it must be paired with a strongly basic metal center for the H_2 activation step (Step A, Eq 7) to be favorable. The free energy of this step is the sum of the free energies for H_2 heterolysis (Eq 8), the hydride acceptor ability of the relay, which is the opposite of the hydricity (Eq 9), and proton transfer to the metal (Eq 10). The free energy of the reaction in Eq 10 is RTlnK_a, where K_a is the acid dissociation constant of MH^+, and at a temperature of 298 K this expression for the free energy converts to 1.364logK_a, in units of kcal/mol. The free energy of the reaction in Eq 10 is therefore expressed as -1.364 pK_a, and Eq 11 gives the relationship between ΔG^o for the H_2 hydrolysis step (76 kcal/mol),[28] $\Delta G^o_{H^-}$ for the relay, and the pK_a of the metal hydride.

Step A:

Eq 7	$M\text{-}L^{BI+} + H_2 \longrightarrow HM^+\text{-}L^{BIH}$	ΔG^o (kcal/mol)
Eq 8	$H_2 \longrightarrow H^+ + H^-$	76
Eq 9	$L^{BI+} + H^- \longrightarrow L^{BIH}$	$-\Delta G^o_{H^-}$
Eq 10	$M + H^+ \longrightarrow M\text{-}H^+$	$-1.364pK_a$
Eq 11	$\Delta G^o = 76 - \Delta G^o_{H^-} - 1.364pK_a$	

Figure 7. Addition of H_2 to M-L^{BI}.

Using Eq 11 with values of $\Delta G^o = 0$ for a thermoneutral reaction step and $\Delta G^o_{H^-}$ = 45 kcal/mol for a benzimidazolium relay, the pK_a of the metal hydride that will give a thermoneutral reaction can be calculated as 23. In this case, Pd^{2+} was chosen as a suitable metal because similar tetraphosphino-Pd^{II} hydride complexes were found to have pK_a

values in this range.[29] Other late transition metals, particularly Ni^{II} complexes, can be expected to have similar values. Finally, in Step C of the catalytic mechanism, a suitable base is required to deprotonate the metal hydride, which must have a pK_a similar to the metal hydride. One such base is DBU (1,8-diazabicyclo[5.4.0]undec-7-ene). Thus, for the hydrogenation of CO_2, a strong hydride relay will require a strong basic metal center.

1.6 Objectives

The goal of this research is to use hydride relays to facilitate hydrogenation catalysis, where the organic hydride donor will accept hydride from H_2 and transfer it to CO_2. This will be a new approach for the reduction of CO_2 and other organic substrates. This project has focused on the synthesis of ligands with this new design, creating metal complexes with these new ligands studying their reactivity and structural properties to evaluate their potential as catalysts.

The primary objectives of this research were to:

1. Synthesize ligands containing organic hydride donors of varying strength.
2. Incorporate the ligands into well defined, low-valent transition metal complexes.
3. Characterize the complexes to evaluate their potential catalytic activity for CO_2 hydrogenation.

CHAPTER II

SYNTHESIS AND CHARACTERIZATION OF REDOX-ACTIVE LIGANDS

2.1 Introduction

In this study, ligands containing reactive functional groups called "hydride-relays" were synthesized. The relays are organic hydride donors that can reversibly accept or donate H^- ions from H_2. The organic hydride donors are *N*-alkylated pyridinium and imidazolium derivatives which are analogous to nicotinamide adenine dinucleotide, NADH, which is considered to be nature's hydride donor.[16] These hydride donors are tethered to a phosphine donor so that they can be incorporated into a metal complex. The design of the bifunctional ligand is shown in Figure 8. It consists of three main parts: (1) a phosphorus donor atom that binds to the metal, (2) an organic hydride relay, and (3) a flexible ethylene linkage that connects the two. Due to the flexible linker between the relay and the phosphine donor, the steric and electronic properties of the relay can be varied without changing the overall ligand design. In this study, ligands containing phenanthridinium, benzimidazolium and 2-phenylbenzimidazolium groups were synthesized.

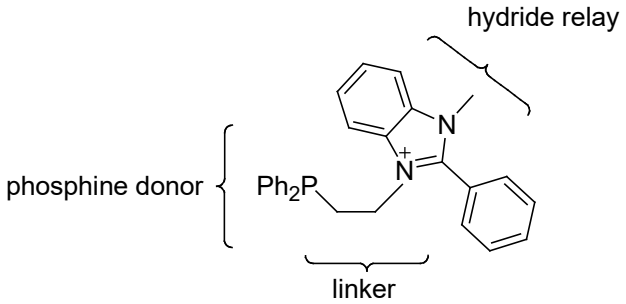

Figure 8. Ligand design using $L^{PhenBI+}$ as hydride relay.

In this study, the hydride donor ability of the relay will work synergistically with the proton acceptor ability of the metal. The modularity of the ligand design allows us to judiciously choose the metal based on the acid-base chemistry and the organic hydride donor based on its hydride transfer ability and combine them to form a bifunctional complex to carry out a variety of hydrogenation reactions. Hydricity (ΔG^{o}_{H}-), or the hydride donor strength of organic hydride relays have been studied for many related hydride donors in the literature.[15,24,25] The ligands synthesized in this study, are shown in Figure 9. Being weak hydride donors, we do not expect L^{PhenH} or L^{Phen+} to be useful for CO_2 reduction, but these were used in initial studies to prove the initial ligand synthesis and to help in studies of H_2 activation.

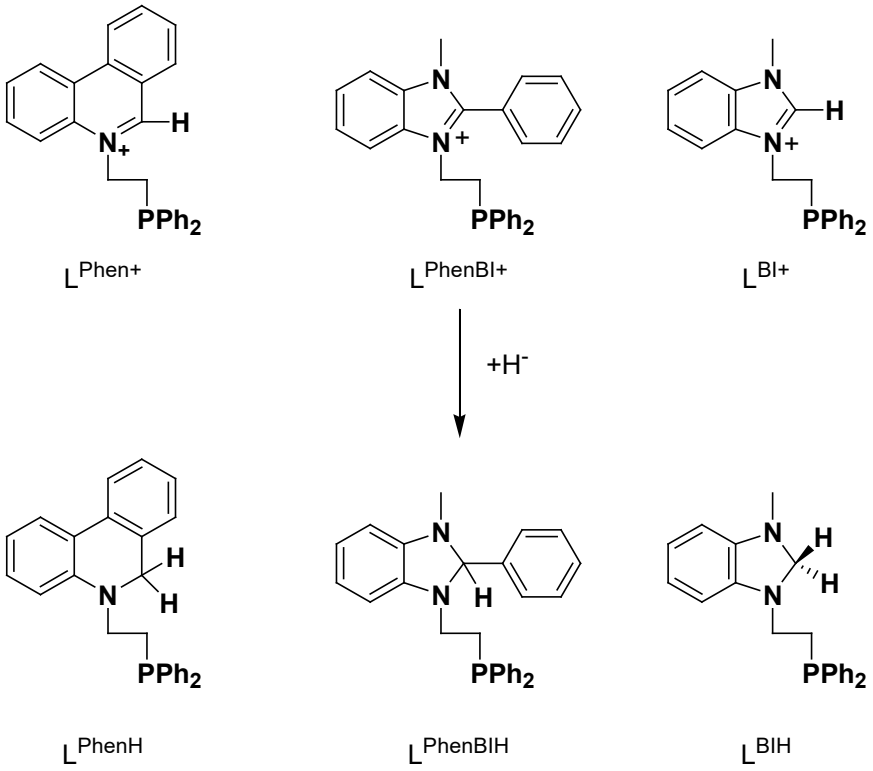

Figure 9. Synthesized redox-active ligands.

2.2 General synthetic approach

The first step in the synthesis of the ligands was the alkylation of the *N*-heterocycle using 1,2-dibromoethane via a nucleophilic substitution reaction (S_N2). Following this, the phosphine group was added to the ligand via a nucleophilic substitution using $KPPh_2$ (shown in Figure 10). The reduction reaction was carried out using $NaBH_4$.[30]

2.3 Results and Discussion

The first step of the synthesis of ligand L^{Phen+} was carried out from a literature precedent by Cronin and co-workers,[31] which was the alkylation of the hydride relay, phenanthrdine using excess of 1,2-dibromoethane.[31] However, the ortho-carbon next to the N atom was susceptible to nucleophilic attack according to the literature report.[31] Therefore, the alkylated phenanthridinium had to be reduced prior to adding the $KPPh_2$ to prevent any nucleophilic attack. For this, we used $NaBH_4$ as the reducing agent.[30] The reduced form of the ligand, L^{PhenH} , was produced in this route, but it can be oxidized by trityl cation in a later step as shown in Figure 10. Diphenylphosphine was then introduced by adding potassium diphenylphosphide ($KPPh_2$), in a nucleophilic substitution that displaces bromide. While the first step of the reaction, that is, addition of the ethylene linker was carried out under air at 100ºC, the later steps were performed using standard Schlenk conditions under nitrogen atmosphere at room temperature. ^{1}H NMR spectroscopy provides evidence for the formation of oxidized and reduced phenanthridinium ligands and addition of the PPh_2 group was confirmed using ^{31}P NMR spectroscopy.

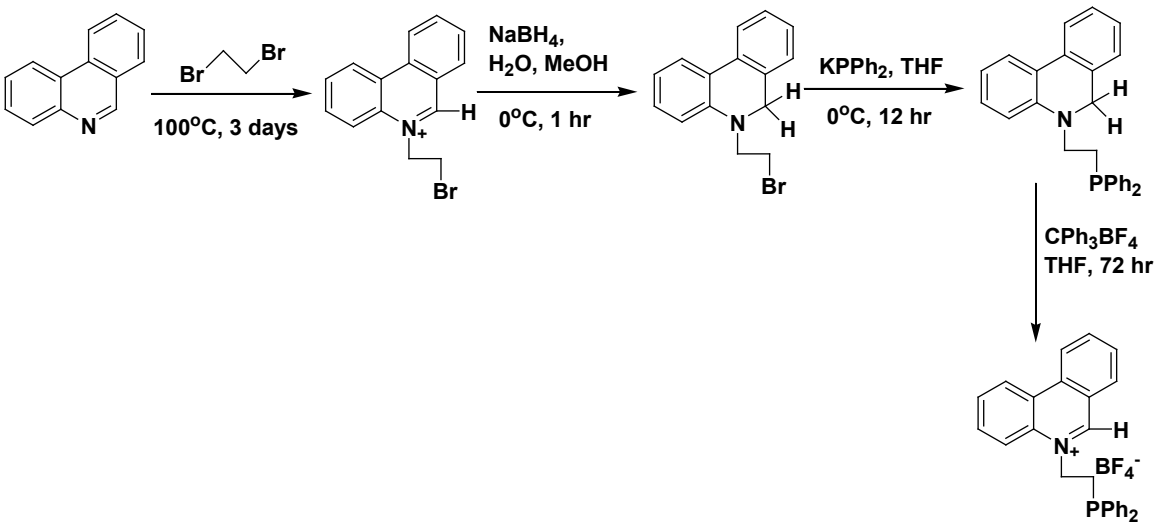

Figure 10. Synthesis of L^{PhenH} and L^{Phen+}.

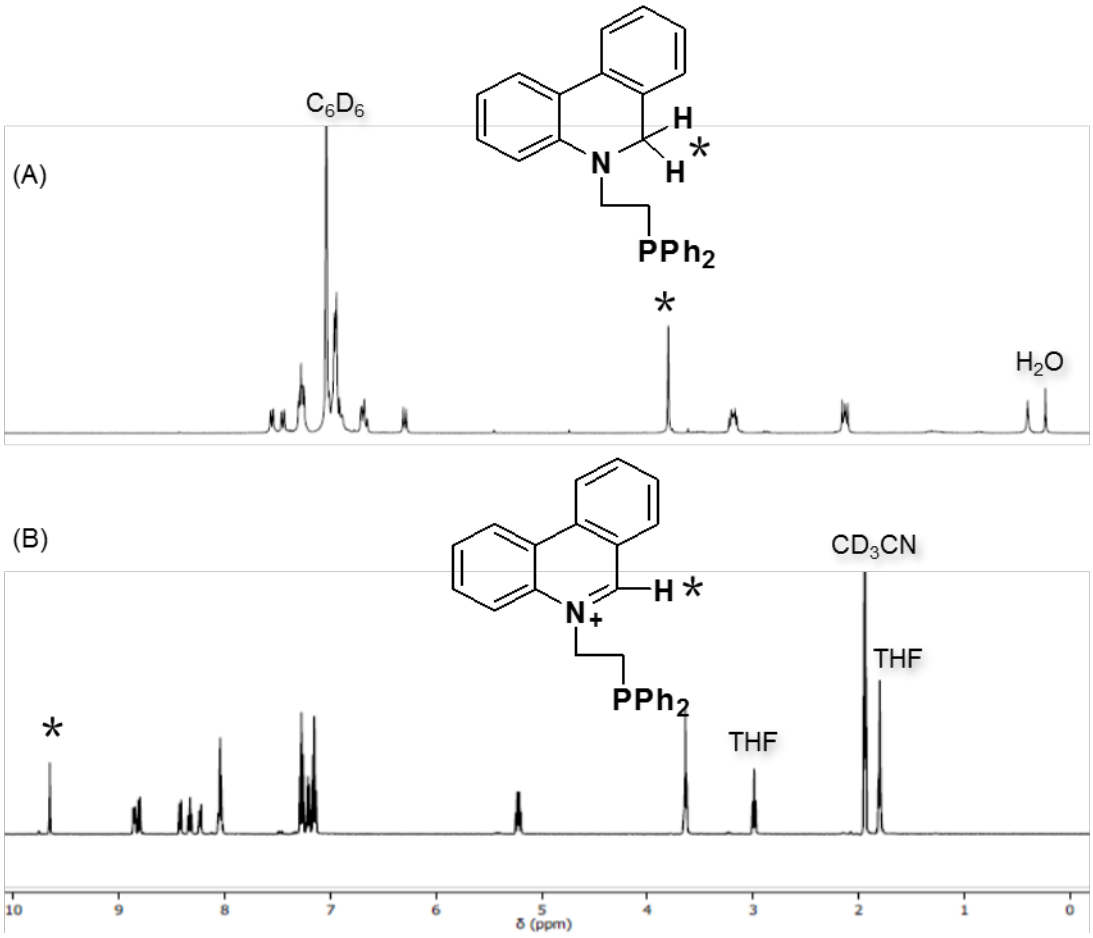

Figure 11. ^{1}H NMR spectra of (A) L^{PhenH} in C_6D_6 (B) L^{Phen+} in CD_3CN (300 MHz).

^{1}H NMR spectroscopy was used to characterize the synthesized ligands, L^{PhenH} and L^{Phen+}, and could be used to distinguish between the two. As shown in Figure 11 (A), the characteristic peak for H on the C at the α-position to the N was seen at δ 3.83 ppm for the reduced ligand whereas for the oxidized ligand it was observed further downfield at δ 9.75 ppm. Also, all the phenanthridinium peaks were recorded at a shift downfield of 8 ppm for the oxidized ligand and upfield of 8 ppm for the reduced ligand. This downfield shift could be explained due to the presence of the positively charged N in the oxidized ligand. The peaks for two CH_2 groups in the ethylene linker were observed at δ 5.21 ppm and δ 2.99 ppm for the oxidized ligand, whereas for the reduced ligand these peaks were observed at a chemical shift of 3.22 ppm and 2.15 ppm, respectively, as shown in Figure 11 (B). These differences in chemical shift confirm that the oxidized ligand (L^{Phen+}) is significantly more electron rich than the reduced ligand (L^{PhenH}). However, the peaks for the PPh_2 protons have nearly the same shifts in both the complexes, indicating that the difference in electron density is in the hydride relay, and not the phosphine. The peaks in the ^{31}P NMR spectra for both the complexes have nearly the same chemical shift values: δ -19.66 ppm for L^{PhenH} and -19.51 ppm for L^{Phen+}, as shown in Figure 44 and 46, respectively.

The synthesis of L^{BI+} ligand started with the alkylation of the relay followed by the addition of $KPPh_2$ (as shown in Figure 12). Because the benzimidazolium group is not as susceptible to nucleophilic attack, it does not need to be reduced prior to introduction of the phosphine. The formation of L^{BI+} ligand was characterized using ^{1}H NMR and ^{31}P NMR spectroscopy.

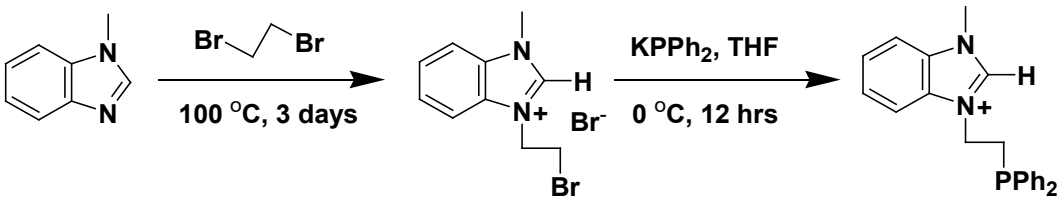

Figure 12. Synthesis of L^{BI+}.

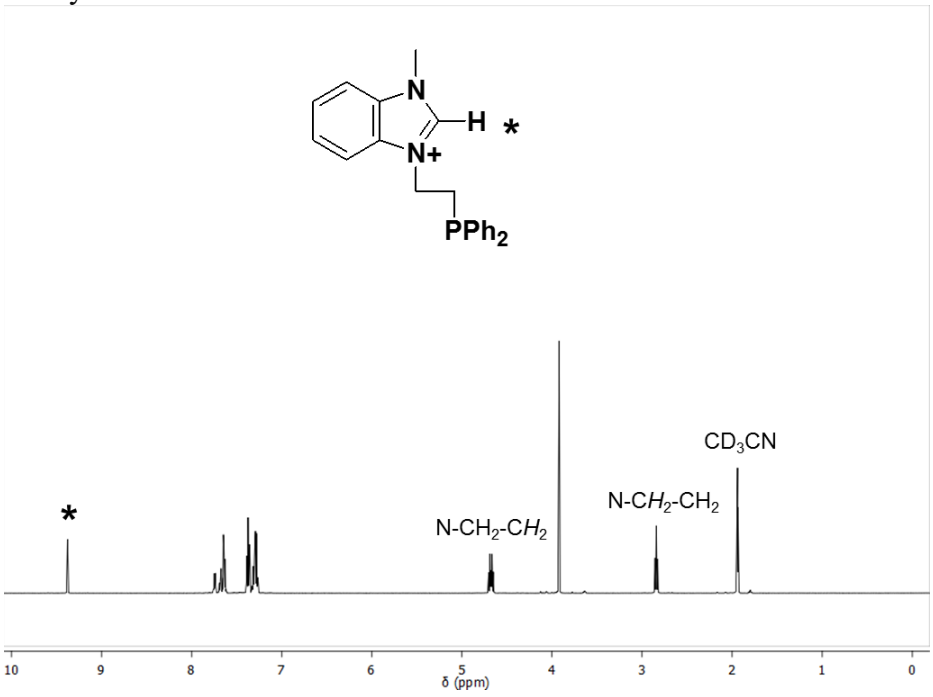

Figure 13. ^{1}H NMR spectrum of L^{BI+} in CD_3CN (300 MHz).

A ^{1}H NMR spectrum (Figure 13) was obtained in acetonitrile-d_3. A peak for the CH_3 group attached to the N was observed at δ 3.9 ppm and a singlet due to the H at the α-position to both the N was observed at δ 9.3 ppm. Also, the peaks for the two CH_2 groups in the ethylene linker were clearly observed at δ 4.6 ppm as a quartet and at δ 2.8 ppm as a triplet, respectively. The quartet is a result of coupling to the two neighboring H's and the P from the PPh_2 group. These peaks are upfield compared to L^{Phen+}, which suggests that L^{BI+} is not as electron deficient as L^{Phen+}. This is consistent with L^{BI+} being a

good hydride donor compared to L^{Phen+}. The ^{31}P NMR spectra showed a singlet at -20.01 ppm (Figure 16).

L^{BI+} was selected based on its predicted hydricity; however, it is susceptible to deprotonation, forming an N-heterocyclic carbene, in the presence of strong bases like DBU (1,8-diazabicycle[5.4.0]undec-7-ene). Therefore, to avoid these deactivation pathways, a 2-phenyl substituted benzimidazolium ligand was synthesized which is robust towards deprotonation while maintaining sufficient donor strength.

The synthesis of the $L^{PhenBI+}$ required a series of additional steps. The commercially available form was not alkylated. Hence the first step was to alkylate one of the N atoms[32] followed by the addition of the 1,2-dibromoethane to alkylate the second N atom, as shown in Figure 14. The diphenylphosphine was then introduced using $KPPh_2$. The product was characterized using ^1H NMR and ^{31}P NMR spectroscopy.

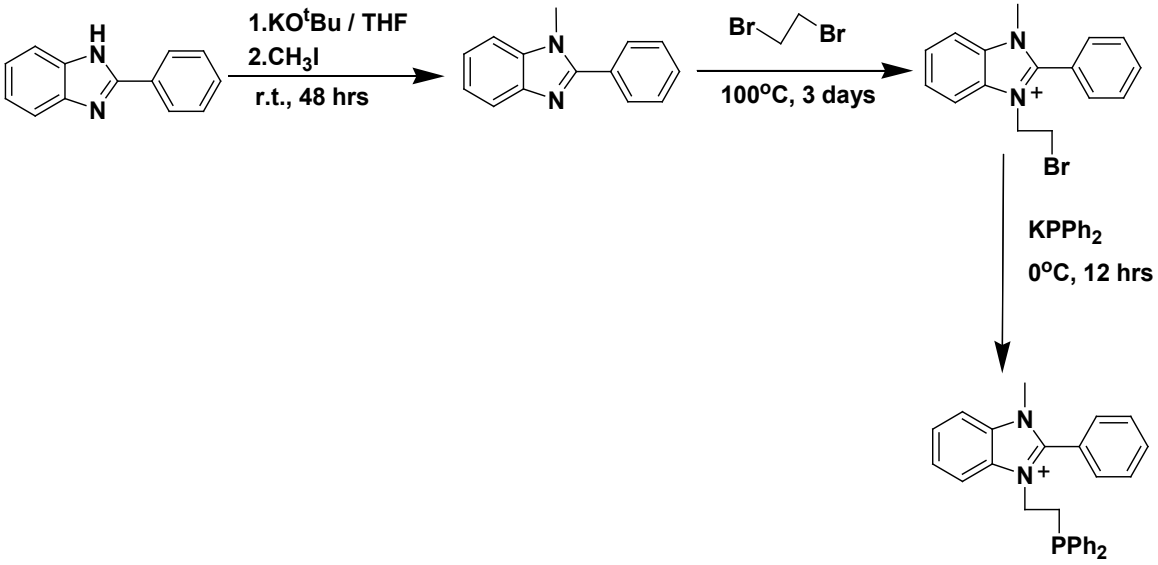

Figure 14. Synthesis of $L^{PhenBI+}$.

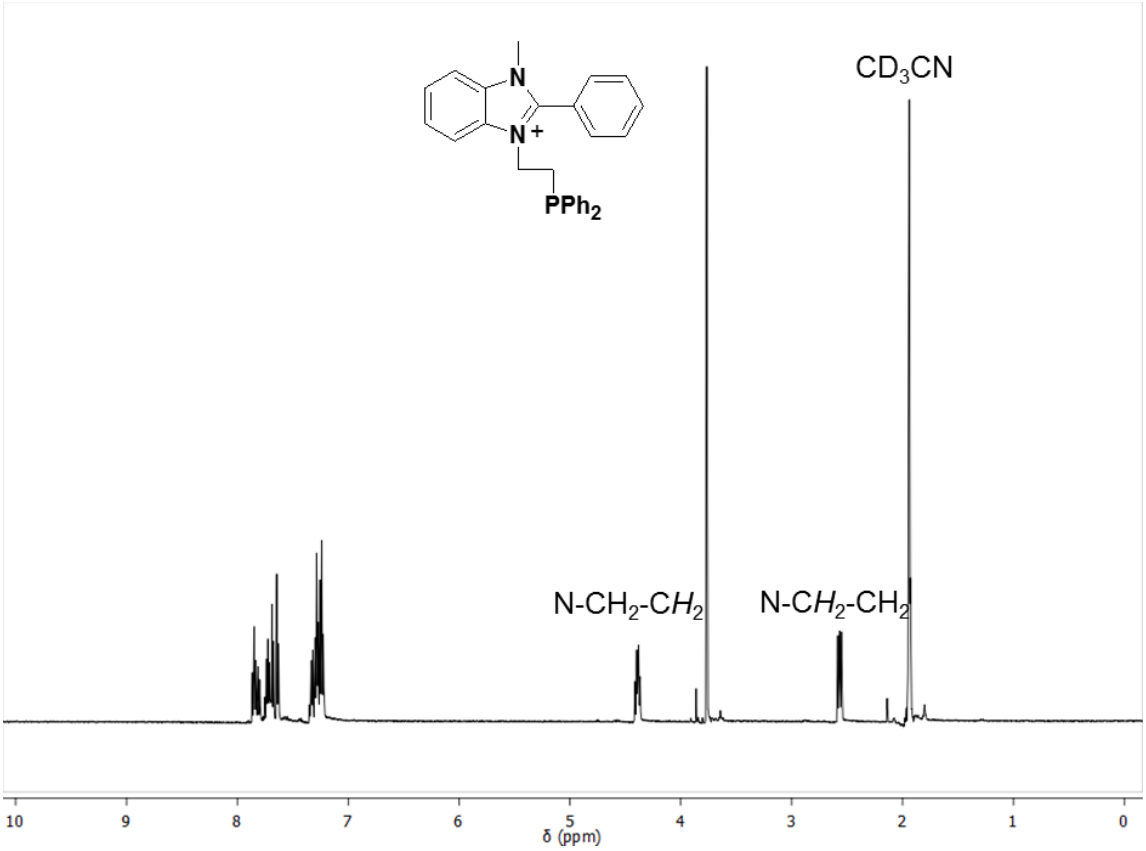

Figure 15. ^{1}H NMR spectrum of $L^{PhenBI+}$ in CD_3CN (300 MHz).

The ^{1}H NMR spectrum (Figure 15) in acetonitrile-d_3 showed a distinct peak for the CH_3 group attached to the N at δ 3.76 ppm, as a singlet. Peaks for aromatic H in the region δ 7.84-7.22 ppm and peaks for the two CH_2 groups in the ethylene linker were observed at δ 4.39 ppm as a quartet and δ 2.57 ppm as a triplet, respectively. The quartet is a result of coupling to the two neighboring H's and the P from the PPh_2 group. For all of the above ligands, a peak for the phosphine group attached to the ethylene linker was recorded by ^{31}P NMR spectroscopy. For L^{BI+}, this signal was observed at a chemical shift of -20.01 ppm as shown in Figure 16. For all of the other ligands, this signal was observed at nearly the same chemical shift value. These chemical shift values for the

phosphine donor, was comparable to the chemical shift for the free phosphine, *t*-$BuPPh_2$ which shows up at -17 ppm.[33]

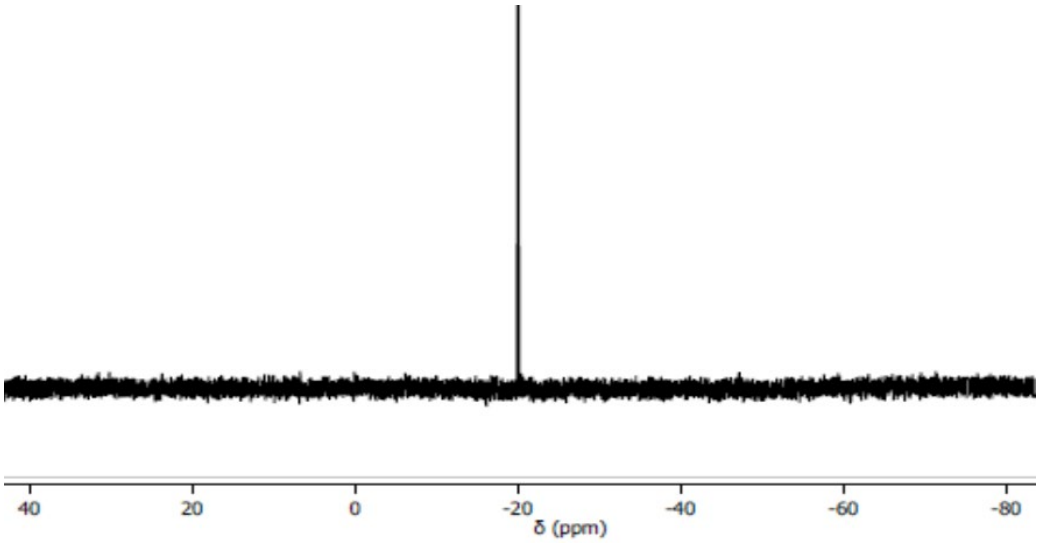

Figure 16. ^{31}P NMR spectrum of L^{BI+} in CD_3CN (300 MHz).

For most of the ligands synthesized above, prior to their addition to a metal center, a metathesis reaction was performed, where the Br^- anion was exchanged with other anions like BF_4^- and PF_6^-, to avoid coordination of Br^- to the metal center. The metathesis reactions of benzimidazolium and phenylbenzimidazolium are shown in Figure 17.

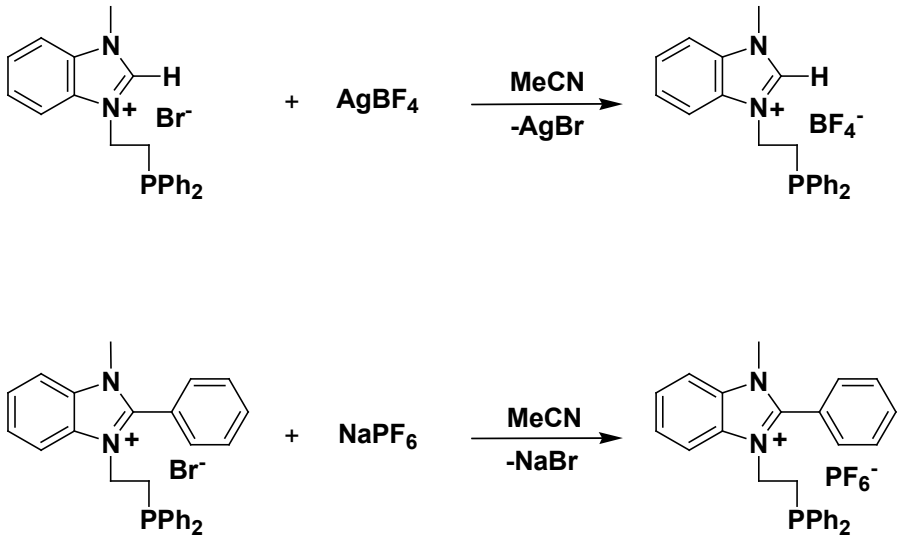

Figure 17. Metathesis reaction of L^{BI+} and $L^{PhenBI+}$.

The ^{1}H NMR spectrum for the products obtained from the anion exchange reactions, as shown in Figure 17, remain unchanged. However, the formation of precipitates, AgBr for the first reaction and NaBr for the second reaction, were observed. The ^{31}P NMR spectrum for $L^{PhenBI}PF_6$ showed a signal for the PF_6 anion at -144.03 ppm, as shown in Figure 70. This signal is integrated to less than a 1:1 ratio vs. the PPh_2 signal, which is likely due to the long relaxation time for the ^{31}P nucleus in PF_6. These provided evidence for the above reactions to have worked.

2.5 Conclusion

Three ligands containing hydride relays, L^{Phen+}, L^{BI+}, and $L^{PhenBI+}$, were synthesized. The former was prepared in its reduced form, and then oxidized. The latter two could be obtained cleanly in their oxidized form without the reduction and oxidation steps. The ^{1}H NMR spectra showed diagnostic shifts for each hydride relay group. The ^{31}P NMR spectra provided evidence for the phosphine group attached to the ethylene linker in each ligand. This fulfilled the first objective of this research which was to

synthesize these redox-active ligands, so that they can then be incorporated into appropriate transition metal complexes in conjunction with other ancillary phosphine ligands. The synthesis of these bifunctional metal complexes will be discussed in Chapter III.

2.6 Experimental section

General. All starting materials and reagents were purchased from commercial sources (Sigma Aldrich and Alfa Aesar) and used without further purification. Most of the air sensitive reactions were performed inside a glove box (VIGOR) under a nitrogen atmosphere. Preliminary steps of the ligand synthesis were performed using standard Schlenk techniques under a nitrogen atmosphere. Solvents were degassed under argon and dried by passage through columns of alumina and molecular sieves and stored inside the glove box. All the air-sensitive reagents were stored inside the glove box under nitrogen atmosphere. Required glassware was oven dried before use. ^{1}H NMR and ^{31}P NMR spectra were recorded on a JEOL Eclipse 300+ spectrometer. The ^{1}H NMR spectra were referenced based on the residual solvent peaks while phosphoric acid was used as the external standard for ^{31}P NMR spectra. Chemical shifts are reported in δ (ppm) relative to ^{1}H (CD_3CN: 1.94, D_2O: 4.79, C_6D_6: 7.16, DMSO-d_6: 2.50) and ^{31}P (H_3PO_4: 0).

Synthesis of discussed compounds

Synthesis of L^{PhenH} and L^{Phen+} ligand.

Step 1. Synthesis of 5-(2-bromo-ethylene)-phenanthridinium bromide: Phenanthridine (30.3 mmol, 5.43 g) was dissolved in 1,2-dibromoethane (608 mmol, 52.4 mL) and stirred at 90ºC for 3 days.[31] A beige color precipitate was observed in the reaction flask and was filtered after 3 days. The residue was washed with 1,2-

dibromoethane and ethyl acetate three times each. The solid experienced a slight change in color from beige to white. The product was dried and collected as a white powder (8.79 g, 79.5%). ^{1}H NMR (D_2O, 300 MHz) (Figure 41): δ 9.71 (s, 1H), 8.61 (dd, *J* = 8.22, 1.44 Hz, 1H), 8.52 (d, *J* = 8.3 Hz, 1H), 8.27 (dd, *J* = 8.05, 1.37 Hz, 1H), 8.15 (dd, *J* = 8.60, 1.22 Hz, 1H), 8.23-8.18 (m, 2H), 8.07 (ddd, *J* = 8.80, 7.02, 1.44 Hz, 1H), 7.88 (ddd, *J* = 1.10, 7.10, 8.35 Hz, 1H) 5.27 (t, *J* = 5.81 Hz, N-C*H*$_2$-CH$_2$-Br, 2H), 3.96 (t, *J* = 5.73 Hz, N-CH$_2$-C*H*$_2$-Br, 2H).

Step 2. Synthesis of 5-(2-bromo-ethylene)-5,6-dihydro-phenanthridine: The oxidized phenanthridinium was reduced using $NaBH_4$ (4.998 mmol, 189.1 mg) in a 2:1 mixture of MeOH-H_2O solvent. The reaction mixture was stirred in an ice bath.[30] A color change was observed from white to red immediately after the $NaBH_4$ was added. The color however faded in the course of time. After 1 hour, a beige precipitate was observed on addition of 100 mL H_2O. The solution was filtered, residue collected and dried under vacuum (1.008 g, 87.45%). ^{1}H NMR (C_6D_6, 300 MHz) (Figure 42): δ 7.57 (dd, *J* = 7.77, 1.61 Hz, 1H), 7.16-6.39 (m, 6H), 6.40 (dd, *J* = 8.28, 1.08, 1H), 3.22 (t, *J* = 8.45 Hz, N-C*H*$_2$-CH$_2$-Br, 2H), 2.96 (t, *J* = 8.26 Hz, N-CH$_2$-C*H*$_2$-Br, 2H), 3.71 (s, THF), 0.41 (s).

Step 3. Synthesis of 5-(2-diphenylphosphanyl-ethylene)-5,6-dihydro-phenanthridine: The above product (0.912 mmol, 0.250 g) was dissolved in minimum THF (30 ml) under positive N_2 using Schlenk techniques. The reaction mixture was cooled in an ice-bath and 1.82 mL $KPPh_2$ solution (0.5 M in THF) was added dropwise. A cloudy beige precipitate was observed initially when adding the drops of $KPPh_2$ and the red color of $KPPh_2$ disappeared with each drop. Later the solution turned cloudy

yellow. After 12 hours, white precipitate was observed at the bottom of the flask with a yellow solution above. The yellow solution was transferred to another round bottom flask (RBF) using cannula transfer. The solid was further washed with THF and the solvent was removed under vacuum. MeOH was added to the solid to quench any remaining $KPPh_2$, and the solid was washed with acetonitrile, then hexane. The product was dried under vacuum and weight recorded. A yield of 960 mg (74.3%) was recorded. ^{1}H NMR (C_6D_6, 300 MHz) (Figure 43): δ 7.68 (dd, *J* = 7.85, 1.57 Hz, 1H), 7.59-7.56 (d, *J* = 7.58, 1H), 7.43-7.34 (m, 3H), 6.83-6.77 (m, 2H), 6.41 (d, *J* = 8.14 Hz, 1H), 3.88 (s, 2H), 3.28 (q, *J* = 7.22 Hz, N-CH_2-C*H*$_2$-PPh_2, 2H), 2.21 (t, *J* = 8.17, 7.96 Hz, N-C*H*$_2$-CH_2-PPh_2, 2H), 0.47 (s, H_2O), 0.30 (s). ^{31}P NMR (C_6D_6, 300 MHz) (Figure 44): δ -19.66 (s).

Step 4. Synthesis of 5-(2-diphenyphosphanyl-ethylene)-phenanthridinium tetrafluoroborate:

To synthesize the oxidized ligand, the above product (0.3505 mmol, 137.9 mg) was then dissolved in THF (10 mL) and a solution of CPh_3BF_4 (0.3505 mmol, 115.7 mg) was added in THF. The reaction mixture experienced a color change from red to pale pink and was stirred for 3 days. The solution, now beige in color, was filtered and the residue collected as a powder. A yield of 131.8 mg (78.45%) was obtained. ^{1}H NMR (CD_3CN, 300 MHz) (Figure 45): δ 9.66 (s, 1H), 8.87-8.85 (m, 1H), 8.81 (d, *J* = 8.43 Hz, 1H), 8.42 (d, *J* = 8.04 Hz, 1H), 8.33 (ddd, *J* = 8.4, 7.1, 1.4 Hz, 1H), 8.24-8.22 (m, 1H), 8.07-8.02 (m, 1H), 7.27 (ddd, *J* = 10.46, 7.94, 1.06 Hz, 1H), 7.21 (m, 1H), 7.15 (ddd, *J* = 7.35, 7.13, 1.23 Hz, 1H), 5.22 (q, *J* = 8.25 Hz, 2H), 2.99 (t, *J* = 7.2 Hz, 2H), 2.10 (s, H_2O), 1.94 (p, CD_3CN). ^{31}P NMR (C_6D_6, 300 MHz) (Figure 46): δ -19.51 (s).

Synthesis of L^{BI+} ligand.

Step 1. Synthesis of 1-(2-bromo-ethylene)-3-methyl-3*H*-benzimidazol-1-ium bromide:

1-Methylbenzimidazole (30.3 mmol, 4.01 g) was dissolved in 1,2-dibromoethane (608 mmol, 52.4 mL) and heated to 90°C. After 3 days, a beige precipitate was observed in the reaction flask and filtered. The residue was washed with 1,2-dibromoethane and ethyl acetate three times each. The solid experienced a slight color change from beige to white (2.25 g, 87.8%). ^{1}H NMR (CD_3CN, 500 MHz) (Figure 47): δ 9.96 (s, 1H), 7.97-7.95 (m, 1H), 7.88-7.86 (m, 1H), 7.71-7.69 (m, 2H), 4.96 (t, *J* = 5.94 Hz, N-C*H*$_2$-CH$_2$-Br, 2H), 4.11 (s, 3H), 3.97 (t, *J* = 5.90 Hz, N-CH$_2$-C*H*$_2$-Br, 2H), 1.94 (p, CD_3CN).

Step 2. Synthesis of 1-(2-diphenylphosphany-ethylene)-3-methyl-3*H*-benzimidazol-1-ium bromide:

The above product was dissolved in 50 mL THF making it cloudy white. 14.5 mL $KPPh_2$ (0.5 M in THF) solution was added dropwise giving a bright yellow solution. After 12 hours, the pale pink reaction mixture was then filtered, and the residue collected. It was further washed with THF and extracted with MeCN. A yield of 2.02 g (75.2%) was recorded. ^{1}H NMR (CD_3CN, 500 MHz) (Figure 48): δ 9.38 (s, 1H), 7.76-7.26 (m, 14H), 4.68 (q, *J* = 7.23 Hz, N-CH$_2$-C*H*$_2$-PPh$_2$, 2H), 3.92 (s, 3H), 2.84 (t, N-C*H*$_2$-CH$_2$-PPh$_2$, *J* = 7.21 Hz, 2H), 1.94 (p, CD_3CN). ^{31}P NMR (CD_3CN, 500 MHz) (Figure 49): δ -20.01 (s).

Synthesis of $L^{PhenBI+}$ ligand.

Step 1. Synthesis of 1-methyl-2-phenyl-1*H*-benzimidazole:

2-Phenylbenzimidazole (3.615 mmol, 702.2 mg) was dissolved in 20 mL THF. Methyl iodide (4.1 mmol, 0.25 mL) was added dropwise, followed by potassium tert-butoxide

(3.700 mmol, 419.9 mg). The reaction mixture experienced a color change from bright yellow to cloudy white. After 2 days, the solution was filtered, and residue collected. It was further washed with dichloromethane and extracted with water. The residue was dried under vacuum (666.4 mg, 88.78%). ^{1}H NMR (CD_3CN, 500 MHz) (Figure 50): δ 7.77 (m, 3H), 7.55 (m, 3H), 7.32 (ddd, *J* = 8.00, 7.18, 1.11 Hz, 1H), 7.26 (m, 2H), 3.85 (s, 3H), 2.15(s, H_2O), 1.94 (p, CD_3CN).

Step 2. Synthesis of 1-(2-bromo-ethylene)-3-methyl-2-phenyl-3*H*-benzimidazol-1-ium bromide:

In the next step, 1,2-dibromoethane (68.8 mmol, 5.93 mL) was added to the above residue in a 100 mL Schlenk flask and allowed to react at 100^{o}C for 3 days. The reaction mixture was beige in color. The solution was filtered, and the residue collected. It was washed with ethyl acetate three times and dried under vacuum (715 mg, 52.6%). ^{1}H NMR (CD_3CN, 500 MHz) (Figure 51): δ 8.07-7.76 (m, 9H), 4.78 (t, *J* = 6.30 Hz, N-CH_2-CH_2-Br, 2H), 3.85 (s, 3H), 3.74 (t, *J* = 6.31 Hz, N-CH_2-CH_2-Br, 2H), 1.94 (p, CD_3CN).

Step 3. Synthesis of 1-(2-diphenylphosphanyl-ethylene)-3-methyl-2-phenyl-3*H*-benzimidazol-1-ium bromide:

2.62 mL $KPPh_2$ (0.5 M in THF) solution was added to the above product (1.14 mmol, 450 mg) in 30 mL THF in a Schlenk flask (100 mL). The cloudy white solution turned yellow after adding the $KPPh_2$ dropwise. The reaction mixture was filtered after 12 hours, the residue was collected and dried under vacuum. A yield of 445 mg (80.0%) was obtained. ^{1}H NMR (CD_3CN, 500 MHz) (Figure 52): δ 7.84 (m, 2H), 7.85-7.63 (m, 3H), 7.35-7.22 (m, 4H), 4.39 (q, *J* = 7.74 Hz, N-CH_2-CH_2-PPh_2, 2H), 3.77 (s, 3H), 2.57 (t, N-

CH_2-CH_2-PPh_2, J = 8.46 Hz, 2H), 1.94 (p, CD_3CN). ^{31}P NMR (CD_3CN, 500 MHz) (Figure 53): δ -21.33 (s).

CHAPTER III

SYNTHESIS AND CHARACTERIZATION OF TRANSITION METAL COMPLEXES CONTAINING REDOX-ACTIVE LIGANDS

3.1 Introduction

The newly synthesized redox-active ligands (phenanthridinium, benzimidazolium, phenylbenzimidazolium) were added to the metal center containing commercially available ancillary polydentate phosphine ligands as shown in Figure 18. In most cases, well-defined metal-phosphine complexes were prepared first by adding the ancillary ligand to weakly-coordinated metal salts like $[Pd(MeCN)_4](BF_4)_2$. The bifunctional ligand was then added in a second step.

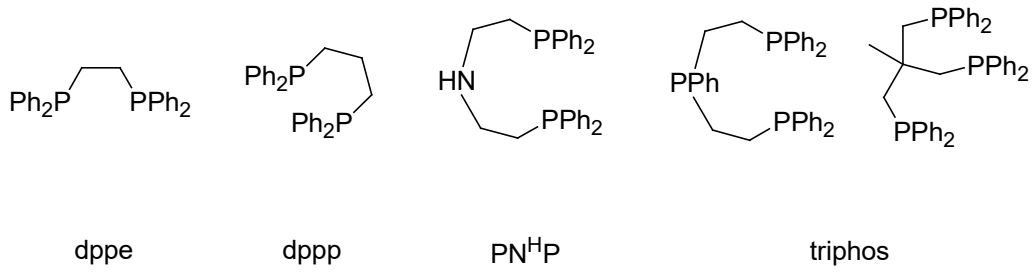

Figure 18. Various bidentate and polydentate phosphine ligands used in the synthesis of metal complexes.

In this study, tetraphosphine complexes of Group 10 metals were chosen because their coordination chemistry has been extensively studied, especially the acidity or hydricity of their hydrides.[26,34–36] We chose to use heteroleptic triphosphine/ monophosphine complexes of the type $[M(PP_2)(P')]$, where P' is the new, monophosphine ligand, containing the hydride relay, and PP_2 is the commercially available ligand, bis(2-diphenylphosphinoethyl)phenylphosphine (triphos). These complexes have the advantage that the precursor complexes, $[M(PP_2)(MeCN)]^{2+}$ and

$[M(PP_2)Cl]^+$ are known.[37,38] The monodentate ligand, P', should be able to easily displace the acetonitrile or chloro ligands in these precursors, forming the M^{II} tetraphosphine. The general strategy for the synthesis of these complexes is shown in Figure 19.

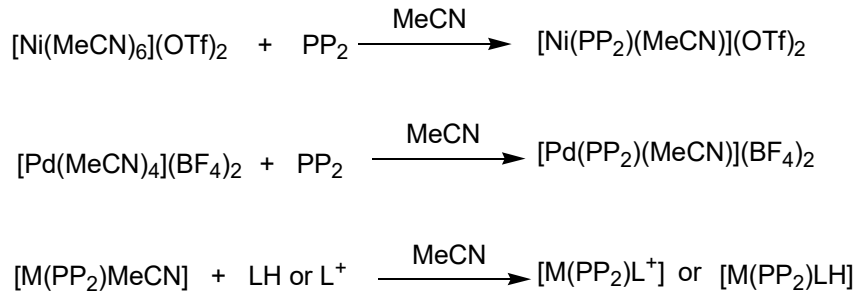

Figure 19. General synthetic route to synthesize metal complexes using PP_2 ligand.

We expected that the presence of both the sterically bulky PP_2 and the relatively bulky LH ligands might make the complexes too sterically hindered for the monodentate ligand to bind strongly. However, Pd and Pt complexes containing the PP_2 and a monodentate phosphine ligand are known in the literature.[38–40] Ni complexes, on the other hand, are not reported, although a Co analogue, $[CoBr(PP_2)(PPh_3)]^+$ is known.[41]

In addition to this, we also used the PNP ($Ph_2PCH_2CH_2NHCH_2CH_2PPh_2$) analogue of PP_2, in which the central phosphorus donor of PP_2 is replaced by NH.[42–44] PNP was used because it is somewhat less sterically hindered than PP_2 and the NH can be deprotonated to create a basic site. During the synthesis of these complexes, a route that allowed addition of either the reduced (L^H) or oxidized (L^+) form of the ligands was preferred. The general synthetic route for synthesizing the $[M(PN^HP)L^H]$ or $[M(PN^HP)L^+]$ complexes is shown in Figure 20. M^0 species were synthesized using $NaBH_4$.

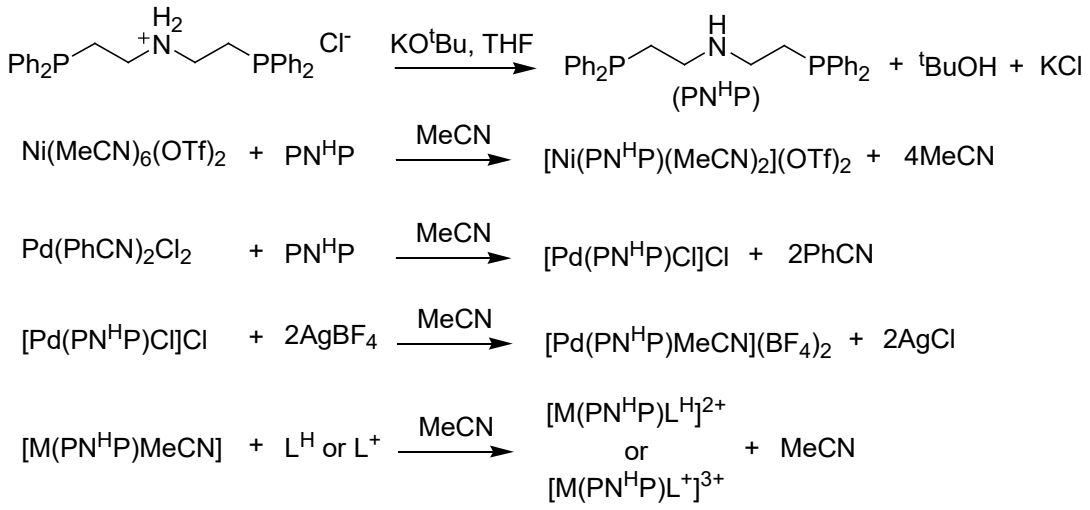

Figure 20. General synthetic route for synthesizing $[M(PN^HP)L^H]$ and $[M(PN^HP)L^+]$.

3.2 Results and Discussions

The synthesis of metal complexes using Ni was attempted first. Previous work in the laboratory showed that $[Ni(PP_2)(L)]^{2+}$ complexes of this type do not form in solution. The monophosphine ligand did not bind to the $[Ni(PP_2)(MeCN)_2]^{2+}$ complex probably due to the expected steric crowding and the small size of the metal. Therefore, three alternative strategies were explored to synthesize the Group 10 complexes.

(1) Using diphosphines, which are less sterically crowded than triphos ligands.

(2) Synthesizing homoleptic complexes using only monodentate ligands.

(3) Changing from Ni to Pd complexes.

The first strategy we explored was using a bidentate ligand, 1,2-bis(diphenylphosphino)ethane (dppe), which was less sterically hindered than triphos. The attempted series of reactions using dppe and a monophosphine ligand is shown in Figure 21.

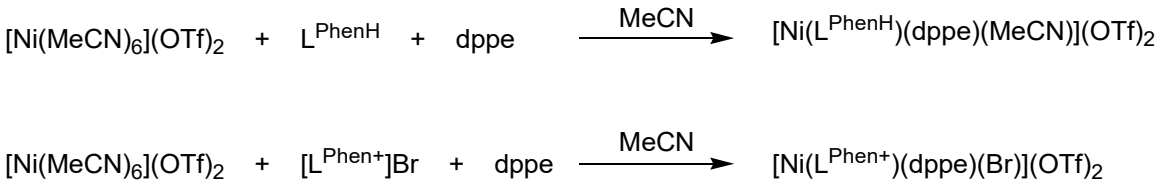

Figure 21. Synthesis of Ni^{2+}complexes using dppe and L^{PhenH}/L^{Phen+} ligands.

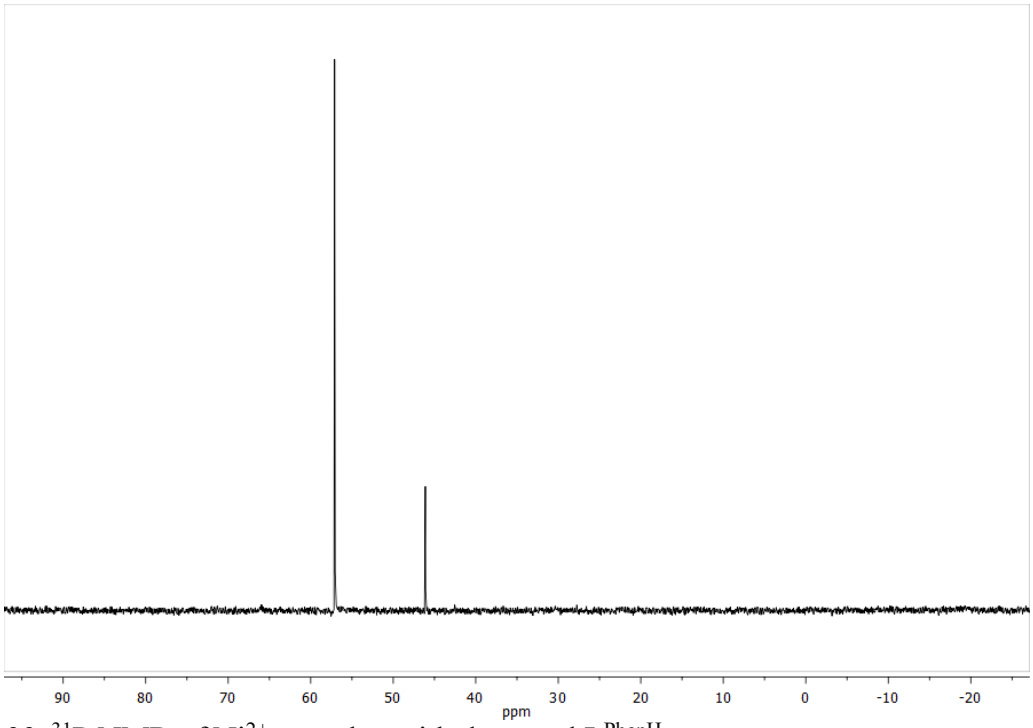

Figure 22. ^{31}P NMR of Ni^{2+} complex with dppe and L^{PhenH}.

The ^{31}P NMR spectroscopy was the most informative for these complexes. The ^{31}P NMR spectrum of the reaction using the reduced ligand, L^{PhenH} showed two singlets at 57.09 and 46.10 ppm (as shown in Figure 22). The singlets indicated that homoleptic complexes, containing only one equivalent type of phosphine each, were forming in the solution. Based on literature values,[45] the peak at 57.09 ppm was identified as $[Ni(dppe)_2]^{2+}$. The peak at 46.10 ppm is attributed to $[Ni^0(dppe)_2]$, for which no literature

shift has been reported in acetonitrile. Similar $Ni^0(diphosphine)_2$ complexes have upfield shifts compared to their Ni^{II} precursors.[46] There was however no free ligand peak or other signal for L^{PhenH} observed in the spectrum. Presumably some of the reduced monophosphine ligand, L^{PhenH} reduced the Ni^{2+} to Ni^0 and was oxidized to L^{Phen+}. Either form of ligand could coordinate to the remaining Ni species, forming $[Ni(L^{Phen+})_n]^{n+2}$ and $[Ni(L^{PhenH})_n]^{2+}$ complexes. These species could be high spin paramagnetic complexes that do not show up in the ^{31}P NMR spectrum. However, due to the complex mixture of species observed in this solution, detailed measurements of the paramagnetism were not conducted.

Heteroleptic complexes containing diphosphine ligands like dppe have been found to be difficult to form. In most cases, homoleptic complexes like $[Ni(dppe)_2]^{2+}$ are observed. To explore the chemistry of these reactions, we used monophosphine ligands without any supporting chelating phosphines, to create homoleptic complexes. A reaction using $L^{PhenBI+}$ has been shown in Figure 23.

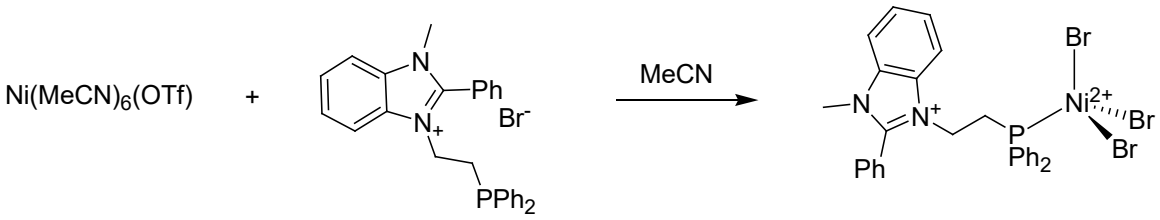

Figure 23. Synthesis of $[NiBr_3(L^{PhenBI+})]$.

The above reaction was also conducted using $[L^{BI+}][Br]$, $[L^{BI+}][BF_4]$ and $[L^{PhenBI+}][PF_6]$. In all the cases, only paramagnetic products were observed, indicating that the phosphines bind to give only high-spin complexes. Addition of up to 4 equivalents of ligand did not result in any changes. The results were not different with variations in stoichiometry which is consistent with a reaction in which fewer than four

phosphines bind. The product of the reaction using [$L^{PhenBI+}$][Br] was characterized by X-ray diffraction. Single crystals were grown by vapor diffusion of diethyl ether into a saturated acetonitrile solution. The structure was found to be that of [$NiBr_3(L^{PhenBI+})$] (Figure 24). This is a neutral complex with three bromide ions balancing the charge of the Ni^{II} ion and the positively charged, cationic benzimidazolium group on the phosphine ligand. The Ni center is roughly tetrahedral, as expected for a high spin Ni^{II} ion with weak field bromide ligands.

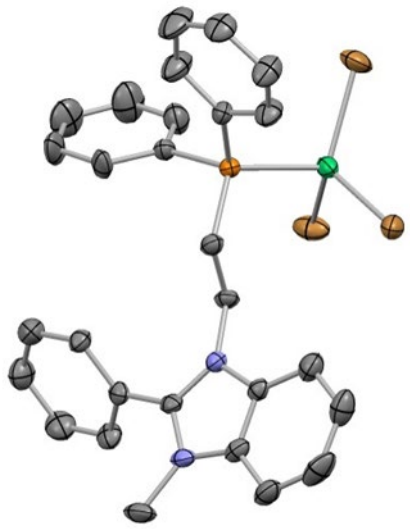

Figure 24. Structure of [$NiBr_3(L^{PhenBI+})$] determined by X-ray crystallography. The H-atoms have been removed and only one of the two molecules in the asymmetric unit is shown. Selected bond distances (Å) and angles (°): Ni1-P1 2.305(2); Ni1-Br1 2.339(1); Ni1-Br2 2.351(1); Ni1-Br3 2.370(1); P1-Ni1-Br2 108.77(6); P1-Ni1-Br2 108.77(6); P1-Ni1-Br3 100.95(6)

After using dppe, we tried to synthesize [Ni(PNP)P'] complexes, where PNP is the deprotonated form of bis(2-diphenylphosphinoethyl)ammonium chloride. The PNP ligand is slightly less sterically hindered than the triphosphine ligand due to its smaller central N atom which we hoped might allow a monophosphine ligand to bind at the fourth position. However, no ligand binding was observed.

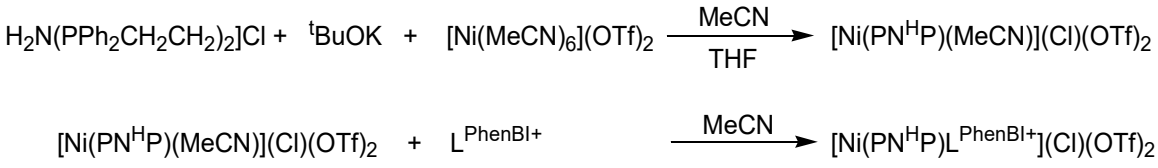

Figure 25. Synthesis of $[Ni(PN^{H}P)(L^{PhenBI+})]^{3+}$ complex.

Instead of the product expected in Figure 25, we saw a signal for free ligand at the ^{31}P NMR spectrum at -20.33 ppm which indicated that the ligand did not bind to the metal complex. Also, in the ^{1}H NMR spectrum, only the starting materials were observed.

The synthesis of $[NiBr_3(L^{PhenBI+})]$ confirmed that hydride-relay containing ligands could be incorporated into a metal complex, and the reduction of Ni^{II} to $[Ni^{0}(dppe)_2]$ suggests that these groups can react with the metal itself. However, the paramagnetic Ni complexes were difficult to study by NMR spectroscopy.

After Ni, we moved on to Pd complexes. Pd, being a second-row transition element, was larger in size, compared to Ni, and gives exclusively low spin complexes. We first synthesized Pd complexes in conjunction with the PP_2 ligand and L^{PhenH}. The series of steps involved in this synthesis are shown in Figure 26.

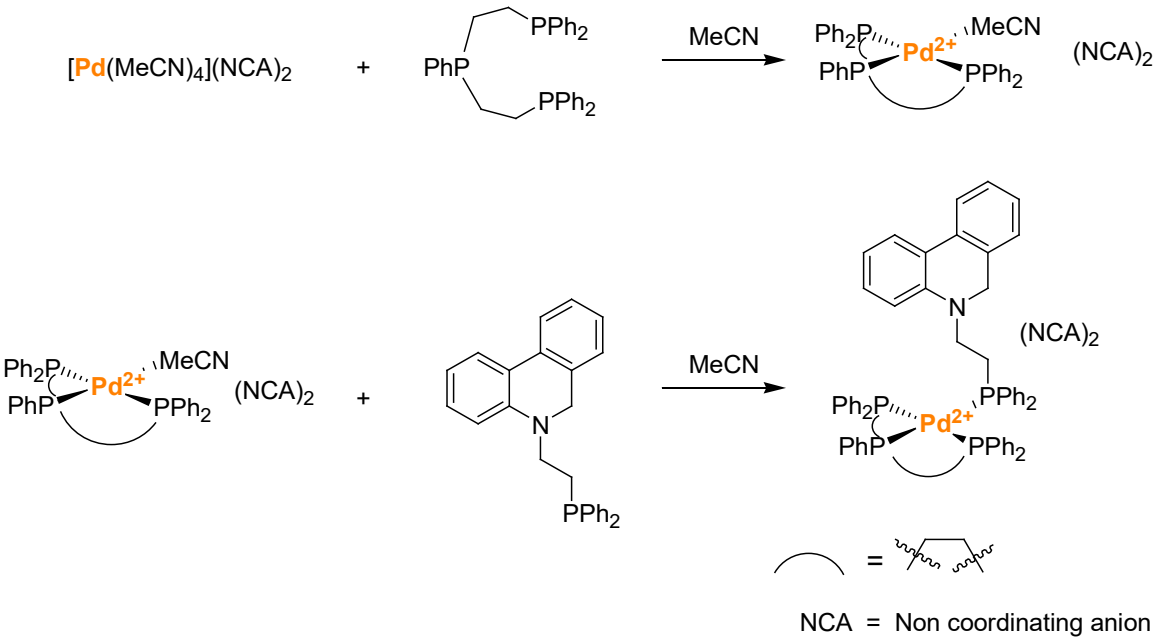

Figure 26. Synthesis of $[Pd(PP_2)(MeCN)]^{2+}$ and $[Pd(PP_2)(L^{PhenH})]^{2+}$ complexes.

These complexes were characterized using ^{1}H NMR and ^{31}P NMR spectroscopy. As expected, in the ^{31}P NMR spectrum for the complex, $[Pd(PP_2)(MeCN)]^{2+}$, a doublet and triplet were observed at 53.68 ppm and 117.08 ppm, respectively, as shown in Figure 63. This was due to the presence of two equivalent terminal phosphine groups, R-PPh_2 and one inequivalent central R-PPh-R group. The ^{1}H NMR spectrum (Figure 62), was less informative as the aromatic protons from the two terminal PPh_2 groups and the central PPh group largely overlap, and the aliphatic protons from the ethylene linkers appear as multiplets due to the asymmetry of the complex.

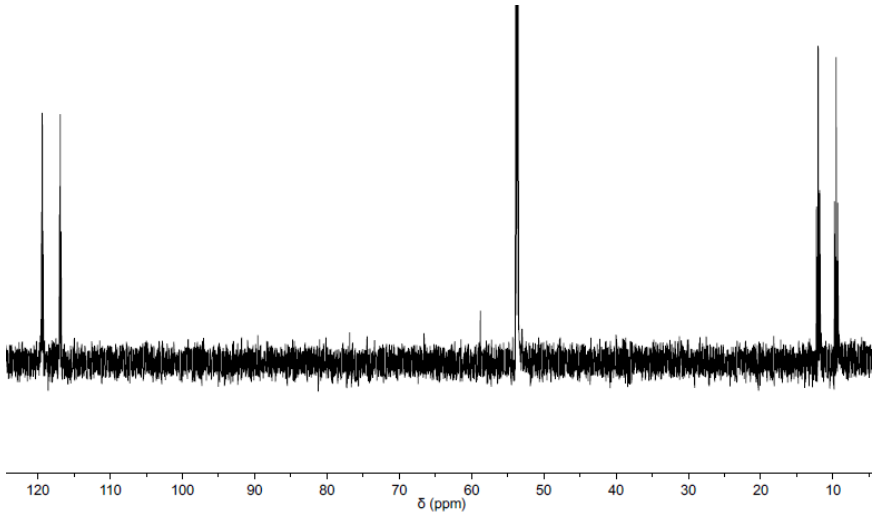

Figure 27. ^{31}P NMR spectrum of [Pd(PP$_2$)L^{PhenH}] (BF$_4$)$_2$ in CD$_3$CN (300 MHz).

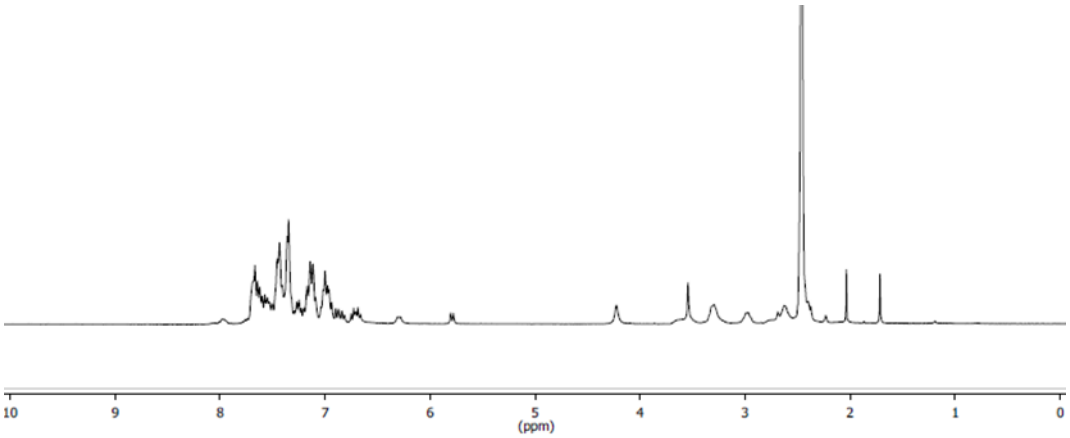

Figure 28. ^{1}H NMR spectrum of [Pd(PP$_2$)L^{PhenH}] (BF$_4$)$_2$ in CD$_3$CN (300 MHz).

On addition of L^{PhenH}, the splitting changes to two doublets of triplets (dt) and a doublet of doublets (dd) at 118.08, 53.73 and 10.81 ppm (Figure 27). The presence of cis and trans PPh$_2$ groups were confirmed from the *J* values obtained: 303.78 Hz for the trans coupling which was greater than 28.06 Hz for the cis coupling between the terminal phosphines. These splitting patterns confirmed the binding of the monophosphine ligand, L^{PhenH} to the Pd center, which was not successful with the Ni complexes.

Another key aspect of these reactions was that the ligand, L^{PhenH} did not reduce the metal, nor did it oxidize. This was observed in the ^{1}H NMR spectrum (Figure 28). The peaks for the reduced ligand were clearly observed and shift in peaks were observed from the starting material. No peak was recorded at around 9.6 ppm, where we would expect to see the peak for α-H, next to the positively charged N, for an oxidized L^{Phen+} ligand. This peak for the α-H was observed at 4.26 ppm, slightly downfield compared to the corresponding peak of the free ligand, which was recorded at 3.83 ppm. This could be explained because of the lower electron density since the phophine group has donated its electrons by binding to the metal center. The peaks for the two CH_2 groups from the ethylene linker in L^{PhenH} were also shifted downfield, 3.30 ppm and 2.62 ppm, compared to its chemical shift values in the free ligand, which were observed at 3.22 ppm and 2.15 ppm, respectively.

Table 1

Selected distances (Å) and angles (°) for palladium complexes determined by X-ray crystallography, along with τ_4 and τ_4' values used to distinguish square planar ($\tau = 0$) and tetrahedral structures ($\tau = 1$). Labeling scheme for Pd-P', Pd-P_t1, P_t2, and P_c are shown in Figure 29, as well as the definitions of α and β used to calculate the τ_4 and τ_4' values.

Distances (Å)	$[Pd(PP_2)(L^{PhenH})][BF_4]_2$	$[Pd(PP_2)(L^{Phen+})][BF_4]_3$	$Pd(PP_2)(L^{PhenH})$
Pd–P'	2.379(2)	2.355(1)	2.331(1)
Pd–P_t1	2.334(2)	2.314(1)	2.315(1)
Pd–P_t2	2.375(2)	2.355(1)	2.316(1)
Pd–P_c	2.299(2)	2.311(1)	2.343(2)
Bond Angles (°)			
P'–Pd–P_t1	98.75(7)	100.07(4)	108.63(5)
P'–Pd–P_t2	97.04(6)	97.98(4)	119.99(5)
P_c–Pd–P_t1	82.88(7)	82.07(4)	87.83(6)
P_c–Pd–P_t2	81.71(7)	80.49(4)	86.61(5)
P'–Pd–P_c	177.81(7)	176.05(5)	124.15(5)
P_t1–Pd–P_t2	159.62(6)	159.65(5)	124.23(5)
τ_4	0.16	0.17	0.79
τ_4'	0.10	0.12	0.79

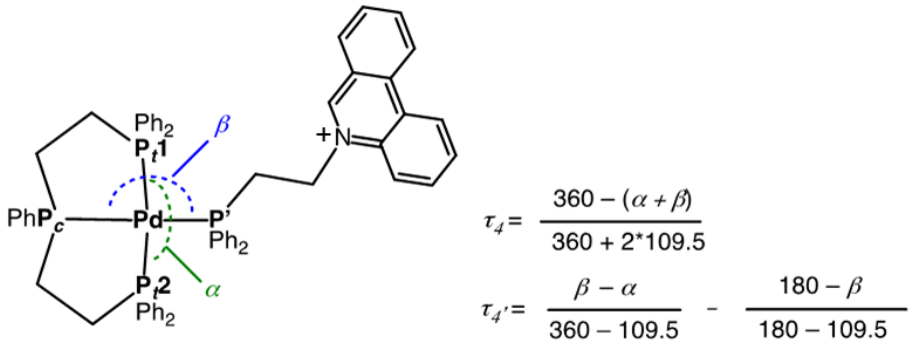

Figure 29. Labelling scheme for Pd and P atoms and formula for τ_4 and τ_4' values shown in Table 1.

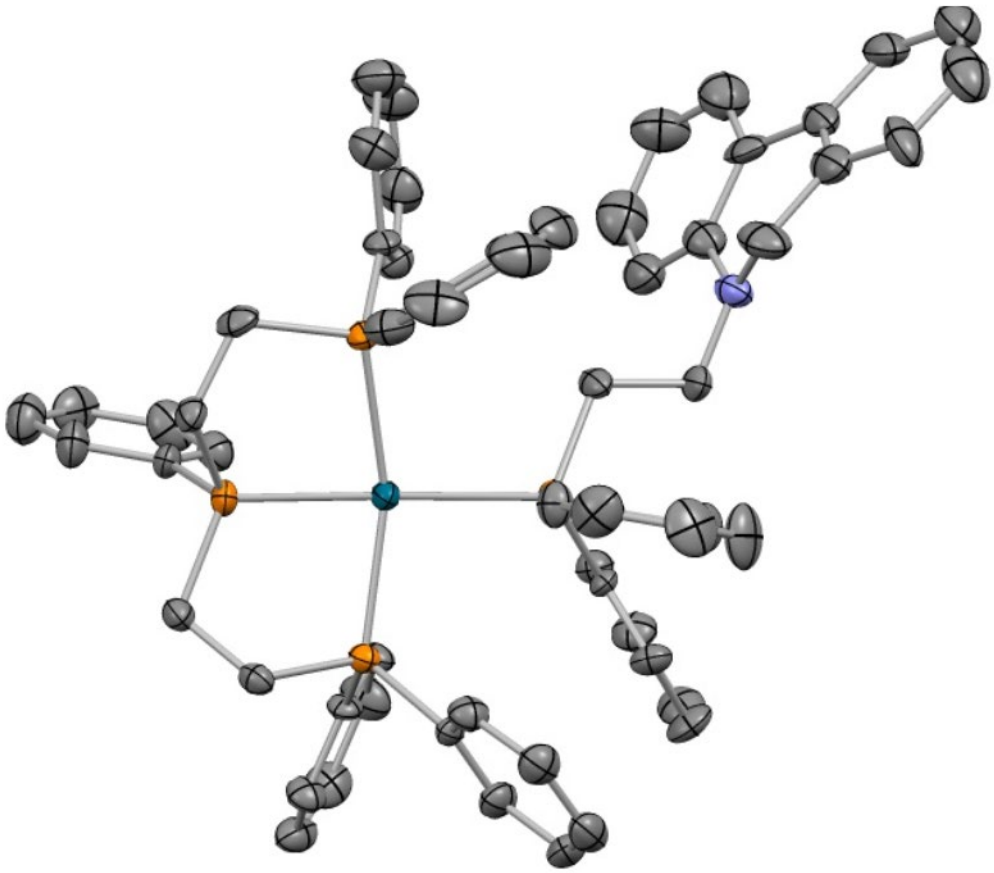

Figure 30. Structure of the cationic portion of $[Pd(PP_2)(L^{PhenH})][BF_4]_2$. The H-atoms and BF_4 counterions have been removed.

Single crystals were grown by vapor diffusion of diethyl ether into saturated acetonitrile solutions. The structures determined from the X-ray data were consistent with the solution NMR spectrum. Each of these shows a four-coordinate Pd center bound to the four phosphine donors in a distorted square-planar geometry. The four phosphines and the Pd atom are nearly planar, as seen in Figure 30. Since X-ray diffraction data cannot be used to reliably determine the positions of H atoms, all H atoms were placed and refined ideally based on the non-H atom coordinates. However, we can be assertive of the redox states of the ligand. The reduced ligand in $[Pd(PP_2)(L^{PhenH})]^{2+}$ has a

nonaromatic dihydropyridinium ring in the center of the reduced phenanthridine relay. Due to the non-aromaticity, the ring is puckered rather than planar. Also, two BF_4 counterions are present in the structure, confirming that $[Pd(PP_2)(L^{PhenH})](BF_4)_2$ is the formula for this compound, as expected. The Pd ion is square planar and possesses somewhat similar Pd-P distances. The terminal "R-PPh_2" phosphines on the PP_2 ligand are eclipsed, with one phenyl group from each phosphorus atom pointing "up", on the same side of the Pd center as the Ph of the central R-PPh-R group. The central phosphorus atom and the monodentate phosphine, however, are mutually staggered, such that one phenyl group from the monophosphine ligand is on the opposite side of the square plane from the phenyl group of the R-P(Ph)-R donor. This means that the phenanthridinium group is oriented away from the Pd center, to one side of the square plane. Thus, in the solid state, the two R-PPh_2 donors are not equivalent: one is nearer to the hydride relay. However, the equivalence of these groups in the ^{31}P NMR spectra indicate that the P' ligand rotates rapidly to exchange these positions in solution.

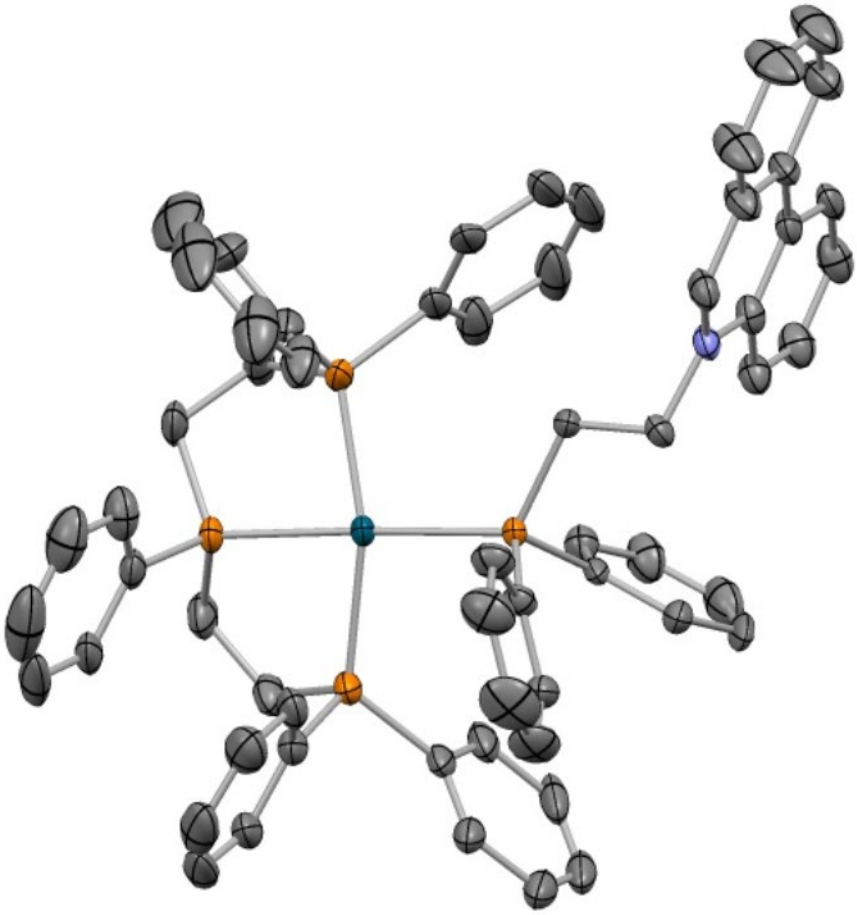

Figure 31. Structure of the cationic portion of $[Pd(PP_2)(L^{Phen+})][BF_4]_3$ determined by X-ray crystallography. The H-atoms and BF_4 counterions have been removed.

The Pd complex, $[Pd(PP_2)L^{Phen+}][BF_4]_3$, using the oxidized ligand, L^{Phen+}, was synthesized by another member in our research group. This complex is offered here for comparison. A single crystal of the complex was obtained by vapour diffusion of diethyl ether into a saturated solution of acetonitrile. The crystal structure of the complex, $[Pd(PP_2)L^{Phen+}][BF_4]_3$, showed three BF_4 counterions, which is consistent with the extra charge due to the oxidized phenanthridinium groups. As expected, the oxidized L^{Phen+} ligand has a fully planar phenanthridinium ring system, due to the aromaticity of the

oxidized central pyridinium ring. Interestingly, the central phosphine donor in the PP_2 ligand is eclipsed with the monodentate phosphine, whereas in $[Pd(PP_2)(L^{PhenH})]^{2+}$ these groups are mutually staggered. Rather than having phenyl groups on the opposite faces of the Pd atom, the phenyl groups are aligned on the same face. Despite this difference, the structures of $[Pd(PP_2)(L^{PhenH})]^{2+}$ and $[Pd(PP_2)(L^{Phen+})]^{3+}$ are otherwise similar. In both cases, the phenanthridinium group is pointed to one side, making the terminal phosphine groups inequivalent. However, the NMR signals for these phosphines are equivalent, indicating that the monophosphine can rotate freely in solution.

The Pd^{II} complexes were reduced to form Pd^0. Either a reduced Pd^0 center or a Pd^{II} hydride is a necessary species in the proposed catalytic mechanism. $[Pd^{II}(H)(L^{PhenH})]^+$, containing a Pd^{II} hydride and an organic hydride donor, should be a strong proton and hydride donor that reduces the substrate and forms $[Pd^0(L^{Phen+})]^+$. This Pd^0 species can then react with H_2, regenerating $Pd^{II}(H)(L^{PhenH})]^+$.The reaction scheme for both the reactions are shown in Figure 32. An excess of $NaBH_4$ was used as the reductant to drive this reaction. A color change in the reaction mixture from orange-yellow to dark brown was observed which was consistent with what we would expect to see for a Pd^0 species.[47]

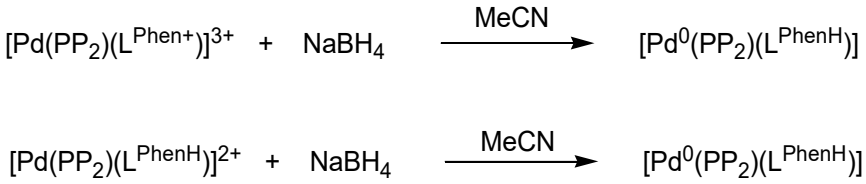

Figure 32. Synthesis of Pd^0 complexes using L^{Phen+} and L^{PhenH}.

$$Pd^{0}(PP_2)(L^{Phen+}) \quad + \quad H_2 \longrightarrow HPd^{II}(PP_2)(L^{PhenH})$$

Figure 33. Oxidation of Pd^0 to Pd^{2+}.

$NaBH_4$ is a hydride donor that could in principle form a Pd hydride species. In practice, however, Pd hydrides are rare and unstable, so the $Pd^{II}H$ presumably disproportionates to $[Pd^{II}(PP_2)(L^{PhenH})]$ and $[Pd^0(PP_2)(L^{PhenH})]$.

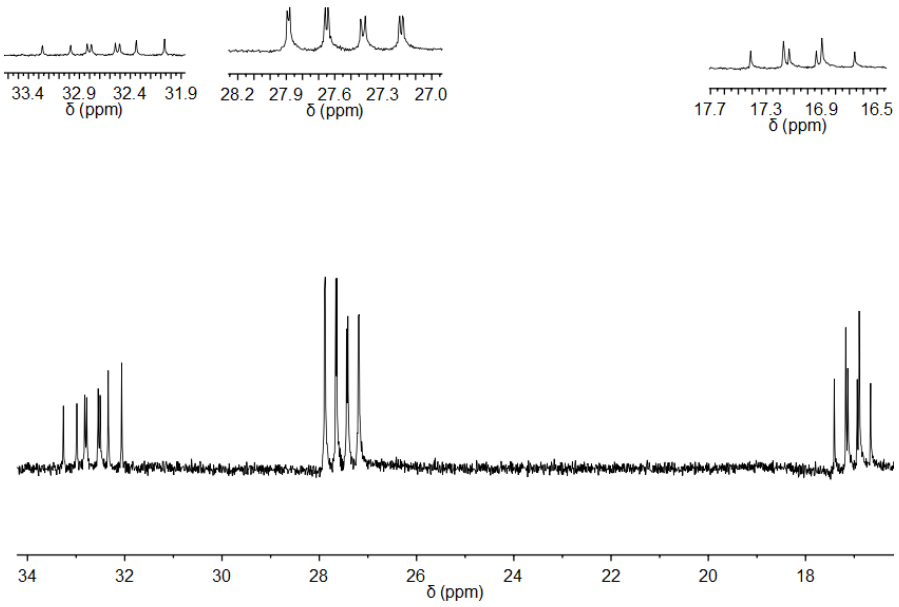

Figure 34. ^{31}P NMR spectrum of $[Pd^0(PP_2)L^{PhenH}]$.

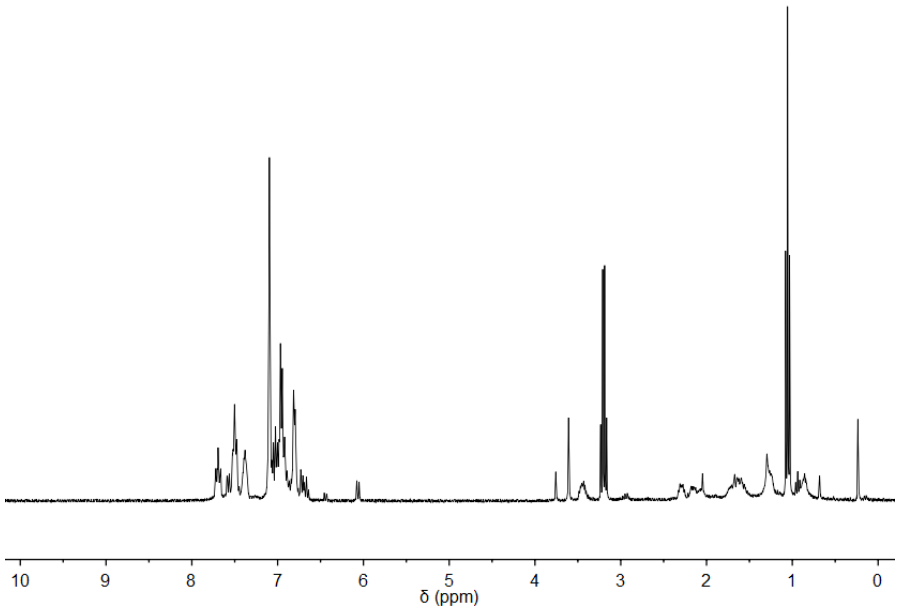

Figure 35. ^{1}H NMR spectrum of [$Pd^{0}(PP_2)(L^{PhenH})$].

The products obtained from both reactions appeared identical by ^{1}H NMR and ^{31}P NMR spectroscopy. All ^{1}H signals in the aromatic region are upfield of 8 ppm, as observed previously for [$Pd^{II}(PP_2)(L^{PhenH})]^{2+}$, indicating that the phenanthridinium ligand is reduced in both complexes, as seen in Figure 35. This means that we were unable to reduce the Pd species without also reducing the ligand. The large number of inequivalent peaks for the PPh_2 and PPh goups suggest significant asymmetry and a lack of free rotation. The ^{31}P signals also shift significantly upfield and no Pd-H signal was observed, both of which are consistent with an electron rich Pd^{0} center. Pd^{0} species are expected to be tetrahedral. Three signals were observed in the ^{31}P NMR spectrum, as expected. However, the splitting patterns were more complicated than expected for the simple [$P(PP_2)(P')$] complex with two equivalent R-PPh_2 groups. Instead, each ^{31}P signal shows

additional coupling which suggested that the two terminal phosphines are not equivalent. Instead, it shows two sets of inequivalent $RPPh_2$ which are at similar but not identical shifts and a resulting pair of doublet of doublets was observed (as seen in Figure 34).

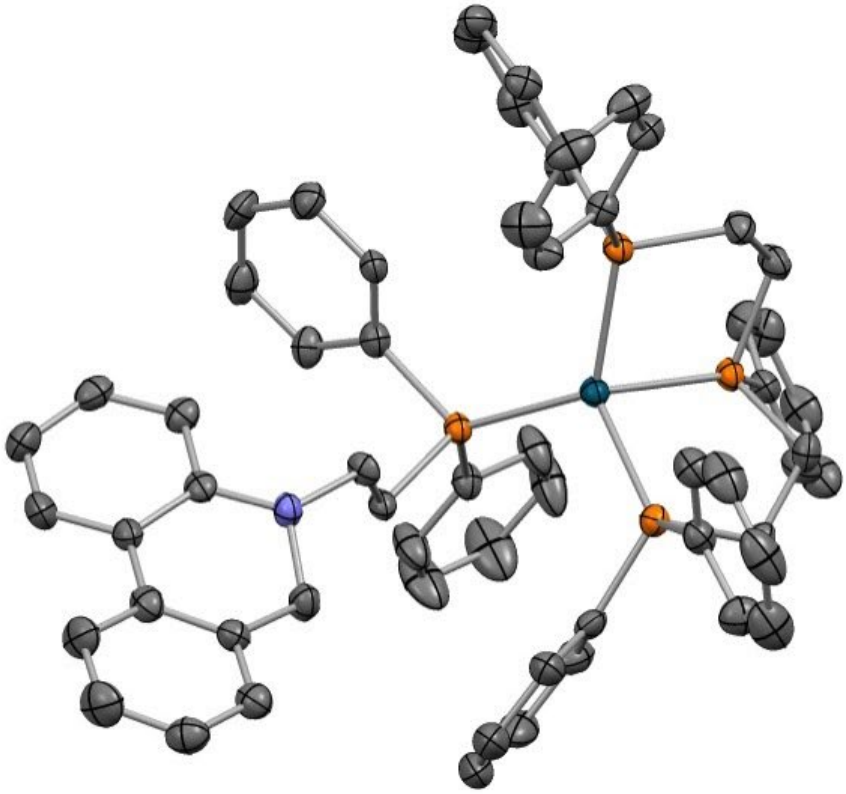

Figure 36. Structure of $[Pd^0(PP_2)(L^{PhenH})]$ determined by X-ray crystallography. The H-atoms have been removed.

The crystal structure obtained for the complex $[Pd^0(PP_2)(L^{PhenH})]$, shows a distorted tetrahedral geometry, as expected (as seen in Figure 36). All four phosphorus donors remain closely coordinated, and the phenanthridine remains unbound and oriented to the side, away from the metal center. Like in the Pd^{II} complexes, the orientation of the phenanthridinium group makes the $RPPh_2$ groups of the triphos ligand inequivalent. In the case of Pd^0 however, the asymmetry observed in the NMR spectra indicates that the monodentate ligand cannot rotate freely to relieve this asymmetry. The solution and

solid-state data, therefore, suggest that the hydride relay is locked into a position away from the metal center and is therefore, not well poised for bifunctional metal-ligand cooperativity.

A Pd^0 complex was also synthesized using PP_2 and $L^{PhenBI+}$ ligands in MeCN. This was a one pot synthesis, where $[L^{PhenBI+}](BF_4)$ was added to the $[Pd(PP_2)(MeCN)](BF_4)_2$ complex and subsequently, 4 equivalents of $NaBH_4$ were used as the reductant. A color change from pale yellow to red was observed in the reaction mixture, consistent with the color of a Pd^0 species. The reaction has been shown in Figure 37.

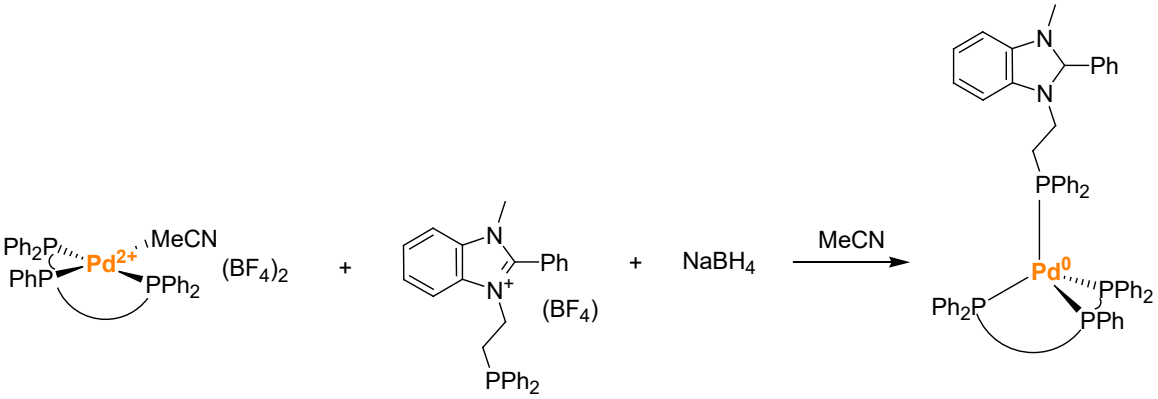

Figure 37. Synthesis of $[Pd^0(PP_2)L^{PhenBI+}](BF_4)$ complex.

The ^{31}P NMR signals, as seen in Figure 69, shift significantly upfield, consistent with a Pd^0 center,[48] and the complex splitting patterns are similar to those in the phenanthridinium complex. As with the phenanthridinium complex, in the ^1H NMR spectrum (Figure 68), all aromatic signals are upfield of 8 ppm, indicating that the benzimidazolium group is reduced. A similar degree of asymmetry is also observed for the PPh_2 and PPh protons, consistent with the asymmetric and inflexible conformation indicated by the ^{31}P NMR signals.

After investigating the Pd^0 complexes, we synthesized [Pd(PN^HP)(L')] complex using the ligand, $L^{PhenBI+}$. We expected that the PN^HP ligand, which was less sterically crowded that PP_2 will be better able to position the hydride relay in the metal complex. The series of steps involved in the synthesis of this complex has been shown in Figure 38.

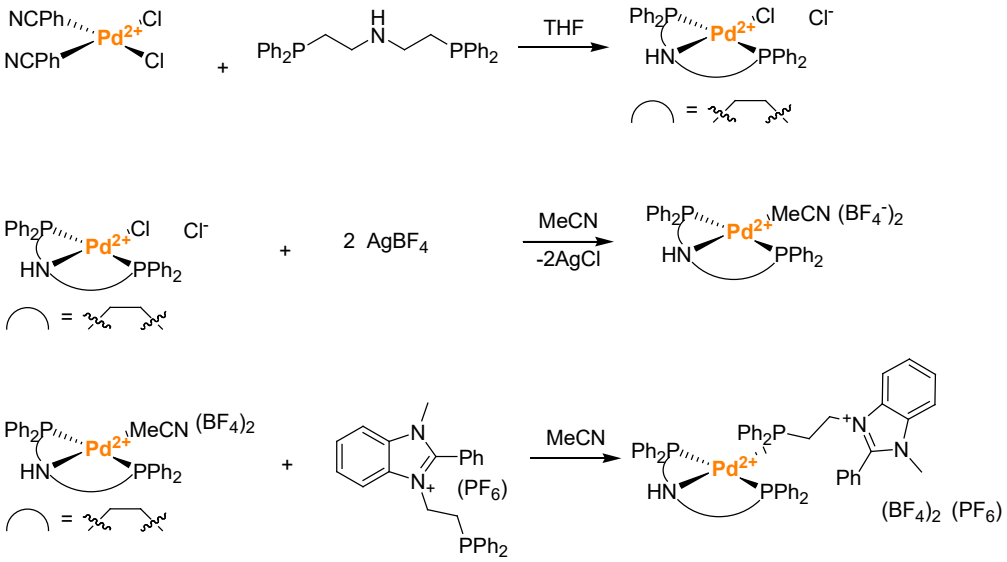

Figure 38. Synthesis of [Pd(PN^HP)($L^{PhenBI+}$)]$^{3+}$.

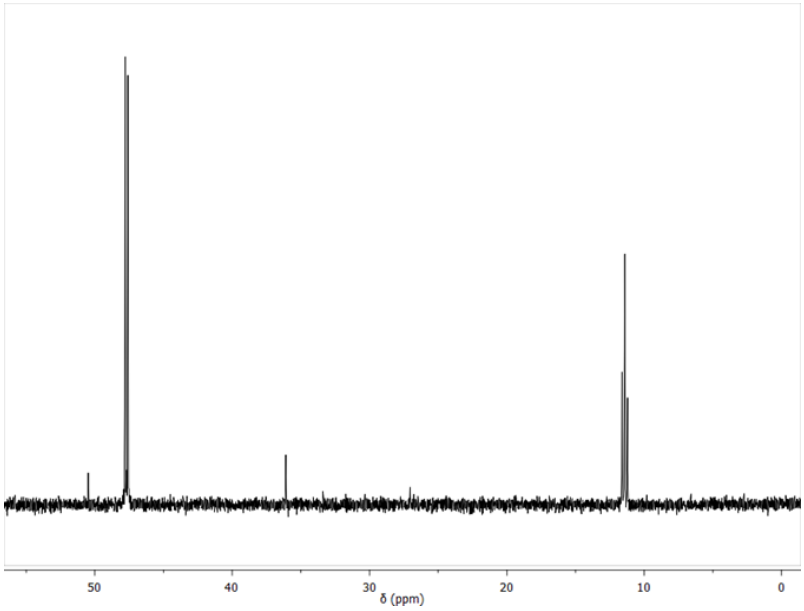

Figure 39. ^{31}P NMR spectrum of [Pd(PN^HP)($L^{PhenBI+}$)]$^{3+}$ in CD_3CN (300 MHz).

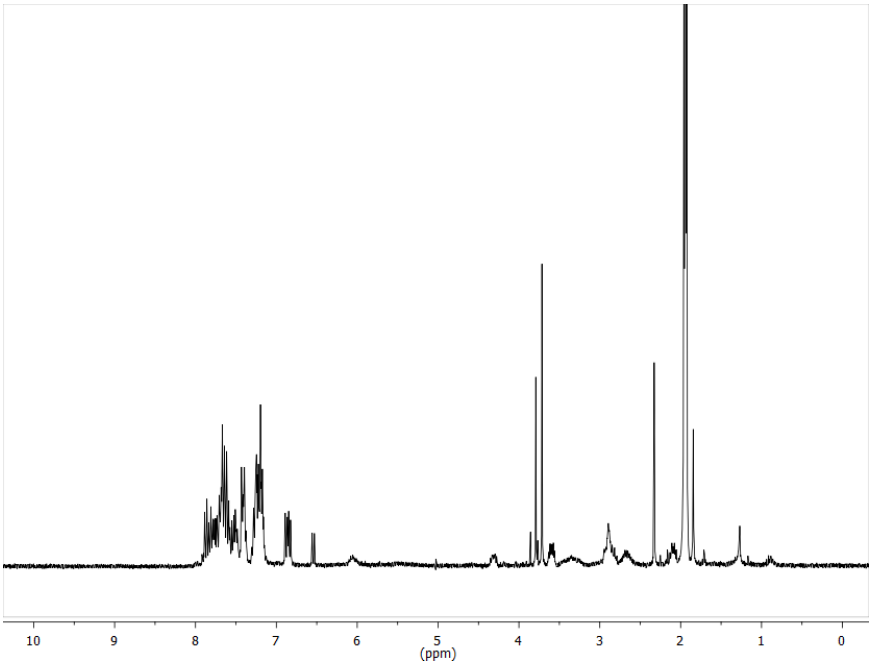

Figure 40. ^{1}H NMR spectrum of $[Pd(PN^{H}P)(L^{PhenBI+})]^{3+}$ in CD_3CN (300 MHz).

The ^{31}P NMR spectrum, as seen in Figure 39, clearly showed the binding of the hydride relay to the Pd center. Also, the doublet and triplet observed at 47.70 and 11.42 ppm showed the presence of two equivalent terminal phosphines, R-PPh_2 and one inequivalent phosphine from the hydride relay. As observed in Figure 40, all ^{1}H signals in the aromatic region are upfield of 8 ppm and peaks for the aliphatic protons from the ethylene linker in the oxidized ligand were observed at 3.79 and 2.33 ppm, and the signal for the -CH_3 group attached to the N atom of the ligand was observed at 3.72 ppm. This Pd(PNP) complex has an advantage due to the presence of the H at the central N atom of the PNP ligand, which could be deprotonated, using a base like potassium tert-butoxide, that can act as a basic center, without reducing the Pd^{2+} species to Pd^{0}. This will help to retain the square planar geometry of the Pd complex which is capable of free rotation, as well as, create a basic center within the ligand.

3.3 Conclusion

A set of transition metal complexes using the synthesized redox-active ligands were synthesized. Most reactions using Ni were not successful presumably because of the small size of the metal and the presence of the bulky phosphine groups. These complexes also tended to form paramagnetic complexes that were not observed by ^{1}H or ^{31}P NMR spectroscopy. We obtained a crystal structure of $[NiBr_3(L^{PhenBI+})]$ which indicated that the redox active ligand was able to bind to the metal center. Pd^{2+} complexes were synthesized using both reduced (L^{PhenH}) and oxidized (L^{Phen+}) forms of the ligand. These products were characterized by ^{1}H and ^{31}P NMR spectroscopy and crystal structures for both the complexes were obtained using X-ray crystallography. Pd^{0} species, being catalytic intermediates in the proposed catalytic cycle, were synthesized using L^{PhenH} and $L^{PhenBI+}$ and each of these was used in conjunction with PP_2 as the ancillary phosphine ligand. These complexes were characterized by ^{1}H and ^{31}P NMR spectroscopy. Lastly, a Pd^{2+} complex using $L^{PhenBI+}$ in conjunction with $PN^{H}P$ ligand was synthesized and characterized using ^{1}H and ^{31}P NMR spectroscopy.

The results from these studies demonstrate that the originally proposed ligand design can be used to create metal-phosphine complexes with a hydride relay in the vicinity of the metal. The modularity of the design allows a variety of hydride relays to be used with minimal changes at the metal center. As such, the first and second objectives of this research, which were to synthesize the redox active ligands and incorporate these ligands into transition metal centers, were fulfilled. The third objective was to characterize these complexes to evaluate their suitability for catalysis. Analysis of the crystal structures revealed conformational and steric issues that will be useful to

future catalyst design. Specifically structural characterization of the Pd(PP_2) complexes showed that the hydride relay could freely rotate, and therefore approach the metal center, in the Pd^{II} complexes but not the Pd^0 complexes. Instead the tetrahedral Pd^0 geometry and the bulky PP_2 ligand lock the hydride relay away from the metal center. This led to the synthesis of a Pd(PNP) complex that should operate exclusively through Pd(II) intermediates. Other target designs for future catalysts will include:

(a) A shorter linker, like methylene, that does not direct the relay away.

(b) A less hindered phosphine donor group that will be free to position the hydride relay near the metal center and will allow the formation of metal complexes using the smaller first row transition metals.

(c) Further studies on the $[Pd(PNP)(L^{PhenBI+})]^{3+}$ complex: deprotonating the N on the PNP ligand to create a basic center and study hydrogenation reactions using this complex.

3.4 Experimental section

General. All starting materials and reagents were purchased from commercial sources (Sigma Aldrich and Alfa Aesar) and used without further purification, unless otherwise mentioned. Syntheses of the metal complexes were performed inside a glove box (VIGOR) under a nitrogen atmosphere. All deuterated solvents were dried using activated molecular sieves and stored inside the glove box. Solvents were degassed under argon and dried by passage through columns of alumina and molecular sieves and stored inside the glove box. All the air-sensitive reagents were stored inside the glove box under inert atmosphere. Required glassware was oven dried before use. ^1H NMR and ^{31}P NMR spectra were collected using a JEOL Eclipse 300+ spectrometer. Chemical shifts are

reported in δ (ppm) relative to ^{1}H (CD_3CN: 1.94, D_2O: 4.79, DMSO-d_6: 2.50) and ^{31}P (H_3PO_4: 0).

Synthesis of discussed compounds.

Deprotonation of PNP ligand. Bis(2-diphenylphosphinoethylene)ammonium chloride $[(Ph_2PCH_2CH_2)_2NH_2]$ Cl (0.209 mmol, 99.9 mg, 1 equiv) was dissolved in 7 mL THF. This was added to a solution of potassium tert-butoxide (0.209 mmol, 23.5 mg, 1 equiv) in 3 mL THF in a tared vial. A change from clear transparent to cloudy white was observed in the reaction vial. After stirring it overnight, the mixture was filtered the next day and a clear colorless filtrate dried under vacuum leaving a colorless oil. A yield of 81.6 mg (88.4%) was obtained. ^{1}H NMR (CD_3CN, 300 MHz) (Figure 54): δ 7.44-7.28 (m, 21H), 7.17 (dt, J = 15.6, 7.4 Hz, 1H), 2.57 (t, J = 8.0 Hz, 4H), 2.33 (s, 1H), 2.21-2.07 (m, 5H), 1.89 (s, 1H), 1.52 (s, 1H), 1.24 (s, 1H). ^{31}P NMR (CD_3CN, 300 MHz) (Figure 55): δ -20.37 (s).

Synthesis of [Pd($PN^{H}P$)Cl]Cl. $PN^{H}P$ (0.185 mmol, 81.6 mg, 1 equiv) was dissolved in 3 mL THF in a vial and was then added to the Pd complex, $PdCl_2(PhCN)_2$ (0.185 mmol, 71.7 mg, 1 equiv), dissolved in 6 mL THF. This resulted in the appearance of a cloudy pale yellow mixture that was stirred overnight. The mixture was filtered and the residue on the frit (THF solute) was extracted with MeCN. A yellow powdered solid, [Pd($PN^{H}P$)Cl]Cl, giving a yield of 66.6 mg (58.2%). ^{1}H NMR (CD_3CN, 300 MHz) (Figure 56): δ 8.02 (d, J = 6.5 Hz, 1H), 7.90-7.79 (m, 1H), 7.55 (dt, J = 26.5, 10.2 Hz, 3H), 7.17 (dt, J = 15.8, 7.8 Hz, 1H), , 3.26 (s, 1H), 3.07-2.89 (m, 1H), 2.83-2.72 (m, 1H), 1.91 (s, 1H). ^{31}P NMR (CD_3CN, 300 MHz) (Figure 57): δ 37.90

Synthesis of [Pd(PN^{H}P)(CH$_3$CN)](BF$_4$)$_2$. The complex, [Pd(PN^{H}P)Cl]Cl (0.0979 mmol, 60.1 mg, 1 equiv), dissolved in 10 mL MeCN was added to a solution of silver tetrafluoroborate, $AgBF_4$ (0.194 mmol, 37.8 mg, 2 equiv) in 5 mL MeCN in a vial. A color change from pale yellow to cloudy white was observed immediately. After two days, the mixture was filtered and the filtrate was dried under vacuum. A beige colored product, [Pd(PN^{H}P)(CH$_3$CN)](BF$_4$)$_2$, giving a yield of 72.7 mg (49.1%) was obtained. ^{1}H NMR (CD$_3$CN, 300 MHz) (Figure 58): δ 7.81 (t, *J* = 6.7 Hz, 1H), 7.64 (dq, *J* = 23.0, 8.6, 7.9 Hz, 4H), 7.19 (dq, *J* = 15.5, 7.6 Hz, 1H), 3.35 (dd, *J* = 29.9, 11.7 Hz, 0H), 2.30 (s, 1H), 1.91 (s,15H). ^{31}P NMR (CD$_3$CN, 300 MHz) (Figure 59): δ 46.59.

Synthesis of [Pd(PN^{H}P)(L$^{PhenBI+}$)](PF$_6$)(BF$_4$)$_2$. The Pd complex, [Pd(PN^{H}P)CH$_3$CN](BF$_4$)$_2$ (0.0572 mmol, 43.6 mg, 1 equiv), dissolved in 2 mL MeCN was added to a solution of the ligand, [L$^{PhenBI+}$](PF$_6$) (0.0572 mmol, 32.4 mg, 1 equiv) in 3 mL MeCN. A distinct pale yellow solution was observed and allowed to react for two days. The reaction mixture was filtered and the filtrate was dried under vacuum giving a brown powder, [Pd(PN^{H}P) L$^{PhenBI+}$](PF$_6$)(BF$_4$)$_2$ was obtained with a yield of 60.9 mg (82.8%). ^{1}H NMR (CD$_3$CN, 300 MHz) (Figure 60): δ 8.00-7.32 (m, 8H), 7.18 (dd, *J* = 17.5, 7.1 Hz, 4H), 6.88-6.75 (m, 1H), 2.88 (d, *J* = 11.5 Hz, 1H), 2.65 (d, *J* = 14.9 Hz, 1H), 1.91 (s, 27H). ^{31}P NMR (CD$_3$CN, 300 MHz) (Figure 61): δ 47.65 (d, *J* = 24.0 Hz), 11.42 (t, *J* = 24.0 Hz), -144.01 (h, PF$_6$).

Synthesis of [Pd(PP$_2$)(CH$_3$CN)](BF$_4$)$_2$. The Pd complex, [Pd(CH$_3$CN)$_4$](BF$_4$)$_2$ (0.3741 mmol, 166.2 mg, 1 equiv), dissolved in 6 mL MeCN was added to a solution of bis(2-diphenylphosphinoethyl)phenylphosphine (PP_2) ligand (0.3741 mmol, 199.8 mg, 1 equiv) in 12 mL THF giving a bright yellow solution. After stirring overnight, the

reaction mixture was dried under vacuum giving a yellow powder. A yield of 317.8 mg (99.34 %) was recorded. ^{1}H NMR (CD_3CN, 300 MHz) (Figure 62): δ 7.95-7.81 (m, 1H), 7.59 (dq, *J* = 23.0, 9.4, 8.0 Hz, 12H), 3.42 (dt, *J* = 14.0, 5.6 Hz, 1H), 3.22 (dd, *J* = 20.0, 13.5, Hz, 1H), 3.14-2.95 (m, 1H), 2.94 (d, *J* = 9.9 Hz, 1H), 2.45-2.28 (m, 1H), 1.94 (s, 1H), 1.81 (s, 1H). ^{31}P NMR (CD_3CN, 300 MHz) (Figure 63): δ 117.08 (t), 53.68 (d).

Synthesis of $[Pd(PP_2)(L^{PhenH})](BF_4)_2$. The Pd complex, $[Pd(PP_2)CH_3CN](BF_4)_2$ (0.0221 mmol, 15.4 mg, 1 equiv) was dissolved in 1 mL MeCN and added to a solution of L^{PhenH} (0.0221 mmol, 69.3 mg, 1 equiv) in 1 mL MeCN. After 2 hours, the reaction mixture was dried under vacuum. A dark brown solid was obtained with a yield of 16.9 mg (84.9%). ^{1}H NMR (CD_3CN, 300 MHz) (Figure 64): δ 7.82-7.64 (m, 2H), 7.59 (dt, *J* = 21.0, 6.3 Hz, 2H), 7.54-7.3 (m, 7H), 7.35-7.21(m, 1H), 7.17 (ddd, *J* = 16.4, 10.4, 6.2 Hz, 3H), 7.14-6.81 (m, 4H), 6.85-6.63 (m, 1H), 4.23 (s, 1H), 3.30 (t, *J* = 7.6 Hz, 1H), 3.02-2.91 (m, 1H), 2.62 (q, *J* = 6.7 Hz, 1H), 2.46-2.34 (m, 1H). ^{31}P NMR (CD_3CN, 300 MHz) (Figure 65): δ 118.08 (dd, *J* = 302.5, 12.2 Hz), 53.73 (dd, *J* = 27.8, 12.2 Hz), 10.81 (dt, *J* = 302.7, 27.8 Hz).

Synthesis of $[Pd^0(PP_2)(L^{PhenH})]$. The Pd^{2+} complex, $[Pd(PP_2)L^{PhenH}](BF_4)_2$ (0.0420 mmol, 50.7 mg, 1 equiv) dissolved in 3 mL MeCN giving a dark orange solution. $NaBH_4$ (0.17 mmol, 6.3 mg, 4 equiv) was added and the solution turned dark brown after 15 minutes of addition. The reaction mixture was filtered, and filtrate was dried under vacuum. The remaining solid in the vial was extracted using ether. A dark brown oily solid was obtained as product giving a yield of 41.6 mg (28.6%). ^{1}H NMR (CD_3CN, 300 MHz) (Figure 67): δ 7.82-7.64 (m, 1H), 7.65-7.48 (m, 6H), 7.48-7.33 (m, 1H), 7.39 (m, 1H), 7.31-7.19 (m, 3H), 7.24-7.01 (m, 8H), 6.99 (q, *J* = 7.1 Hz, 2H), 6.56 (s, 1H), 5.62

(d, J = 7.7 Hz, 0H), 3.49 (s, 1H), 3.08 (p, J = 6.9, 6.1 Hz, 1H), 2.14 (d, J = 8.3 Hz, 1H), 2.07-1.62 (m, 3H), 1.06 (s, 2H). ^{31}P NMR (CD_3CN, 300 MHz) (Figure 66): δ 118.08 (dd, J = 302.5, 12.2 Hz), 53.73 (dd, J = 27.8, 12.2 Hz), 10.81 (dt, J = 302.7, 27.8 Hz).

Synthesis of $[Pd^0(PP_2)(L^{PhenBI+})](BF_4)$. The Pd complex, $[Pd(PP_2)CH_3CN](BF_4)_2$ (0.0501 mmol, 42.9 mg, 1 equiv) was dissolved in 2 mL MeCN. This bright yellow mixture was added to a solution of $L^{PhenBI+}$ (0.0501 mmol, 25.1 mg, 1 equiv) in 5 mL MeCN. A change from bright yellow to pale yellow cloudy solution was recorded. After 1 hour, $NaBH_4$ (0.21 mmol, 7.5 mg, 4 equiv) was added and the solution turned brown. After 30 minutes, the reaction mixture was filtered, and brown filtrate was dried under vacuum. 3 mL THF was added to the brown solid left in the vial and the solution was filtered. The filtrate was then dried under vacuum and brown oily solid was obtained. The yield was 53.1 mg (28.8%). ^{1}H NMR (CD_3CN, 300 MHz) (Figure 68): δ 7.63-7.26 (m, 5H), 7.25 (s, 3H), 7.21-7.09 (m, 1H), 7.07 (s, 1H), 7.02 (t, J = 7.6 Hz, 1H), 3.61 (s, 6H), 3.24 (s, 1H), 1.76 (d, J = 6.5 Hz, 6H), 1.16-1.04 (m, 1H), 1.04 (s, 3H). ^{31}P NMR (CD_3CN, 300 MHz) (Figure 69): δ 33.55-32.34 (m), 27.56-26.80 (m), 16.11-15.37 (m).

X-Ray Crystallographic Data Collection and Refinement of the Structures. Single crystals of $Pd(PP_2)(L^{PhenH})$ were grown by vapor diffusion of diethyl ether into a concentrated THF solution. Single crystals of $[Pd(PP_2)(L^{PhenH})][BF_4]_2$, $[Pd(PP_2)(L^{Phen+})][BF_4]_3$ and $[Ni(L^{PhenBI+})Br_3]$ were grown by vapor diffusion of diethyl ether into concentrated acetonitrile solutions. A yellow plate of $[Pd(PP_2)(L^{PhenH})][BF_4]_2$ (0.2 mm x 0.1 mm x 0.025 mm), a colorless block of $[Pd(PP_2)(L^{Phen+})][BF_4]_3$ (0.1 mm x 0.1 mm x 0.05 mm), a red block of $[Pd(PP_2)(L^{PhenH})]$ (0.1 mm x 0.1 mm x 0.05 mm), and

a green block of [Ni($L^{PhenBI+}$)Br_3] (0.1 mm x 0.05 mm x 0.05 mm) were placed on the tip of a nylon fiber and mounted on a Rigaku XtaLab Mini II CCD diffractometer for data collection at 173(2) K. The data collection was carried out using Mo-Kα radiation (graphite monochromator). The data intensity was corrected for absorption and decay (SADABS). Final cell constants were obtained from least squares fits of all measured reflections. The structures were solved using SHELXT-2014 and refined using SHELXL-2014. A direct-methods solution was calculated which provided most non-hydrogen atoms from the E-map. Full-matrix least squares / difference Fourier cycles were performed to locate the remaining non-hydrogen atoms. All non-hydrogen atoms were refined with anisotropic displacement parameters. Hydrogen atoms were placed ideally and refined as riding atoms with relative isotropic displacement parameters. In [Pd(PP_2)(L^{Phen+})][BF_4]$_3$, three of the phenyl groups on the PP_2 ligand were found to be disordered; each group was fit independently to a model containing two positions, with the secondary disordered positions refining to occupancies of 46%, 37%, and 23%. Equal-displacement (EADP) constraints as well as rigid-bond (DELU) and equivalent-distance (SADI and SAME) restraints were used for the carbon atoms in these disordered groups. In addition, two of the three BF_4^- counterions were disordered, one by rotation about a B–F bond and one by inversion. Initially, these groups were modeled over two positions. In this initial refinement, a large void space was observed in the structure, with diffuse electron density corresponding to partial solvent occupation. The PLATON program, SQUEEZE function was used to remove the contribution of this void space from the refinement. In total, 226 electrons were removed from a volume of 1165 $Å^3$, equally distributed between two locations at 0.000 -0.010 0.000 and 0.000 -0.020 0.500

in the unit cell. The R1 value dropped from 8.80% to 7.24%. Ultimately, to improve the refinement of the Pd complex of interest, the PLATON program, SQUEEZE function was used to remove the contribution of all electron density from the solvent-accessible void space from the refinement, including that of all three BF_4^- counterions. In total, 787 electrons were removed from a total volume of 2366 $Å^3$, centered around a position of (0.000 -0.010 -0.005) in the unit cell. This represents the contribution of 504 electrons corresponding to the BF_4^- ions as well as 283 additional electrons, corresponding to approximately 13 CH_3CN molecules per unit cell, or 3.25 per asymmetric unit.

The PLATON program, SQUEEZE function was also used to remove the contribution from a similar solvent-accessible void space in the structure of $[Pd(PP_2)(L^{PhenH})][BF_4]_2$. This process removed a total of 436 electrons in a total volume of 1195 $Å^3$ from two large void spaces of 600 $Å^3$ each, equally distributed between two positions at (0.000 0.500 0.000) and (0.500 0.000 0.500) in the unit cell. These large void spaces contained four of the eight BF_4^- ions in the unit cell, which contribute a total of 168 electrons, with the remaining 268 electrons in this void space corresponding to approximately 12 CH_3CN molecules. The automated SQUEEZE process also found and removed a total of 176 electrons from four well-defined positions corresponding to BF_4^- positions, located at (0.207 0.813 0.806), (0.293 0.313 0.694), (0.707 0.687 0.306), and (0.793 0.187 0.194) in the unit cell and containing a volume of 64 $Å^3$ each.

Crystallographic data are summarized in Table 2.

Table 2

Crystallographic details for $[Pd(PP_2)L^{PhenH}][BF_4]_2$, $[Pd(PP_2)L^{Phen+}][BF_4]_3$ and $[Pd(PP_2)L^{PhenH}]$

	$[Pd(PP_2)(L^{PhenH})][BF_4]_2 \bullet (CH_3CN)_{3.25}$	$[Pd(PP_2)(L^{Phen+})][BF_4]_3 \bullet (CH_3CN)_3$	$Pd(PP_2)(L^{PhenH})$
chemical formula	$C_{67.5}H_{67.75}B_2F_8N_{4.25}P_4Pd$	$C_{67}H_{65}B_3F_{12}N_4P_4Pd$	$C_{61}H_{57}NP_4Pd$
formula weight	1207.97	1293.77	1034.35
crystal system	Monoclinic	Monoclinic	Triclinic
space group	$P2_1/n$	$P2_1/c$	$P\text{-}1$
a (Å)	11.2927(4)	21.822(2)	11.5406(6)
b (Å)	41.743(1)	13.632(1)	12.6451(6)
c (Å)	12.9751(4)	22.575(2)	18.3167(7)
α (deg)	90	90	79.558(4)
β (deg)	90.251(3)	91.116(8)	80.469(4)
γ (deg)	90	90	78.061(4)
V (Å^3)	6116.3(3)	6714.3(1)	2549.0(2)
Z	4	4	2
D_{calcd} (g cm^{-3})	1.458	1.403	1.348
λ (Å), μ (mm^{-1})	0.71073, 0.479	0.71073, 0.448	0.71073, 0.530
Temperature (K)	173(2)	173(2)	173(2)
θ range (°)	2.505 to 25.030	2.569 to 27.484	2.612 to27.485
reflns collected	39351	34204	11652
unique reflns	10810	15329	6270
data/restraint/parameters	10810 / 0 / 604	15329 / 128 / 615	11652 / 0 / 604
R_1, wR_2 ($I > 2\sigma(I)$)	0.0772, 0.1483	0.0632, 0.1349	0.0680, 0.1176

Table 3

Atomic coordinates and equivalent isotropic atomic displacement parameters ($Å^2$) for $[Pd(PP_2)(L^{PhenH})]^{2+}$

$U_{(eq)}$ is defined as one third of the trace of the orthogonalized U_{ij} tensor.

	x/a	*y/b*	*z/c*	*U(eq)*
Pd1	0.51921(4)	0.34720(2)	0.34525(4)	0.02946(17)
P1	0.31763(14)	0.35314(5)	0.29483(13)	0.0310(4)
P2	0.71220(14)	0.33963(5)	0.39683(14)	0.0348(5)
P3	0.55028(15)	0.29724(5)	0.26935(13)	0.0316(4)
P4	0.55648(15)	0.40060(5)	0.39966(14)	0.0357(5)
N1	0.0491(5)	0.40706(16)	0.4307(5)	0.0472(17)
C1	0.2417(5)	0.38189(18)	0.3796(6)	0.0414(19)
C2	0.1047(5)	0.38038(19)	0.3802(6)	0.049(2)
C3	0.0478(8)	0.4371(2)	0.3700(8)	0.074(3)
C4	0.9543(7)	0.4589(2)	0.4093(8)	0.066(3)
C5	0.8955(7)	0.4794(2)	0.3364(8)	0.075(3)
C6	0.8074(8)	0.4984(3)	0.3737(10)	0.094(4)
C7	0.7781(9)	0.4988(3)	0.4804(9)	0.081(3)
C8	0.8364(8)	0.4784(2)	0.5488(8)	0.074(3)
C9	0.9282(7)	0.4586(2)	0.5117(8)	0.057(2)
C10	0.9891(7)	0.4358(2)	0.5816(7)	0.054(2)
C11	0.9825(9)	0.4390(3)	0.6842(9)	0.085(3)
C12	0.0302(10)	0.4156(3)	0.7482(8)	0.083(3)
C13	0.0837(9)	0.3893(3)	0.7070(8)	0.087(3)
C14	0.0933(7)	0.3859(2)	0.5983(8)	0.066(3)
C15	0.0484(7)	0.4094(2)	0.5359(7)	0.054(2)
C16	0.3001(6)	0.36907(18)	0.1649(5)	0.0390(18)
C17	0.3974(6)	0.3815(2)	0.1148(6)	0.051(2)
C18	0.3859(9)	0.3952(2)	0.0185(7)	0.073(3)

C19	0.2785(9)	0.3957(2)	0.9709(7)	0.076(3)
C20	0.1818(8)	0.3829(3)	0.0203(7)	0.081(3)
C21	0.1897(7)	0.3699(2)	0.1167(6)	0.055(2)
C22	0.2258(5)	0.31741(16)	0.3028(5)	0.0276(15)
C23	0.1948(6)	0.30672(19)	0.3998(6)	0.045(2)
C24	0.1232(7)	0.2793(2)	0.4095(6)	0.052(2)
C25	0.0843(7)	0.2640(2)	0.3247(8)	0.066(3)
C26	0.1155(7)	0.2741(2)	0.2277(7)	0.059(2)
C27	0.1856(6)	0.30125(18)	0.2178(5)	0.0414(19)
C28	0.7089(5)	0.29676(18)	0.2351(5)	0.0358(17)
C29	0.7828(6)	0.30688(18)	0.3275(5)	0.0392(18)
C30	0.7864(6)	0.37694(17)	0.3728(5)	0.0393(18)
C31	0.7173(6)	0.40333(18)	0.4260(6)	0.047(2)
C32	0.5278(6)	0.43042(17)	0.3018(5)	0.0394(18)
C33	0.6087(8)	0.4343(2)	0.2221(7)	0.064(3)
C34	0.5862(11)	0.4569(2)	0.1447(7)	0.081(3)
C35	0.4806(11)	0.4741(3)	0.1457(8)	0.086(3)
C36	0.4051(9)	0.4705(2)	0.2244(8)	0.074(3)
C37	0.4265(7)	0.44881(19)	0.3017(7)	0.054(2)
C38	0.4943(6)	0.41608(18)	0.5182(6)	0.0406(18)
C39	0.5120(7)	0.4481(2)	0.5450(7)	0.063(2)
C40	0.4739(8)	0.4589(2)	0.6399(7)	0.071(3)
C41	0.4209(8)	0.4388(3)	0.7082(7)	0.068(3)
C42	0.4028(7)	0.4080(3)	0.6818(6)	0.065(3)
C43	0.4395(6)	0.3965(2)	0.5876(5)	0.045(2)
C44	0.5259(6)	0.26373(16)	0.3536(5)	0.0323(16)
C45	0.4553(6)	0.26763(19)	0.4396(5)	0.0440(19)
C46	0.4298(7)	0.2414(2)	0.5013(7)	0.066(3)
C47	0.4750(8)	0.2118(2)	0.4773(6)	0.060(2)
C48	0.5473(7)	0.2076(2)	0.3926(6)	0.053(2)
C49	0.5718(6)	0.23410(18)	0.3297(6)	0.0432(19)

C50	0.4761(5)	0.28847(16)	0.1485(5)	0.0295(15)
C51	0.4021(6)	0.2629(2)	0.1368(6)	0.047(2)
C52	0.3438(7)	0.2582(2)	0.0450(6)	0.054(2)
C53	0.3575(7)	0.2793(2)	0.9638(6)	0.055(2)
C54	0.4322(7)	0.3046(2)	0.9752(6)	0.052(2)
C55	0.4937(7)	0.30933(19)	0.0664(5)	0.0436(19)
C56	0.7327(6)	0.33130(18)	0.5327(5)	0.0381(18)
C57	0.6393(7)	0.32354(19)	0.5952(6)	0.046(2)
C58	0.6560(8)	0.3160(2)	0.6977(6)	0.065(3)
C59	0.7700(9)	0.3171(2)	0.7370(6)	0.069(3)
C60	0.8632(8)	0.3247(2)	0.6768(7)	0.071(3)
C61	0.8447(6)	0.3323(2)	0.5730(6)	0.056(2)

Table 4

Atomic coordinates and equivalent isotropic atomic displacement parameters ($Å^2$) for $[Pd(PP_2)(L^{Phen+})]^{3+}$ cation

$U_{(eq)}$ is defined as one third of the trace of the orthogonalized U_{ij} tensor.

	x/a	***y/b***	***z/c***	***U(eq)***
Pd1	0.31675(2)	0.63419(2)	0.36724(2)	0.03288(11)
P1	0.27903(8)	0.65409(8)	0.27146(5)	0.0484(4)
P2	0.33000(7)	0.47476(8)	0.33518(6)	0.0420(3)
P3	0.37626(7)	0.57274(8)	0.44711(6)	0.0431(3)
P4	0.29908(6)	0.79234(7)	0.40519(5)	0.0327(3)
C1	0.2960(8)	0.7726(7)	0.2371(7)	0.041(3)
C2	0.2468(8)	0.8308(8)	0.2191(6)	0.049(3)
C3	0.2572(9)	0.9225(8)	0.1943(7)	0.076(5)
C4	0.3168(10)	0.9560(7)	0.1876(7)	0.081(5)
C5	0.3660(8)	0.8978(9)	0.2056(8)	0.073(4)
C6	0.3556(8)	0.8061(9)	0.2304(8)	0.058(3)
C1'	0.2736(12)	0.7731(14)	0.2343(13)	0.041(3)
C2'	0.2209(11)	0.8240(18)	0.2203(13)	0.049(3)
C3'	0.2282(14)	0.9199(18)	0.1985(16)	0.076(5)
C4'	0.2866(14)	0.9563(17)	0.1930(15)	0.081(5)
C5'	0.3388(13)	0.9053(17)	0.2078(16)	0.073(4)
C6'	0.3325(12)	0.8069(18)	0.2274(15)	0.058(3)
C7	0.201(2)	0.623(3)	0.266(3)	0.062(2)
C8	0.174(3)	0.594(4)	0.213(3)	0.087(4)
C9	0.113(3)	0.564(4)	0.211(3)	0.121(5)
C10	0.079(2)	0.563(4)	0.262(3)	0.119(5)
C11	0.106(3)	0.593(5)	0.316(3)	0.111(4)
C12	0.167(3)	0.622(5)	0.318(3)	0.073(3)
C7'	0.2010(7)	0.6141(12)	0.2593(9)	0.062(2)

C8'	0.1827(8)	0.5689(17)	0.2066(8)	0.087(4)
C9'	0.1243(9)	0.531(2)	0.2009(9)	0.121(5)
C10'	0.0836(8)	0.5408(17)	0.2462(11)	0.119(5)
C11'	0.1007(9)	0.5890(14)	0.2986(12)	0.111(4)
C12'	0.1596(9)	0.6237(13)	0.3045(11)	0.073(3)
C13	0.3248(3)	0.5713(3)	0.2273(2)	0.0630(17)
C14	0.3205(3)	0.4681(3)	0.2550(2)	0.0595(16)
C15	0.4076(3)	0.4401(3)	0.3549(2)	0.0577(15)
C16	0.4299(3)	0.4862(3)	0.4134(2)	0.0572(15)
C17	0.3308(3)	0.5017(3)	0.4975(2)	0.0482(14)
C18	0.2688(3)	0.5149(3)	0.4979(2)	0.0559(15)
C19	0.2321(4)	0.4573(4)	0.5345(3)	0.079(2)
C20	0.2582(5)	0.3859(5)	0.5683(3)	0.088(3)
C21	0.3206(5)	0.3730(4)	0.5687(3)	0.088(3)
C22	0.4268(3)	0.6471(3)	0.4932(2)	0.0491(14)
C23	0.4190(3)	0.6567(3)	0.5535(2)	0.0553(15)
C24	0.4599(3)	0.7139(4)	0.5868(3)	0.073(2)
C25	0.5078(3)	0.7589(4)	0.5615(4)	0.077(2)
C26	0.5164(3)	0.7502(4)	0.5019(4)	0.076(2)
C27	0.4757(3)	0.6936(3)	0.4668(3)	0.0609(16)
C28	0.2794(13)	0.386(2)	0.3669(17)	0.0486(14)
C29	0.2162(14)	0.390(2)	0.3590(15)	0.060(4)
C30	0.1788(11)	0.324(2)	0.3882(14)	0.074(5)
C31	0.2048(15)	0.2534(19)	0.4254(13)	0.087(8)
C32	0.2680(15)	0.249(2)	0.4333(13)	0.077(6)
C33	0.3054(12)	0.315(2)	0.4040(16)	0.058(4)
C28'	0.2778(15)	0.386(3)	0.366(2)	0.0486(14)
C29'	0.2176(17)	0.396(3)	0.3456(18)	0.060(4)
C30'	0.1715(13)	0.340(3)	0.3706(16)	0.074(5)
C31'	0.1858(13)	0.274(2)	0.4156(15)	0.087(8)

C32'	0.2460(15)	0.264(2)	0.4358(14)	0.077(6)
C33'	0.2921(12)	0.320(3)	0.4108(19)	0.058(4)
C34	0.3681(2)	0.8637(3)	0.4174(2)	0.0395(12)
C35	0.4133(3)	0.8539(3)	0.3756(2)	0.0482(13)
C36	0.4642(3)	0.9140(4)	0.3752(3)	0.0665(17)
C37	0.4699(3)	0.9824(4)	0.4175(3)	0.0743(19)
C38	0.4263(3)	0.9947(4)	0.4612(3)	0.0710(18)
C39	0.3740(3)	0.9352(3)	0.4623(2)	0.0487(13)
C40	0.2568(2)	0.7818(3)	0.47235(19)	0.0395(12)
C41	0.1934(3)	0.7679(4)	0.4681(2)	0.0549(14)
C42	0.1598(3)	0.7507(5)	0.5173(3)	0.082(2)
C43	0.1898(4)	0.7460(6)	0.5718(3)	0.092(2)
C44	0.2504(4)	0.7582(5)	0.5776(2)	0.077(2)
C45	0.2856(3)	0.7780(3)	0.5272(2)	0.0504(14)
C46	0.2540(2)	0.8792(3)	0.36013(18)	0.0338(10)
C47	0.2364(2)	0.9740(3)	0.39061(19)	0.0383(11)
C48	0.2922(3)	0.2118(3)	0.2392(2)	0.0491(14)
C49	0.2648(2)	0.0995(3)	0.3145(2)	0.0386(11)
C50	0.2461(2)	0.1641(3)	0.2696(2)	0.0402(12)
C51	0.1829(3)	0.1783(3)	0.2560(2)	0.0474(13)
C52	0.1603(3)	0.2434(4)	0.2116(3)	0.0654(17)
C53	0.0988(4)	0.2535(5)	0.2028(4)	0.094(2)
C54	0.0564(3)	0.2039(5)	0.2371(4)	0.102(3)
C55	0.0769(3)	0.1411(4)	0.2804(3)	0.086(2)
C56	0.1395(3)	0.1291(4)	0.2898(3)	0.0600(15)
C57	0.1611(3)	0.0627(3)	0.3345(2)	0.0475(13)
C58	0.3537(3)	0.1980(4)	0.2528(2)	0.0570(15)
C59	0.3694(3)	0.1343(3)	0.2986(2)	0.0539(14)
C60	0.3266(2)	0.0846(3)	0.3292(2)	0.0469(13)
C61	0.3565(3)	0.4300(3)	0.5353(2)	0.0680(19)
N1	0.21928(19)	0.0483(2)	0.34570(16)	0.0376(9)

Table 5

Atomic coordinates and equivalent isotropic atomic displacement parameters ($Å^2$) for $[Pd^0(PP_2)(L^{PhenH})]$

$U_{(eq)}$ is defined as one third of the trace of the orthogonalized U_{ij} tensor.

	x/a	***y/b***	***z/c***	***U(eq)***
Pd1	0.60821(4)	0.67883(3)	0.68893(2)	0.03128(13)
P1	0.78684(12)	0.71941(12)	0.70999(8)	0.0303(3)
P2	0.55140(12)	0.51496(12)	0.74593(8)	0.0320(3)
P3	0.57748(13)	0.63354(12)	0.57601(8)	0.0331(3)
P4	0.47588(12)	0.84114(12)	0.66312(8)	0.0333(3)
N1	0.7114(4)	0.8674(4)	0.8985(3)	0.0360(11)
C1	0.7773(5)	0.8276(4)	0.7665(3)	0.0334(13)
C2	0.6999(5)	0.8040(4)	0.8424(3)	0.0334(13)
C3	0.6569(5)	0.9817(5)	0.8835(3)	0.0431(15)
C4	0.6463(5)	0.0386(5)	0.9495(3)	0.0372(14)
C5	0.5557(5)	0.1272(5)	0.9600(3)	0.0472(16)
C6	0.5509(6)	0.1838(5)	0.0180(4)	0.0538(17)
C7	0.6328(7)	0.1507(6)	0.0670(4)	0.069(2)
C8	0.7217(6)	0.0609(6)	0.0583(4)	0.0566(18)
C9	0.7304(5)	0.0054(5)	0.9982(3)	0.0431(15)
C10	0.8255(5)	0.9104(5)	0.9851(3)	0.0390(14)
C11	0.9268(6)	0.8835(5)	0.0207(4)	0.0536(18)
C12	0.0107(6)	0.7915(5)	0.0121(4)	0.0572(19)
C13	0.9939(5)	0.7213(5)	0.9671(3)	0.0484(16)
C14	0.8969(5)	0.7453(5)	0.9279(3)	0.0406(14)
C15	0.8122(5)	0.8405(5)	0.9354(3)	0.0348(13)
C16	0.8863(5)	0.7615(5)	0.6253(3)	0.0376(14)
C17	0.8899(6)	0.7105(6)	0.5641(4)	0.059(2)
C18	0.9621(6)	0.7327(7)	0.4982(4)	0.086(3)

C19	0.0325(7)	0.8099(8)	0.4926(4)	0.095(3)
C20	0.0305(7)	0.8621(7)	0.5516(4)	0.090(3)
C21	0.9580(6)	0.8380(6)	0.6173(4)	0.062(2)
C22	0.8918(5)	0.6141(5)	0.7618(3)	0.0367(14)
C23	0.0121(5)	0.6162(5)	0.7567(3)	0.0431(15)
C24	0.0829(5)	0.5416(5)	0.8033(4)	0.0517(17)
C25	0.0344(6)	0.4654(5)	0.8560(4)	0.0556(18)
C26	0.9150(6)	0.4620(5)	0.8617(3)	0.0490(16)
C27	0.8448(5)	0.5373(4)	0.8148(3)	0.0375(14)
C28	0.4511(5)	0.4899(5)	0.8336(3)	0.0355(13)
C29	0.4382(5)	0.5572(5)	0.8860(3)	0.0450(15)
C30	0.3671(6)	0.5414(6)	0.9537(4)	0.068(2)
C31	0.3071(6)	0.4544(6)	0.9695(4)	0.060(2)
C32	0.3187(5)	0.3854(5)	0.9186(4)	0.0520(18)
C33	0.3899(5)	0.4019(5)	0.8508(3)	0.0421(15)
C34	0.6743(4)	0.3964(4)	0.7565(3)	0.0341(13)
C35	0.7709(5)	0.3905(5)	0.7003(3)	0.0438(15)
C36	0.8709(5)	0.3085(6)	0.7080(4)	0.0543(18)
C37	0.8760(6)	0.2335(5)	0.7718(4)	0.0565(18)
C38	0.7819(5)	0.2383(5)	0.8282(4)	0.0490(17)
C39	0.6816(5)	0.3183(5)	0.8200(3)	0.0394(14)
C40	0.4685(5)	0.4788(5)	0.6787(3)	0.0413(15)
C41	0.5260(5)	0.5008(5)	0.5989(3)	0.0427(15)
C42	0.6684(5)	0.6234(5)	0.4841(3)	0.0376(14)
C43	0.6606(5)	0.7095(5)	0.4253(3)	0.0472(16)
C44	0.7355(6)	0.7050(6)	0.3584(4)	0.0564(18)
C45	0.8217(6)	0.6149(6)	0.3498(4)	0.0582(19)
C46	0.8327(6)	0.5307(6)	0.4070(4)	0.0577(18)
C47	0.7582(5)	0.5344(5)	0.4743(4)	0.0496(16)
C48	0.4433(5)	0.7325(5)	0.5521(3)	0.0387(14)
C49	0.4534(5)	0.8462(5)	0.5651(3)	0.0416(14)

C50	0.3192(5)	0.8790(5)	0.7042(3)	0.0396(14)
C51	0.2466(5)	0.9761(5)	0.6791(4)	0.0535(17)
C52	0.1314(6)	0.0019(7)	0.7127(5)	0.070(2)
C53	0.0856(6)	0.9312(7)	0.7693(5)	0.074(3)
C54	0.1539(6)	0.8343(7)	0.7945(4)	0.069(2)
C55	0.2720(5)	0.8075(5)	0.7612(3)	0.0472(16)
C56	0.5313(5)	0.9673(4)	0.6607(3)	0.0384(14)
C57	0.6288(5)	0.9905(5)	0.6091(4)	0.0489(17)
C58	0.6814(6)	0.0779(6)	0.6107(4)	0.063(2)
C59	0.6388(7)	0.1441(6)	0.6649(5)	0.068(2)
C60	0.5427(6)	0.1242(5)	0.7155(4)	0.064(2)
C61	0.4899(5)	0.0362(5)	0.7140(4)	0.0465(16)

Table 6

Crystallographic data for[$NiBr_3(L^{PhenBI+})$].

	$NiBr_3L^{PhenBI+}$
chemical formula	$C_{28}H_{26}Br_3N_2Ni$
formula weight	719.92
crystal system	Monoclinic
space group	$P2_1/c$
a (Å)	18.3574(13)
b (Å)	15.8651(8)
c (Å)	20.1961(12)
α (deg)	90
β (deg)	106.102(7)
γ (deg)	90
V (Å³)	5651.2(6)
Z	4
D_{calcd} *(g cm⁻³)*	1.692
λ (Å), μ (mm⁻¹)	0.71073, 5.005
Temperature (K)	173(2)
θ range (°)	2.642 to 27.484
reflns collected	12948
unique reflns	7003
data/restraint/parameters	12948 / 0 / 631
R_1, wR_2 $(I > 2\sigma(I))$	0.0709, 0.1150

Table 7

Atomic coordinates and equivalent isotropic atomic displacement parameters ($Å^2$) for [$NiBr_3(L^{PhenBI+})$]

	x/a	*y/b*	*z/c*	*U(eq)*
Ni1	0.18724(6)	0.84934(5)	0.23927(4)	0.0385(2)
Ni2	0.32819(6)	0.15357(5)	0.75165(4)	0.0408(2)
Br4	0.22138(6)	0.18325(5)	0.79361(4)	0.0569(2)
Br1	0.07580(5)	0.84924(6)	0.14728(4)	0.0581(2)
Br3	0.29793(6)	0.83254(5)	0.20197(4)	0.0601(3)
Br6	0.43669(5)	0.14282(6)	0.84684(4)	0.0610(3)
Br2	0.16806(5)	0.76512(5)	0.32793(5)	0.0604(3)
Br5	0.33112(6)	0.23324(6)	0.65595(5)	0.0682(3)
P2	0.30659(11)	0.01716(10)	0.71212(9)	0.0310(4)
P1	0.19985(10)	0.98758(10)	0.27583(8)	0.0294(4)
N3	0.2788(3)	0.9159(3)	0.8920(3)	0.0338(13)
N2	0.2107(3)	0.1849(3)	0.0109(3)	0.0364(14)
N1	0.2061(4)	0.0960(3)	0.0921(3)	0.0377(14)
N4	0.2678(4)	0.8319(3)	0.9735(3)	0.0400(15)
C2	0.1785(4)	0.0471(4)	0.1422(3)	0.0330(15)
C112	0.3867(4)	0.7772(4)	0.8660(3)	0.0382(17)
C17	0.2753(4)	0.0045(4)	0.3549(3)	0.0337(15)
C5	0.2715(5)	0.1306(4)	0.0190(3)	0.0421(19)
C103	0.3096(4)	0.8502(4)	0.9304(3)	0.0336(15)
C101	0.2671(4)	0.9518(4)	0.7690(3)	0.0370(16)
C3	0.1718(4)	0.1639(4)	0.0562(3)	0.0360(16)
C1	0.2294(4)	0.0569(4)	0.2155(3)	0.0354(16)
C106	0.2081(4)	0.8874(4)	0.9615(4)	0.0383(17)
C105	0.2131(4)	0.9403(4)	0.9097(3)	0.0330(15)
C23	0.1141(4)	0.0333(4)	0.2881(3)	0.0338(16)
C102	0.3111(4)	0.9643(4)	0.8444(3)	0.0346(16)

C12	0.1019(5)	0.2329(4)	0.1293(4)	0.048(2)
C117	0.3898(4)	0.9641(4)	0.7034(3)	0.0357(16)
C122	0.4515(5)	0.0117(5)	0.6990(5)	0.060(2)
C123	0.2366(4)	0.0069(4)	0.6293(3)	0.0349(16)
C111	0.3790(4)	0.8064(4)	0.9282(3)	0.0361(16)
C11	0.1050(4)	0.2069(4)	0.0641(3)	0.0381(17)
C6	0.2676(4)	0.0738(4)	0.0701(3)	0.0386(17)
C116	0.4361(4)	0.7951(4)	0.9888(4)	0.0450(18)
C9	0.3809(5)	0.0651(5)	0.0078(4)	0.053(2)
C7	0.3217(5)	0.0118(5)	0.0915(4)	0.049(2)
C20	0.3908(5)	0.0261(6)	0.4770(5)	0.071(3)
C28	0.0570(5)	0.9798(5)	0.2950(4)	0.051(2)
C115	0.4998(5)	0.7537(5)	0.9855(4)	0.062(2)
C18	0.3185(5)	0.9387(5)	0.3873(4)	0.052(2)
C110	0.1617(5)	0.0027(5)	0.8853(4)	0.055(2)
C118	0.3961(5)	0.8774(4)	0.6997(4)	0.054(2)
C127	0.1137(5)	0.0437(5)	0.5564(4)	0.061(2)
C8	0.3802(5)	0.0095(5)	0.0602(4)	0.054(2)
C107	0.1494(5)	0.8931(5)	0.9922(4)	0.055(2)
C10	0.3271(5)	0.1264(5)	0.9857(4)	0.047(2)
C14	0.9793(5)	0.2901(5)	0.0805(5)	0.062(2)
C128	0.1701(5)	0.0474(5)	0.6192(4)	0.055(2)
C25	0.0369(6)	0.1505(5)	0.3021(5)	0.066(3)
C114	0.5092(5)	0.7253(5)	0.9243(5)	0.060(2)
C16	0.0459(5)	0.2246(5)	0.0076(4)	0.055(2)
C108	0.0972(6)	0.9539(6)	0.9665(5)	0.070(3)
C24	0.1027(5)	0.1196(5)	0.2919(4)	0.052(2)
C113	0.4536(5)	0.7368(5)	0.8648(4)	0.057(2)
C104	0.2772(5)	0.7571(5)	0.0177(4)	0.061(3)
C15	0.9824(5)	0.2667(5)	0.0151(5)	0.062(2)
C4	0.1997(5)	0.2614(5)	0.9693(4)	0.060(2)

C13	0.0376(6)	0.2733(5)	0.1359(5)	0.062(3)
C19	0.3756(5)	0.9493(6)	0.4469(4)	0.066(3)
C124	0.2515(6)	0.9693(6)	0.5729(4)	0.072(3)
C27	0.9921(5)	0.0110(6)	0.3053(5)	0.066(3)
C26	0.9811(6)	0.0965(7)	0.3081(5)	0.076(3)
C109	0.1021(5)	0.0095(5)	0.9148(5)	0.065(3)
C119	0.4597(6)	0.8402(6)	0.6917(5)	0.074(3)
C126	0.1272(5)	0.0030(6)	0.5028(4)	0.061(2)
C125	0.1962(7)	0.9677(7)	0.5090(5)	0.088(3)
C21	0.3500(6)	0.0947(6)	0.4426(5)	0.088(4)
C120	0.5199(6)	0.8874(7)	0.6872(6)	0.087(3)
C22	0.2934(5)	0.0834(5)	0.3824(5)	0.069(3)
C121	0.5152(6)	0.9741(7)	0.6899(6)	0.090(4)

REFERENCES

(1) Olah, G. A.; Goeppert, A.; Prakash, G. K. S. Chemical Recycling of Carbon Dioxide to Methanol and Dimethyl Ether: From Greenhouse Gas to Renewable, Environmentally Carbon Neutral Fuels and Synthetic Hydrocarbons. *J. Org. Chem.* **2009**, *74*, 487–498.

(2) Huff, C. A.; Sanford, M. S. Cascade Catalysis for the Homogeneous Hydrogenation of CO_2 to Methanol. *J. Am. Chem. Soc.* **2011**, *133*, 18122–18125.

(3) Olah, G. A.; Prakash, G. K. S.; Goeppert, A. Anthropogenic Chemical Carbon Cycle for a Sustainable Future. *J. Am. Chem. Soc.* **2011**, *133*, 12881–12898.

(4) Wang, W.; Himeda, Y.; Muckerman, J. T.; Manbeck, G. F.; Fujita, E. CO_2 Hydrogenation to Formate and Methanol as an Alternative to Photo- and Electrochemical CO_2 Reduction. *Chem. Rev.* **2015**, *115*, 12936–12973.

(5) Jeletic, M. S.; Mock, M. T.; Appel, A. M.; Linehan, J. C. A Cobalt-Based Catalyst for the Hydrogenation of CO_2 under Ambient Conditions. *J. Am. Chem. Soc.* **2013**, *135*, 11533–11536.

(6) Rohmann, K.; Kothe, J.; Haenel, M. W.; Englert, U.; Hölscher, M.; Leitner, W. Hydrogenation of CO_2 to Formic Acid with a Highly Active Ruthenium Acriphos Complex in DMSO and DMSO/Water. *Angew. Chem. Int. Ed.* **2016**, *55*, 8966–8969.

(7) Wesselbaum, S.; vom Stein, T.; Klankermayer, J.; Leitner, W. Hydrogenation of Carbon Dioxide to Methanol by Using a Homogeneous Ruthenium–Phosphine Catalyst. *Angew. Chem. Int. Ed.* **2012**, *51*, 7499–7502.

(8) Tanaka, R.; Yamashita, M.; Nozaki, K. Catalytic Hydrogenation of Carbon

Dioxide Using Ir(III)-Pincer Complexes. *J. Am. Chem. Soc.* **2009**, *131*, 14168–14169.

(9) Inoue, Y.; Izumida, H.; Sasaki, Y.; Hashimoto, H. CATALYTIC FIXATION OF CARBON DIOXIDE TO FORMIC ACID BY TRANSITION-METAL COMPLEXES UNDER MILD CONDITIONS. *Chem. Lett.* **1976**, *5*, 863–864.

(10) Graf, E.; Leitner, W. Direct Formation of Formic Acid from Carbon Dioxide and Dihydrogen using the [{Rh(cod)Cl}$_2$]-$Ph_2P(CH_2)_4PPh_2$ Catalyst System. *J. Chem. Soc. Chem. Commun.* **1992**, 623–624.

(11) Jessop, P. G.; Hsiao, Y.; Ikariya, T.; Noyori, R. Homogeneous Catalysis in Supercritical Fluids: Hydrogenation of Supercritical Carbon Dioxide to Formic Acid, Alkyl Formates, and Formamides. *J. Am. Chem. Soc.* **1996**, *118*, 344–355.

(12) Jessop, P. G.; Ikariya, T.; Noyori, R. Homogeneous catalytic hydrogenation of supercritical carbon dioxide. *Nature* **1994**, *368*, 231–233.

(13) Ezhova, N. N.; Kolesnichenko, N. V; Bulygin, A. V; Slivinskii, E. V; Han, S. Hydrogenation of CO_2 to formic acid in the presence of the Wilkinson complex. *Russ. Chem. Bull.* **2002**, *51*, 2165–2169.

(14) Zhang, Y.; Maclntosh, A. D.; Wong, J. L.; Bielinski, E. A.; Williard, P. G.; Mercado, B. Q.; Hazari, N.; Bernskoetter, W. H. Iron catalyzed CO_2 hydrogenation to formate enhanced by Lewis acid co-catalysts. *Chem. Sci.* **2015**, *6*, 4291–4299.

(15) McSkimming, A.; Colbran, S. B. The coordination chemistry of organo-hydride donors: new prospects for efficient multi-electron reduction. *Chem. Soc. Rev.* **2013**, *42*, 5439–5488.

(16) McSkimming, A.; Bhadbhade, M. M.; Colbran, S. B. Bio-Inspired Catalytic Imine

Reduction by Rhodium Complexes with Tethered Hantzsch Pyridinium Groups: Evidence for Direct Hydride Transfer from Dihydropyridine to Metal-Activated Substrate. *Angew. Chem. Int. Ed.* **2013**, *52*, 3411–3416.

(17) Ohnishi, Y.; Kagami, M.; Ohno, A. Reduction by a Model of NAD(P)H. Effect of Metal Ion and Stereochemistry on the Reduction of α-Keto Esters by 1,4-Dihydronicotinamide Derivatives. *J. Am. Chem. Soc.* **1975**, *97*, 4766–4768.

(18) Tannai, H.; Koizumi, T.; Tanaka, K. Palladium(II) complexes bearing the terpyridine-type tridentate ligand with benzo[b]-1,5-naphthyridin-2-yl groups. *Inorg. Chim. Acta* **2007**, *360*, 3075–3082.

(19) Tanaka, K. Metal-Catalyzed Reversible Conversion between Chemical and Electrical Energy Designed Towards a Sustainable Society. *Chem. Rec.* **2009**, *9* , 169–186.

(20) Koizumi, T.; Tanaka, K. Reversible Hydride Generation and Release from the Ligand of $[Ru(pbn)(bpy)_2](PF_6)_2$ Driven by a pbn-Localized Redox Reaction. *Angew. Chem. Int. Ed.* **2005**, *44*, 5891–5894.

(21) Ohtsu, H.; Tanaka, K. An Organic Hydride Transfer Reaction of a Ruthenium NAD Model Complex Leading to Carbon Dioxide Reduction. *Angew. Chem. Int. Ed.* **2012**, *51*, 9792–9795.

(22) Yang, J. W.; List, B. Catalytic Asymmetric Transfer Hydrogenation of α-Ketoesters with Hantzsch Esters. *Org. Lett.* **2006**, *8*, 5653–5655.

(23) McSkimming, A.; Chan, B.; Bhadbhade, M. M.; Ball, G. E.; Colbran, S. B. Bio-Inspired Transition Metal-Organic Hydride Conjugates for Catalysis of Transfer Hydrogenation: Experiment and Theory. *Chem. - A Eur. J.* **2015**, *21*, 2821–2834.

(24) Zhu, X.; Zhang, M.; Yu, A.; Wang, C.; Cheng, J. Hydride, Hydrogen Atom, Proton, and Electron Transfer Driving Forces of Various Five-Membered Heterocyclic Organic Hydrides and Their Reaction Intermediates in Acetonitrile. *J. Am. Chem. Soc.* **2008**, *130*, 2501–2516.

(25) Zhu, X.; Tan, Y.; Cao, C. Thermodynamic Diagnosis of the Properties and Mechanism of Dihydropyridine-Type Compounds as Hydride Source in Acetonitrile with "Molecule ID Card." *J. Phys. Chem. B* **2010**, *114*, 2058–2075.

(26) DuBois, D. L.; Berning, D. E. Hydricity of transition-metal hydrides and its role in CO_2 reduction. *Appl. Organometal. Chem.* **2000**, *14*, 860–862.

(27) Matsubara, Y.; Fujita, E.; Doherty, M. D.; Muckerman, J. T.; Creutz, C. Thermodynamic and Kinetic Hydricity of Ruthenium(II) Hydride Complexes. *J. Am. Chem. Soc.* **2012**, *134*, 15743–15757.

(28) Curtis, C. J.; Miedaner, A.; Ellis, W. W.; DuBois, D. L. Measurement of the Hydride Donor Abilities of $[HM(diphosphine)_2]^+$ Complexes (M = Ni, Pt) by Heterolytic Activation of Hydrogen. *J. Am. Chem. Soc.* **2002**, *124*, 1918–1925.

(29) Raebiger, J. W.; Miedaner, A.; Curtis, C. J.; Miller, S. M.; Anderson, O. P.; DuBois, D. L. Using Ligand Bite Angles To Control the Hydricity of Palladium Diphosphine Complexes. *J. Am. Chem. Soc.* **2004**, *126*, 5502–5514.

(30) Ostović, D.; Lee, I. H.; Roberts, R. M. G.; Kreevoy, M. M. Hydride Transfer and Oxyanion Addition Equilibria of NAD^+ Analogues. *J. Org. Chem.* **1985**, *50*, 4206–4211.

(31) Parenty, A. D. C.; Smith, L. V.; Pickering, A. L.; Long, D.; Cronin, L. General One-Pot, Three-Step Methodology Leading to an Extended Class of *N*-

Heterocyclic Cations: Spontaneous Nucleophilic Addition, Cyclization, and Hydride Loss. *J. Org. Chem.* **2004**, *69*, 5934–5946.

(32) Rao, Y.; Amarne, H.; Chen, L. D.; Brown, M. L.; Mosey, N. J.; Wang, S. Photo- and Thermal-Induced Multistructural Transformation of 2-Phenylazolyl Chelate Boron Compounds. *J. Am. Chem. Soc.* **2013**, *135*, 3407–3410.

(33) Grim, S. O.; McFarlane, W.; Davidoff, E. F. Group Contributions to Phosphorus-31 Chemical Shifts of Tertiary Phosphines. *J. Org. Chem.* **1967**, *32*, 781–784.

(34) DuBois, D. L.; Miedaner, A.; Haltiwanger, R. C. Electrochemical Reduction of CO_2 Catalyzed by [Pd(triphosphine)(solvent)]$(BF_4)_2$ Complexes: Synthetic and Mechanistic Studies. *J. Am. Chem. Soc.* **1991**, *113*, 8753–8764.

(35) Wiedner, E. S.; Chambers, M. B.; Pitman, C. L.; Bullock, R. M.; Miller, A. J. M.; Appel, A. M. Thermodynamic Hydricity of Transition Metal Hydrides. *Chem. Rev.* **2016**, *116*, 8655–8692.

(36) Berning, D. E.; Miedaner, A.; Curtis, C. J.; Noll, B. C.; DuBois, M. C. R.; DuBois, D. L. Free-Energy Relationships between the Proton and Hydride Donor Abilities of $[HNi(diphosphine)_2]^+$ Complexes and the Half-Wave Potentials of Their Conjugate Bases. *Organometallics* **2001**, *20*, 1832–1839.

(37) Sevillano, P.; Habtemariam, A.; Parsons, S.; Castiñeiras, A.; García, M. E.; Sadler, P. J. Gold(I)-induced chelate ring-opening of palladium(II) and platinum(II) triphos complexes. *J. Chem. Soc. Dalt. Trans.* **1999**, 2861–2870.

(38) DuBois, D. L.; Miedaner, A. Mediated Electrochemical Reduction of CO_2. Preparation and Comparison of an Isoelectronic Series of Complexes. *J. Am. Chem. Soc.* **1987**, *109*, 113–117.

(39) Harmand, L.; Saleh, S.; Andrieu, J.; Cattey, H.; Picquet, M.; Hierso, J. Linear Triphosphines as Ligands for Metal Complexes Immobilization in Ionic Liquids: Palladium-Catalyzed Methoxylation of Alkynes. *Open Org. Chem. J.* **2012**, *6*, 1–11.

(40) Fernández, D.; Sevillano, P.; García-Seijo, M. I.; Castiñeiras, A.; Jánosi, L.; Berente, Z.; Kollár, L.; García-Fernández, M. E. Influence on reactivity of chloro ligand substitution in mononuclear cationic Pd(II) and Pt(II) triphos complexes: X-ray structure of the nitrate derivatives. *Inorganica Chim. Acta* **2001**, *312*, 40–52.

(41) DuBois, D. L.; Meek, D. W. Stereochemistry and Exchange Processes in Five-Coordinate Cobalt(I) Complexes Containing One of Three Triphosphine Ligands. *Inorg. Chem.* **1976**, *15*, 3076–3083.

(42) Curtis, C. J.; Miedaner, A.; Ciancanelli, R.; Ellis, W. W.; Noll, B. C.; DuBois, M. R.; DuBois, D. L. $[Ni(Et_2PCH_2NMeCH_2PEt_2)_2]^{2+}$ as a Functional Model for Hydrogenases. *Inorg. Chem.* **2003**, *42*, 216–227.

(43) Filonenko, G. A.; van Putten, R.; Hensen, E. J. M.; Pidko, E. A. Catalytic (de)hydrogenation promoted by non-precious metals - Co, Fe and Mn: recent advances in an emerging field. *Chem. Soc. Rev.* **2018**, *47*, 1459–1483.

(44) Kothandaraman, J.; Goeppert, A.; Czaun, M.; Olah, G. A.; Prakash, G. K. S. Conversion of CO_2 from Air into Methanol Using a Polyamine and a Homogeneous Ruthenium Catalyst. *J. Am. Chem. Soc.* **2016**, *138*, 778–781.

(45) Berning, D. E.; Noll, B. C.; DuBois, D. L. Relative Hydride, Proton, and Hydrogen Atom Transfer Abilities of $[HM(diphosphine)_2]PF_6$ Complexes (M = Pt, Ni). *J. Am. Chem. Soc.* **1999**, *121*, 11432–11447.

(46) Fisher, K. J.; Alyea, E. C. METAL VAPOUR SYNTHESIS OF ZERO-VALENT NICKEL PHOSPHINE COMPLEXES AND THEIR CHARACTERIZATION BY ^{31}P NMR SPECTROSCOPY. *Polyhedron* **1989**, *8*, 13–15.

(47) Rasheed, L.; Yousuf, M.; Youn, I. S.; Shi, G.; Kim, K. S. An efficient non-reaction based colorimetric and fluorescent probe for the highly selective discrimination of Pd^0 and Pd^{2+} in aqueous media. *RSC Adv.* **2016**, *6*, 60546–60549.

(48) Amatore, C.; Jutand, A.; Khalil, F.; M'Barki, M. A.; Mottier, L. Rates and Mechanisms of Oxidative Addition to Zerovalent Palladium Complexes Generated *in Situ* from Mixtures of Pd°$(dba)_2$ and Triphenylphosphine. *Organometallics* **1993**, *12*, 3168–3178.

APPENDIX

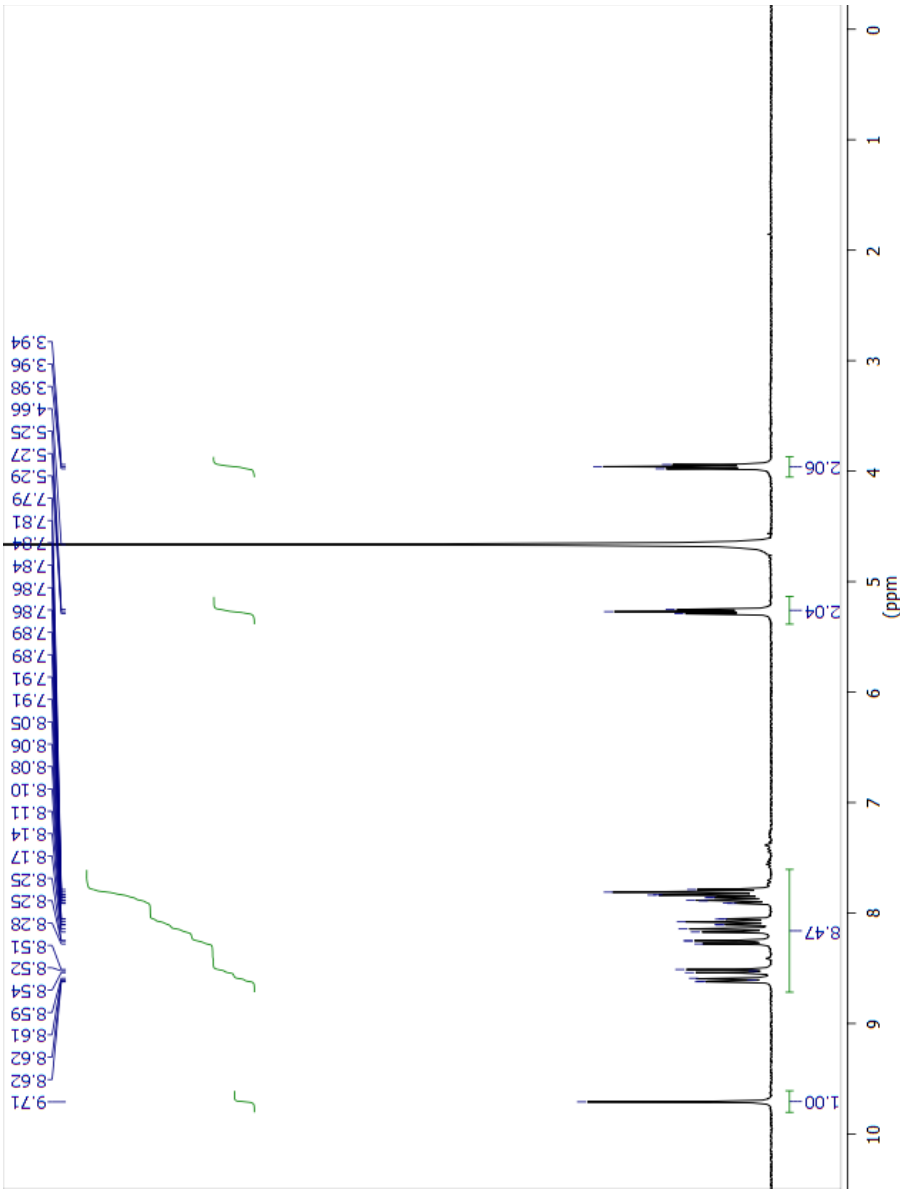

Figure 41. ^{1}H NMR spectrum of 5-(2-bromo-ethylene)-phenanthridinium bromide in D_2O (300 MHz).

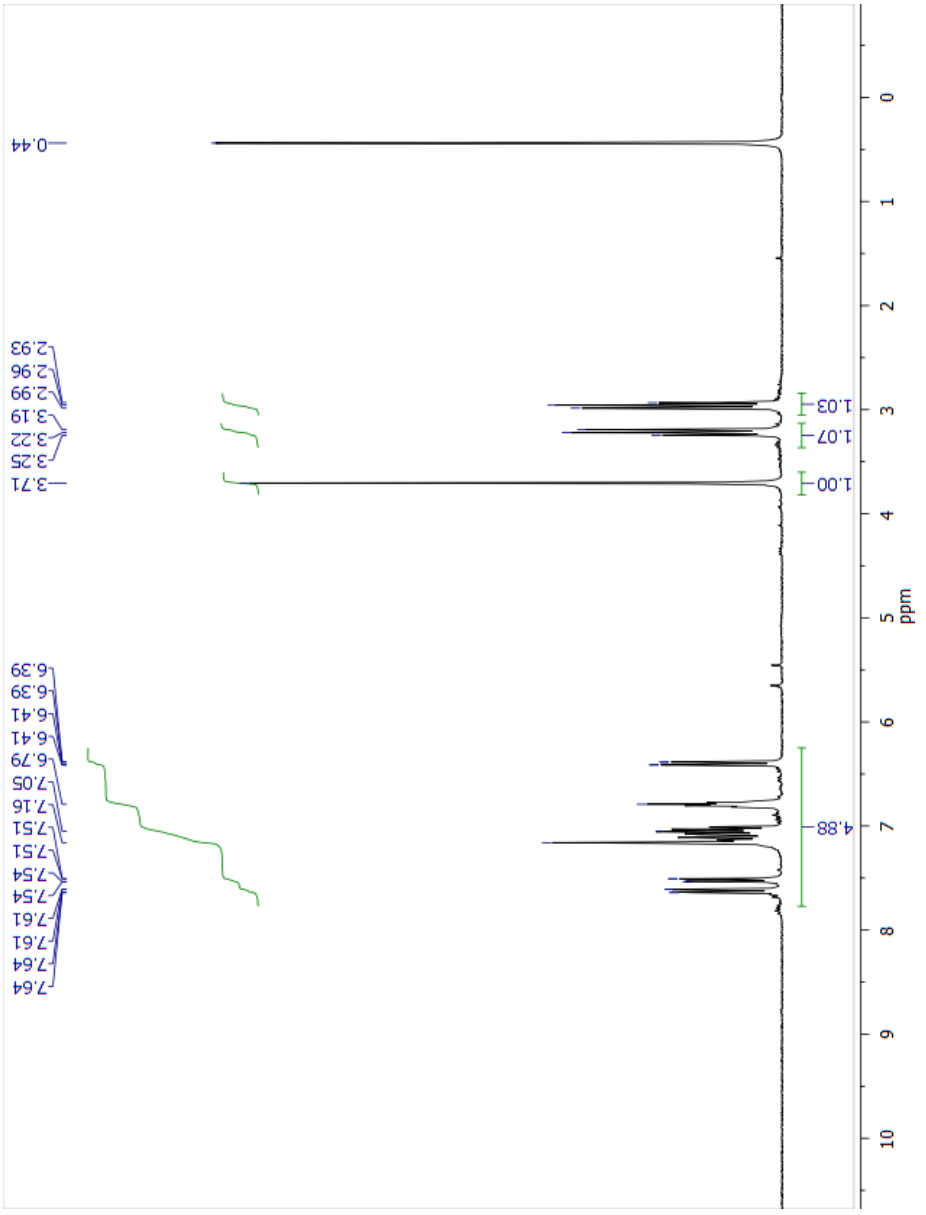

Figure 42. ^{1}H NMR spectrum of 5-(2-bromo-ethylene)-5,6-dihydro-phenanthridine in C_6D_6 (300 MHz).

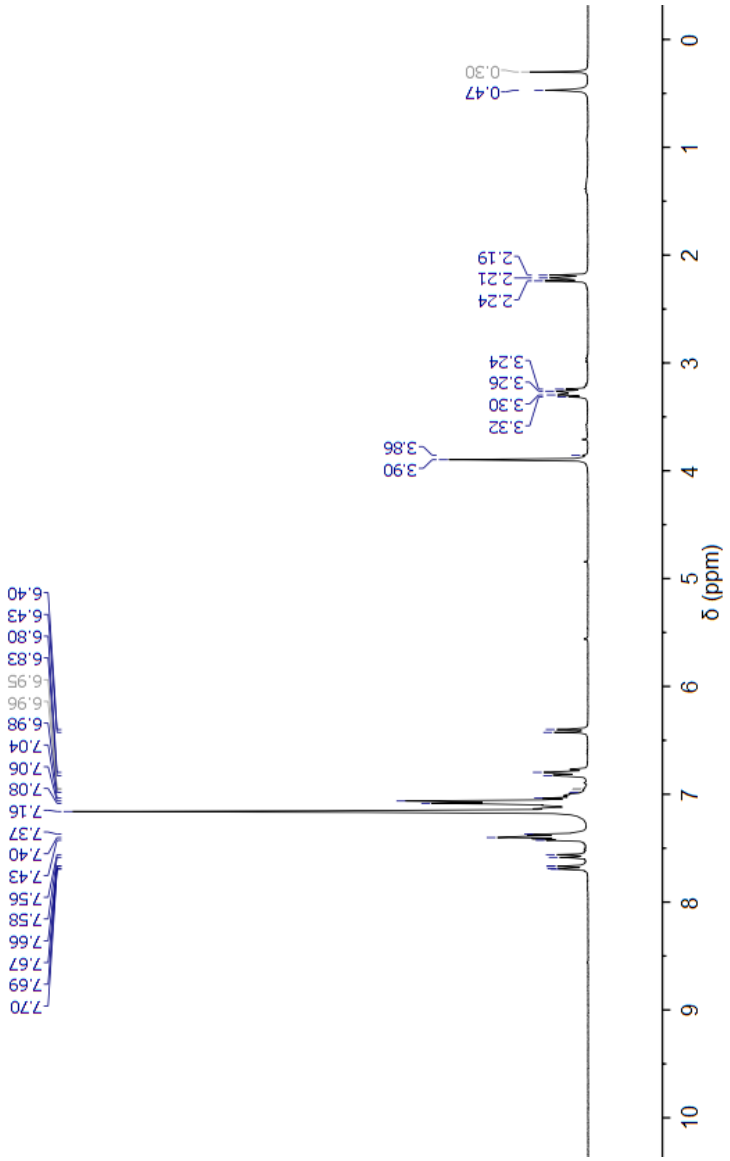

Figure 43. ^{1}H NMR spectrum of 5-(2-diphenylphosphanyl-ethylene)-5,6-dihydro-phenanthridine (L^{PhenH}) in C_6D_6 (300 MHz).

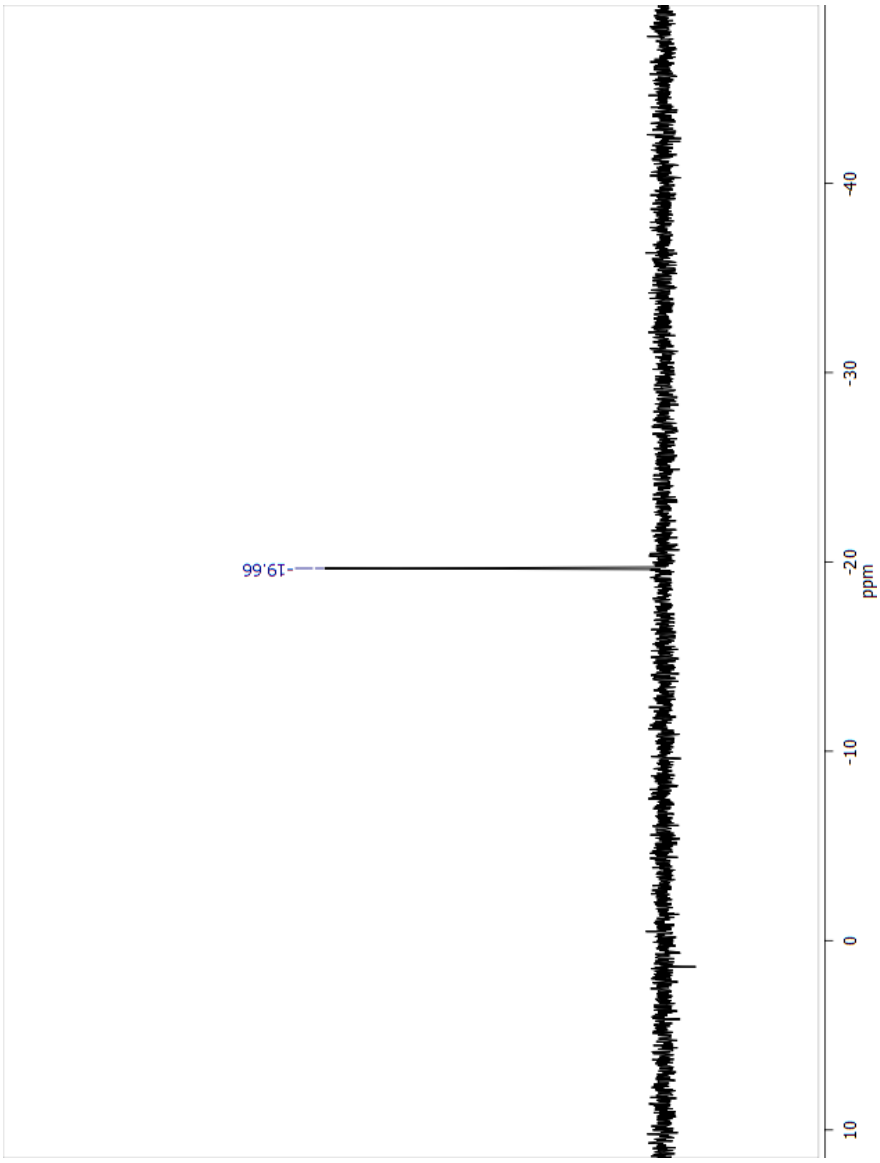

Figure 44. ^{31}P NMR spectrum of 5-(2-diphenylphosphanyl-ethylene)-5,6-dihydro-phenanthridine (L^{PhenH}) in C_6D_6 (300 MHz).

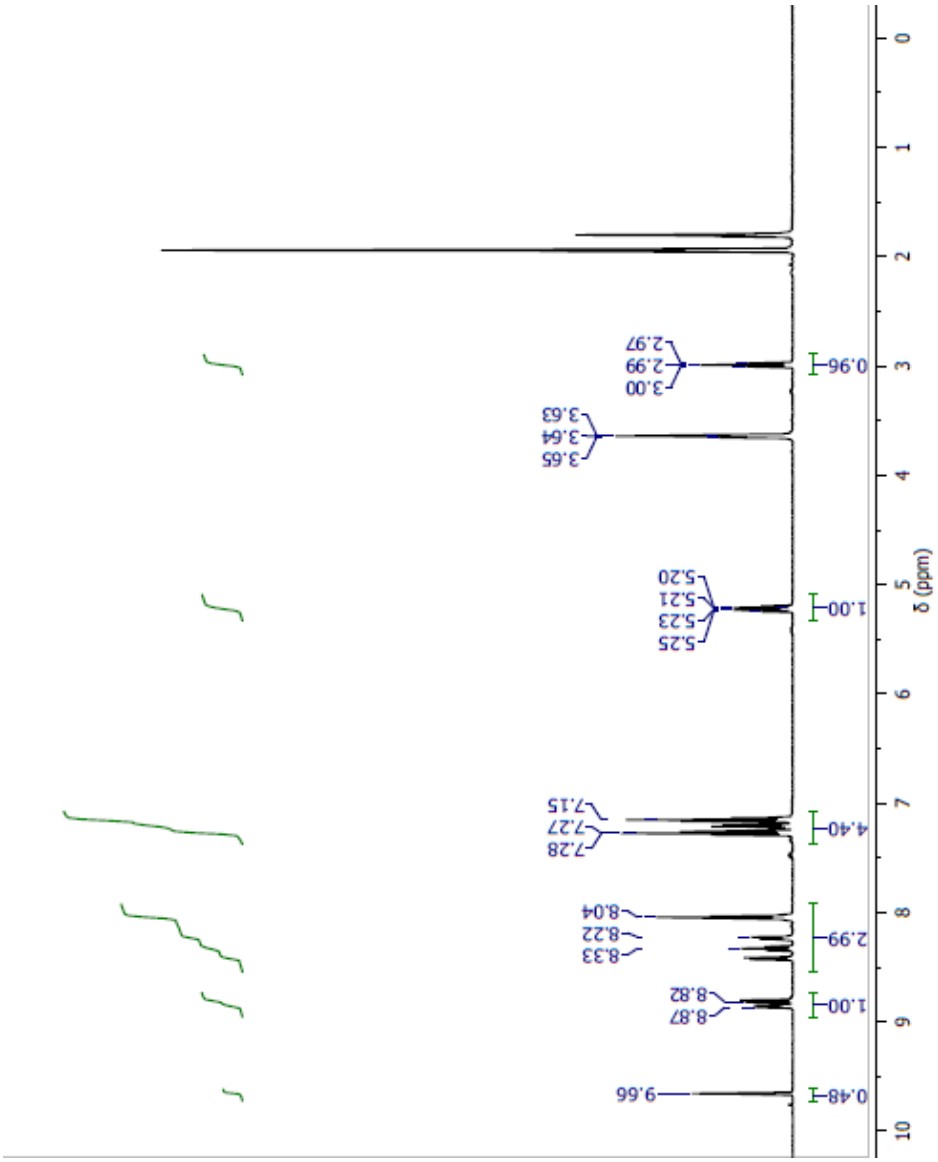

Figure 45. ^{1}H NMR spectrum of 5-(2-diphenylphosphanyl-ethylene)-phenanthridinium tetrafluoroborate (L^{Phen+}) in CD_3CN (300 MHz).

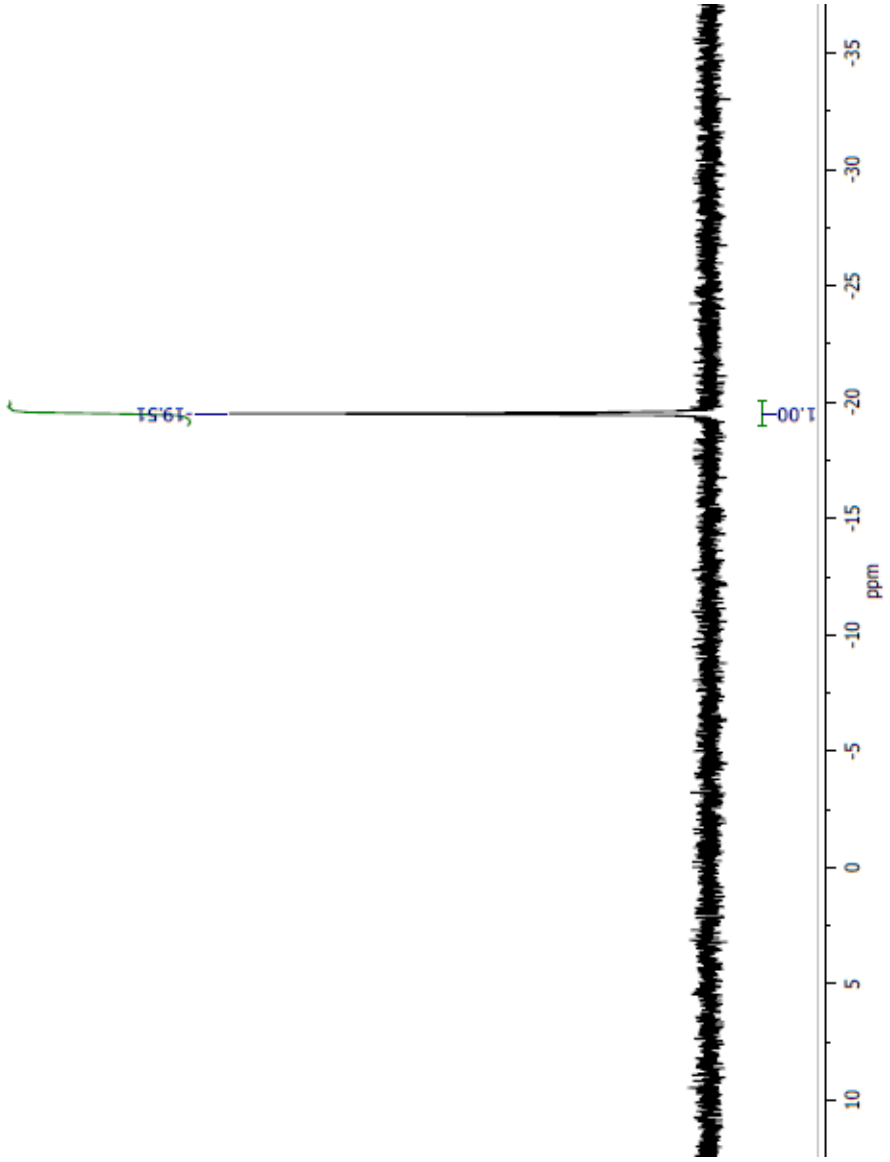

Figure 46. ^{31}P NMR spectrum of 5-(2-diphenylphosphanyl-ethylene)-phenanthridinium tetrafluoroborate (L^{Phen+}) in CD_3CN (300 MHz).

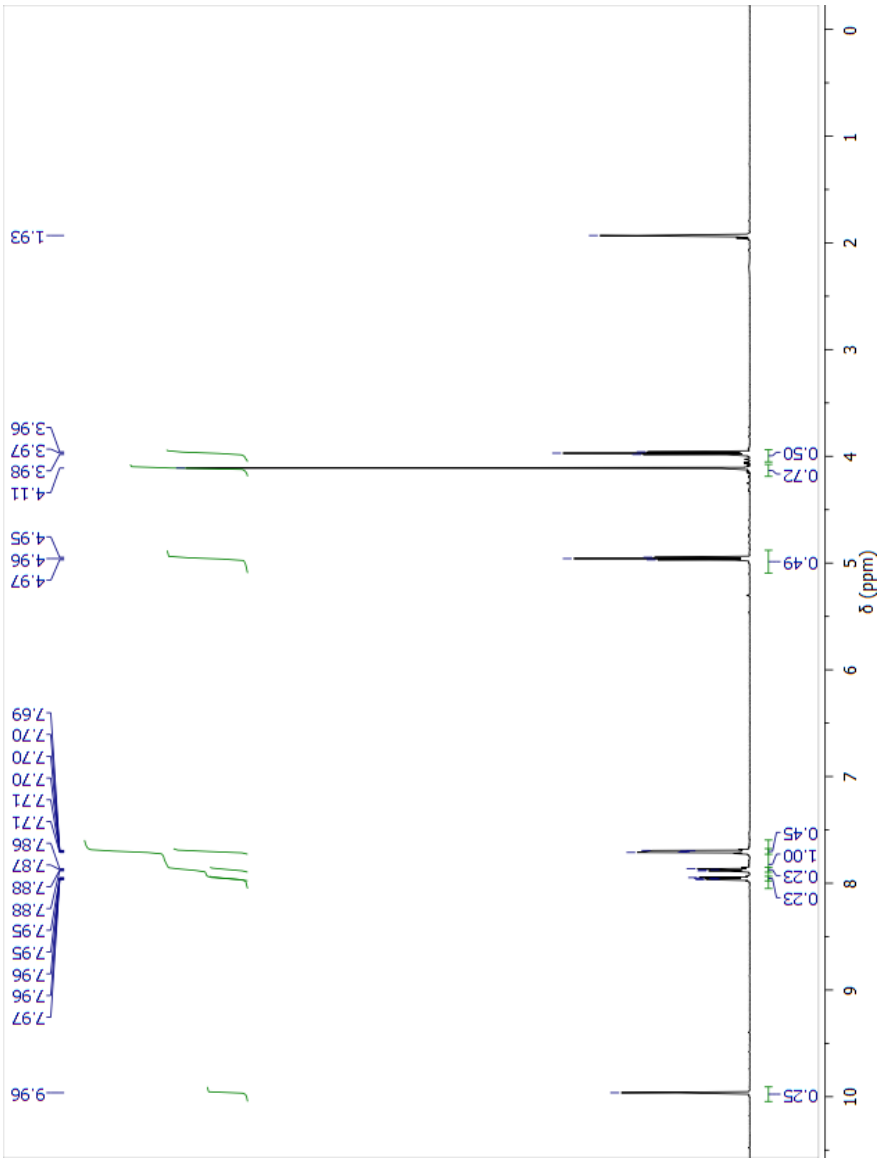

Figure 47. ^{1}H NMR spectrum of 1-(2-bromo-ethylene)-3-methyl-3*H*-benzimidazol-1-ium bromide in CD_3CN (500 MHz).

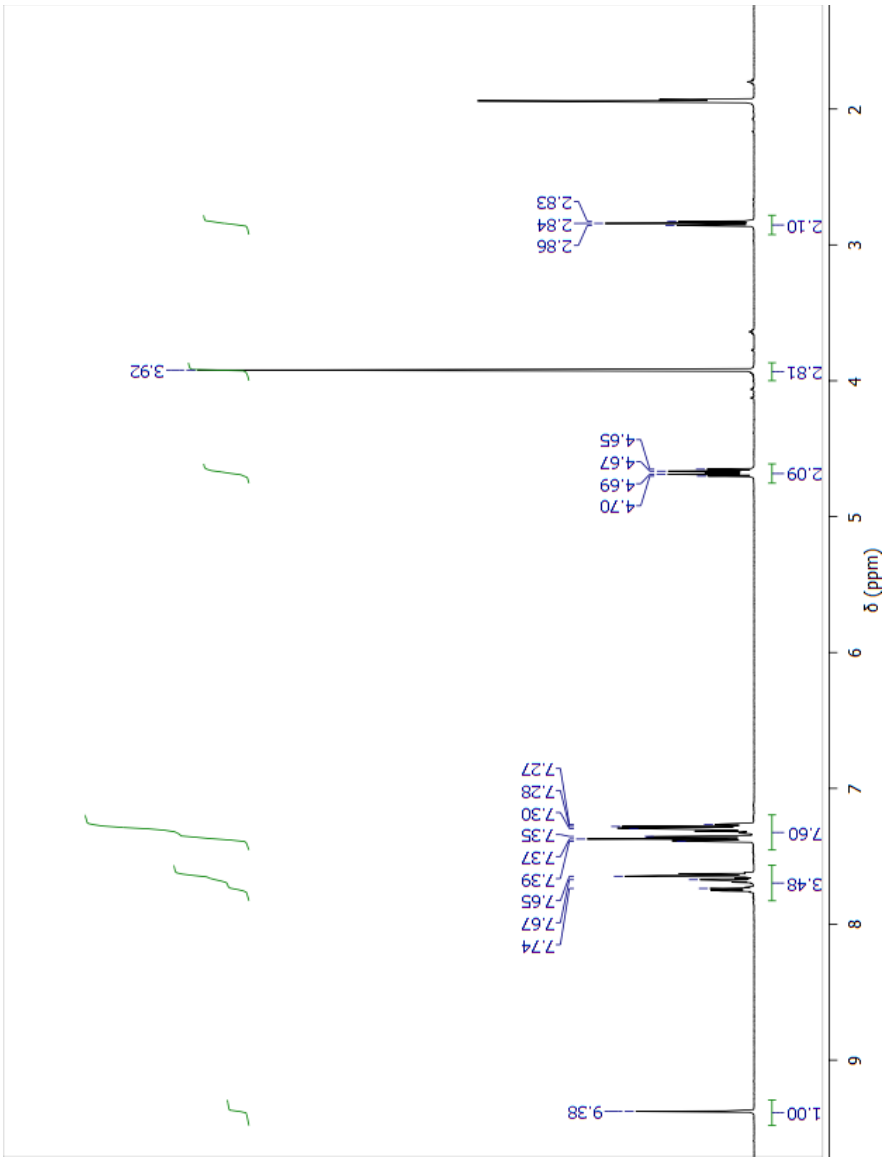

Figure 48. ^{1}H NMR spectrum of 1-(2-diphenylphosphanyl-ethylene)-3-methyl-3*H*-benzimidazol-1-ium bromide (L^{BI+}) in CD_3CN (300 MHz).

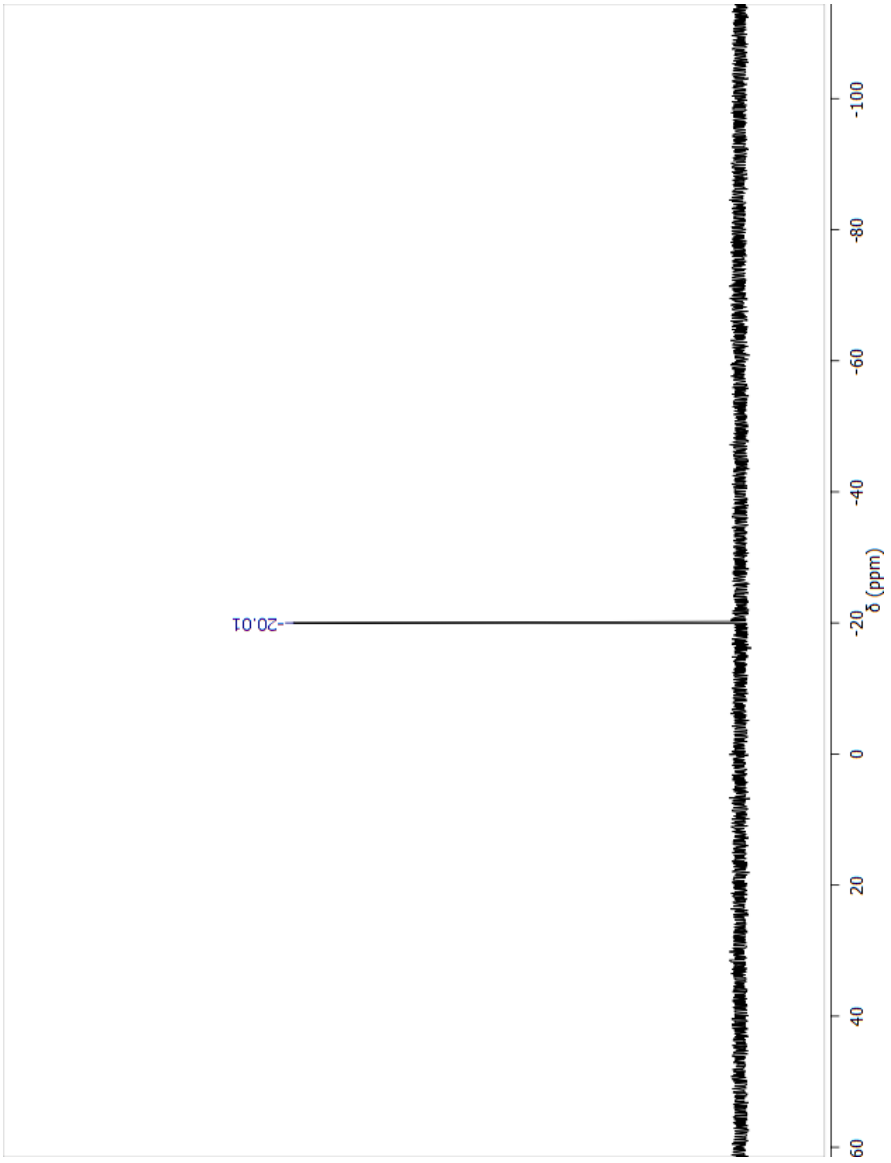

Figure 49. ^{31}P NMR spectrum of 1-(2-diphenylphosphanyl-ethylene)-3-methyl-3*H*-benzimidazol-1-ium bromide (L^{BI+}) in CD_3CN (500 MHz).

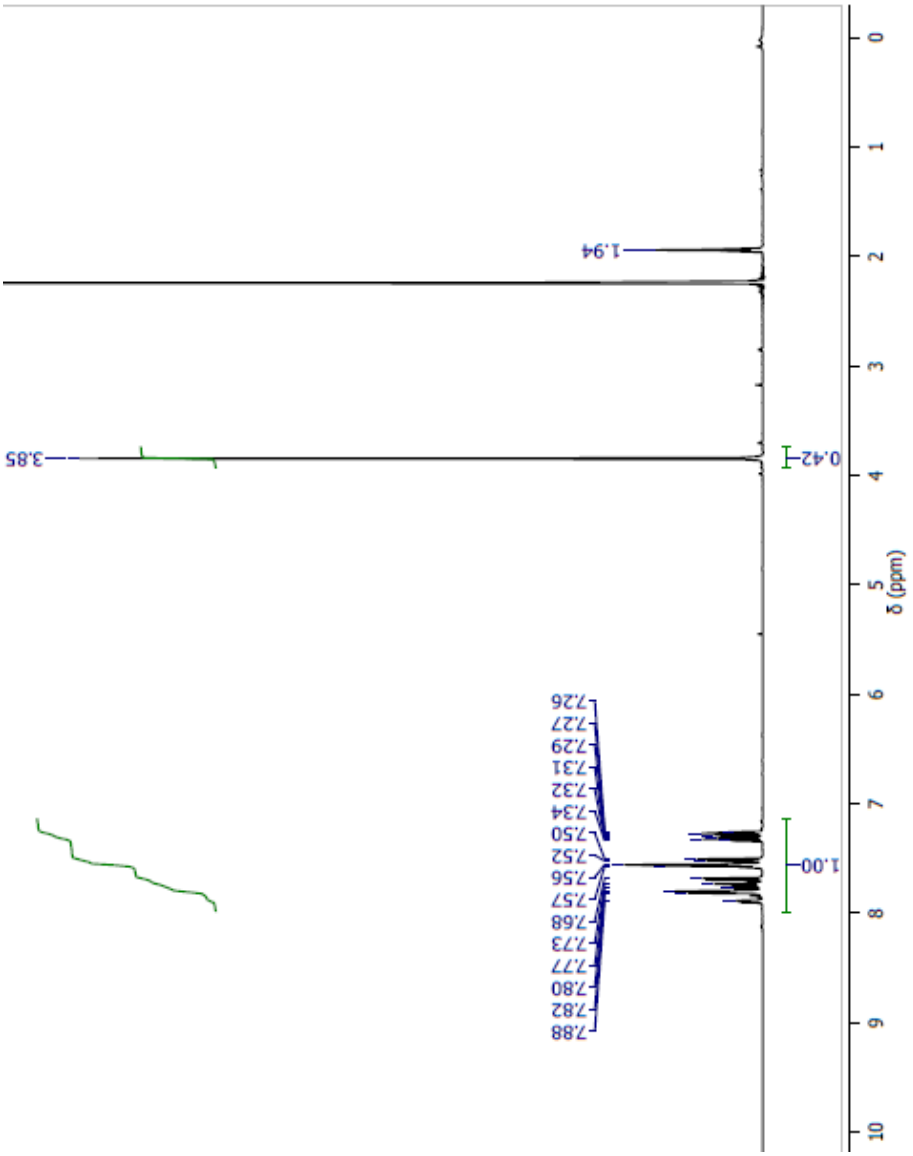

Figure 50. ^{1}H NMR spectrum of 1-methyl-2-phenyl-1*H*-benzimidazole in CD_3CN (500 MHz).

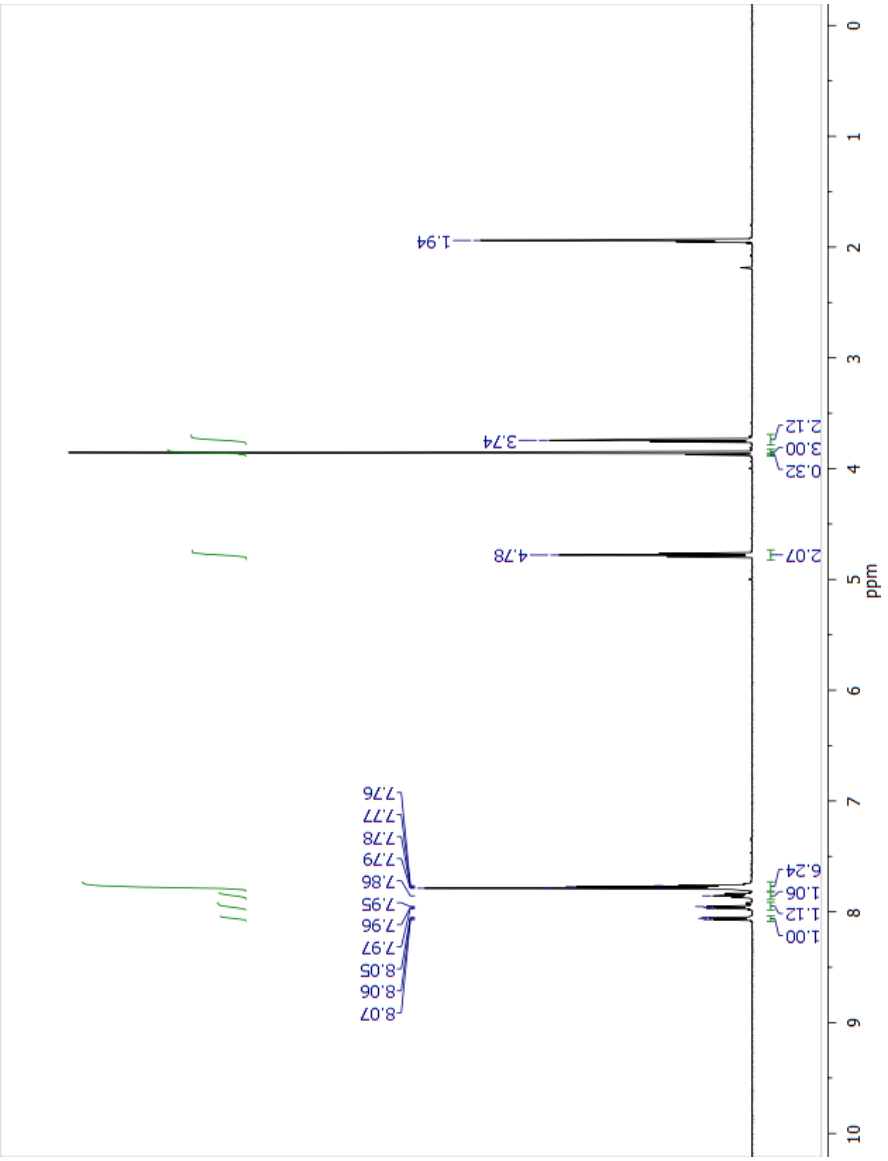

Figure 51. ^{1}H NMR spectrum of 1-(2-bromo-ethylene)-3-methyl-2-phenyl-3*H*-benzimidazol-1-ium bromide in CD_3CN (500 MHz).

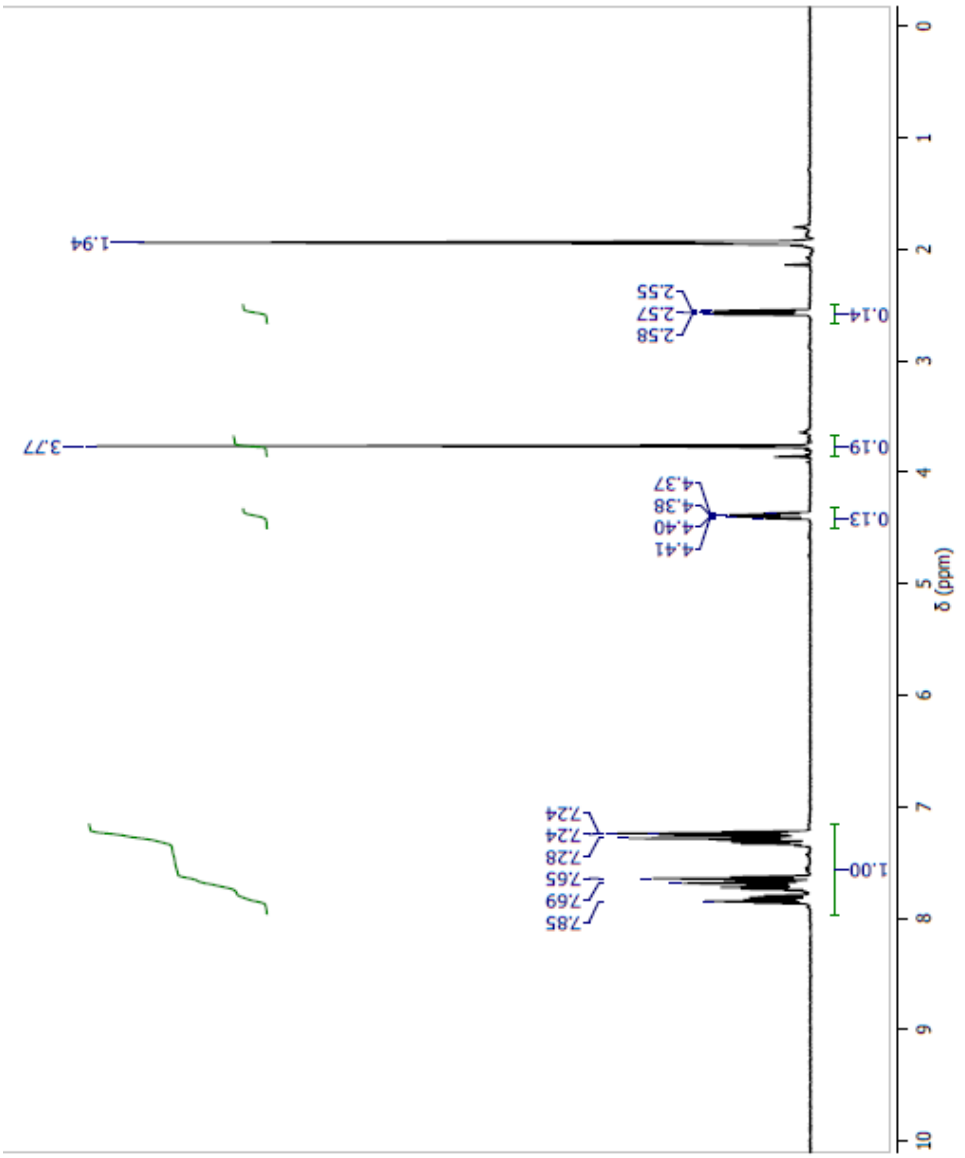

Figure 52. ^{1}H NMR spectrum of 1-(2-diphenylphosphanyl-ethylene)-3-methyl-2-phenyl-3*H*-benzimidazol-1-ium bromide ($L^{PhenBI+}$) in CD_3CN (500 MHz).

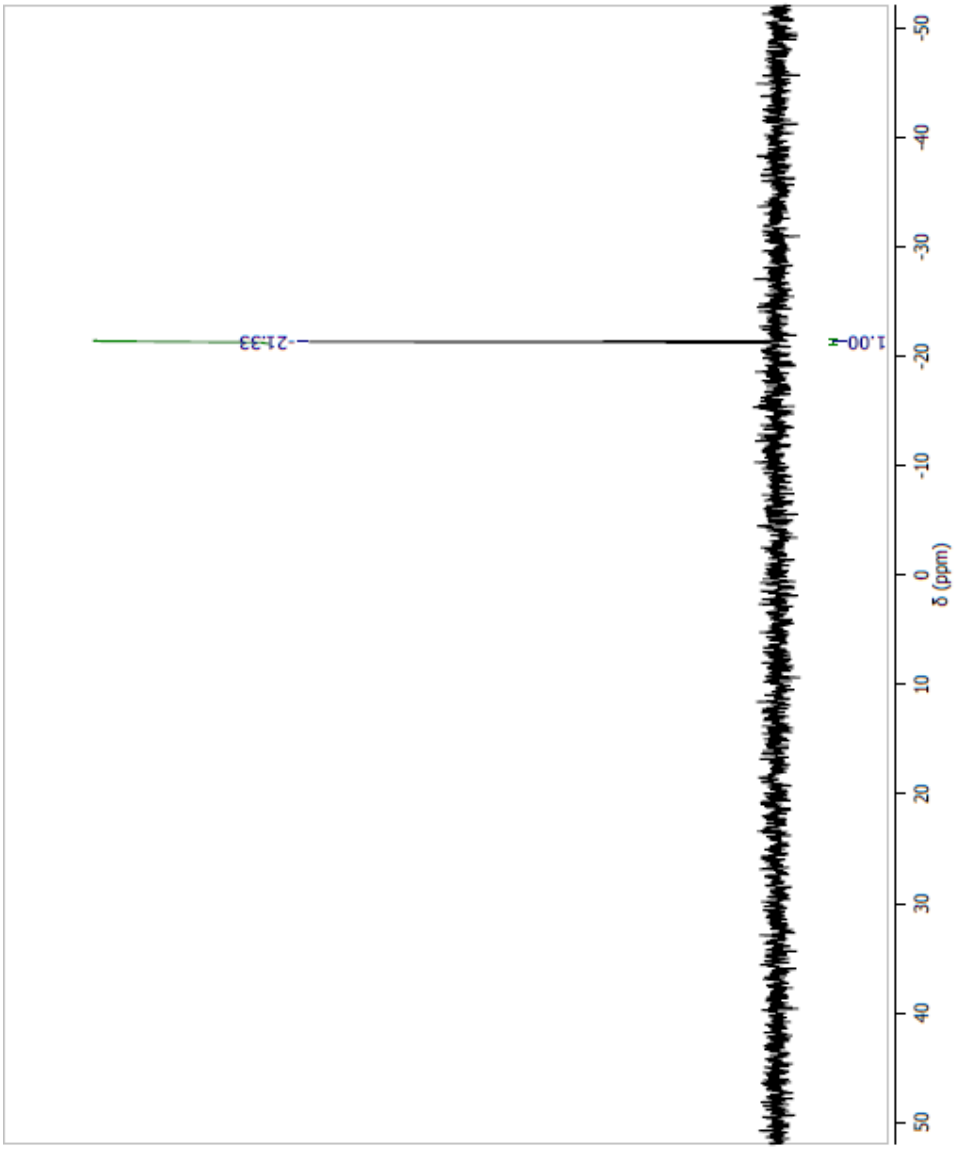

Figure 53. ^{31}P NMR spectrum of 1-(2-diphenylphosphanyl-ethylene)-3-methyl-2-phenyl-3*H*-benzimidazol-1-ium bromide ($L^{PhenBI+}$) in CD_3CN (500 MHz).

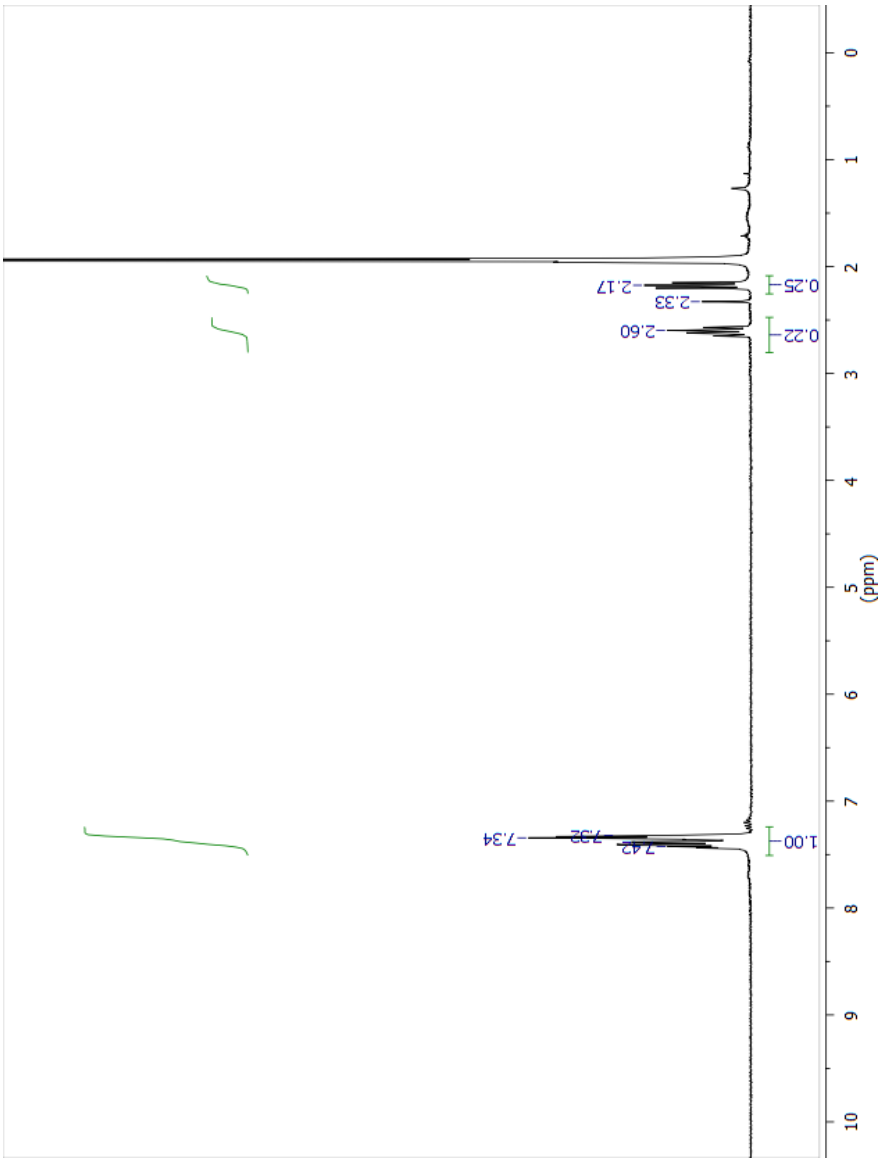

Figure 54. ^{1}H NMR spectrum of PN^{H}P ligand in CD_3CN (300 MHz).

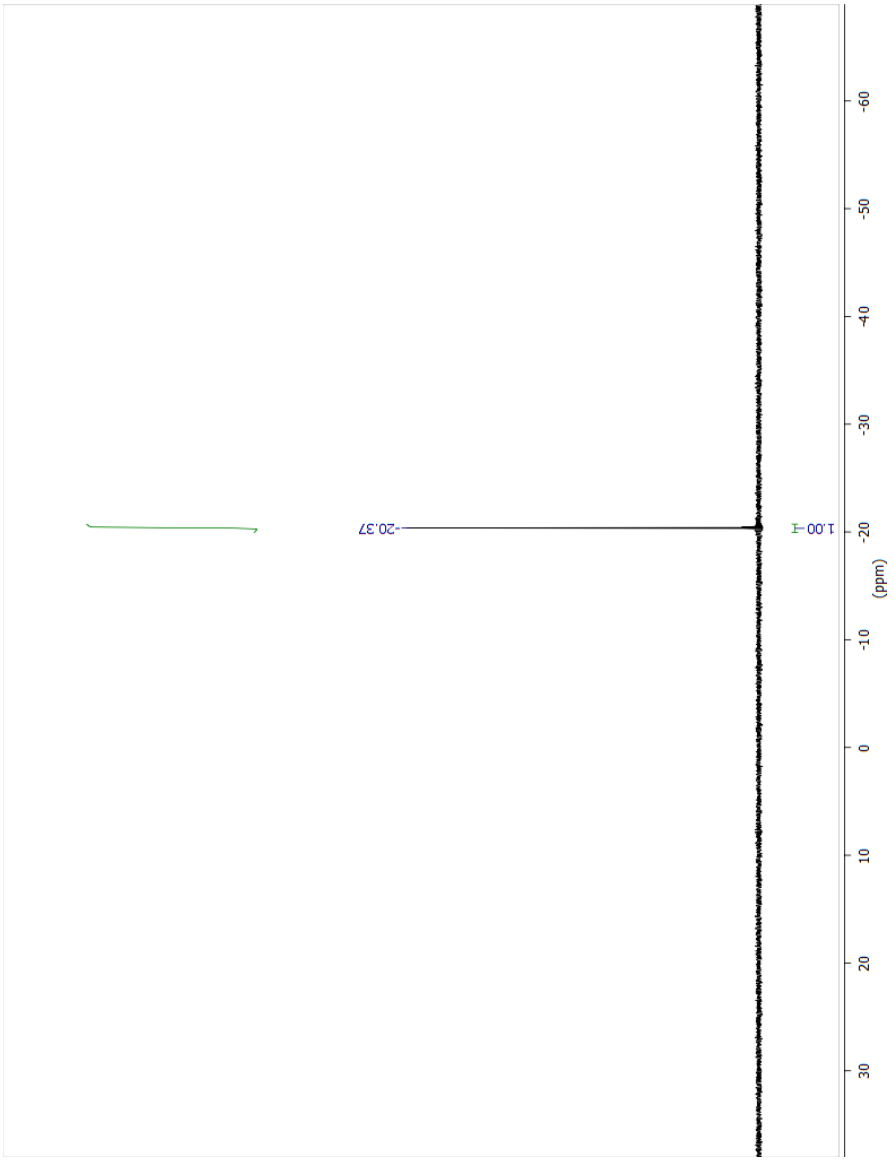

Figure 55. ^{31}P NMR spectrum of PN^{H}P ligand in CD_3CN (300 MHz).

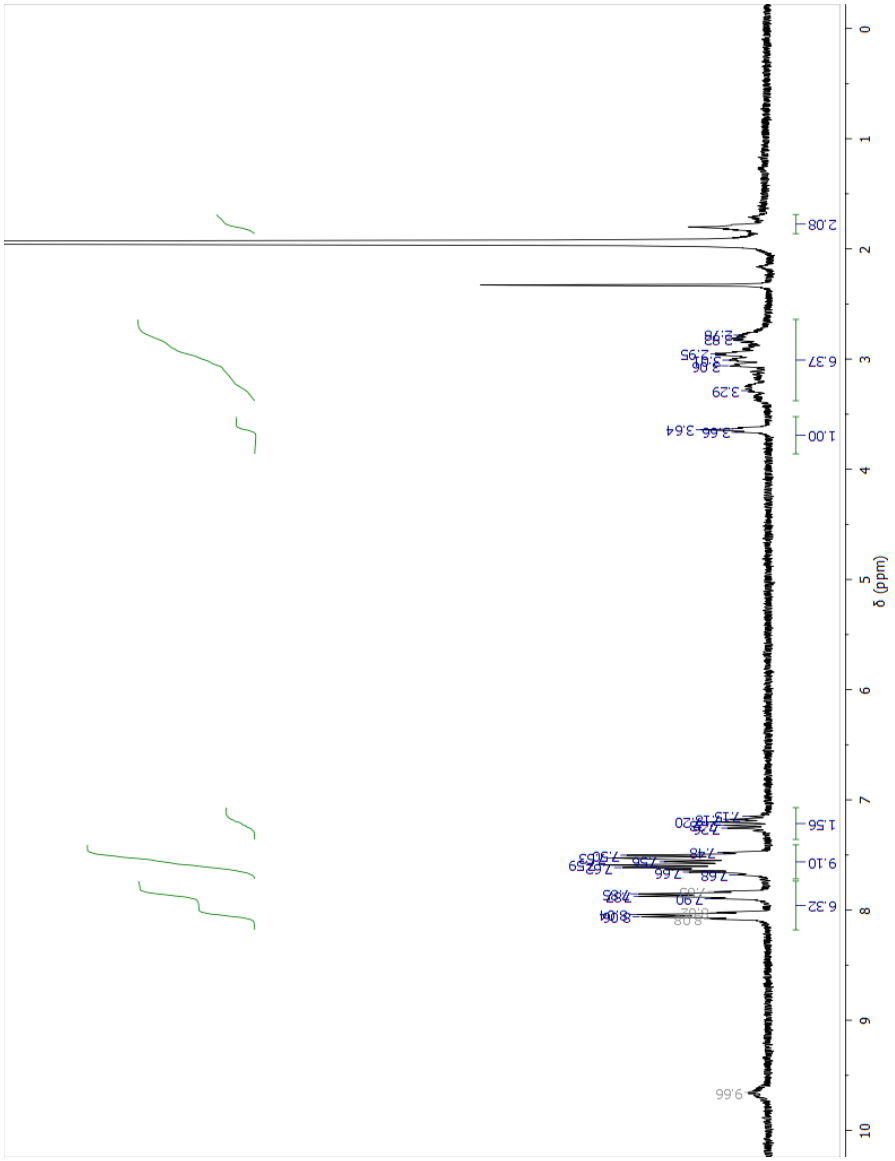

Figure 56. ^{1}H NMR spectrum of [Pd(PN^{H}P)Cl]Cl in CD_3CN (300 MHz).

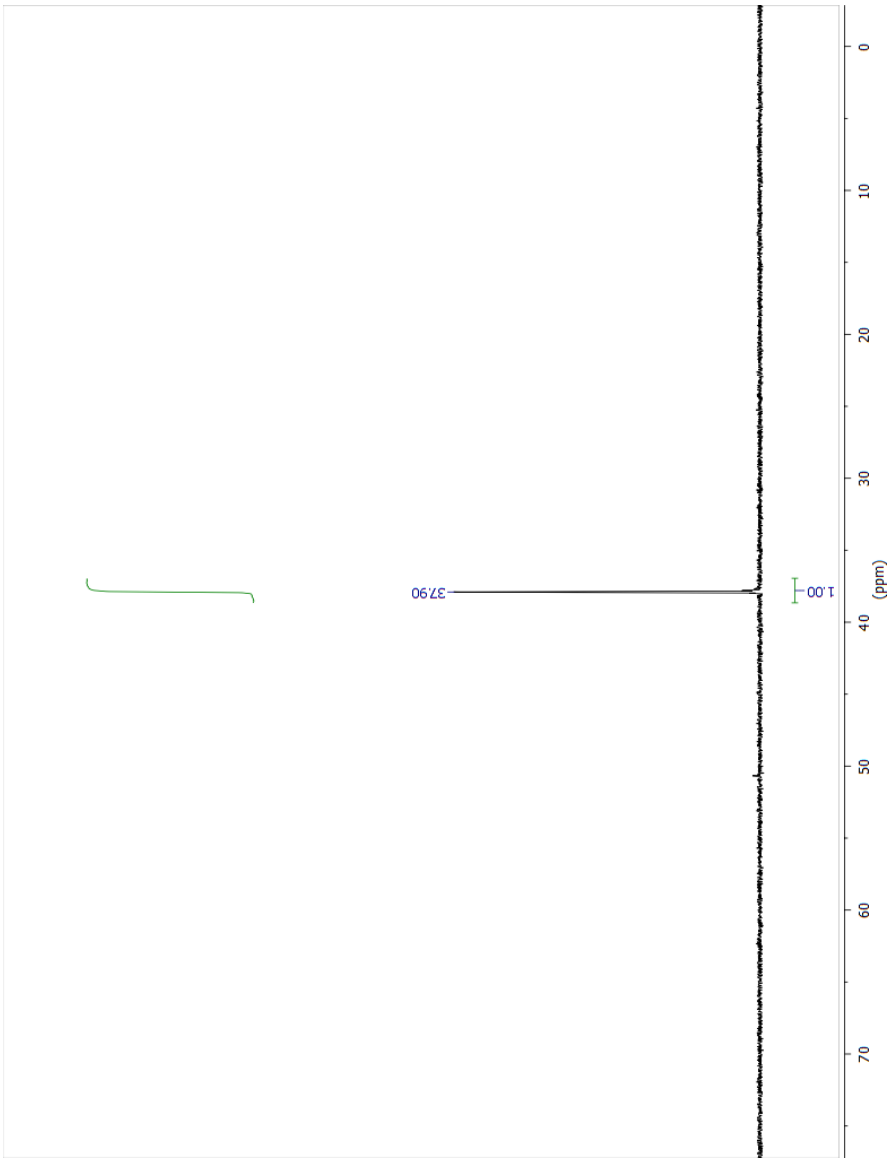

Figure 57. ^{31}P NMR spectrum of [Pd(PN^{H}P)Cl]Cl in CD_3CN (300 MHz).

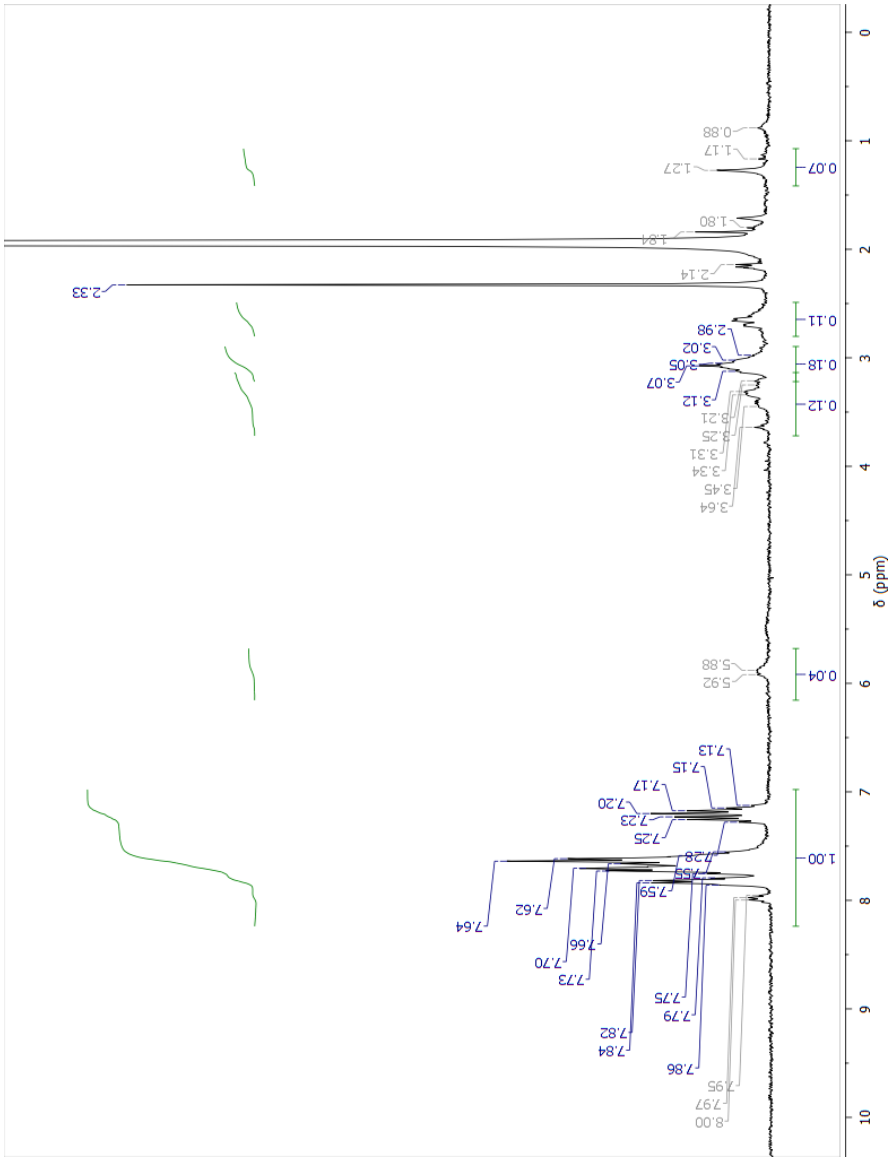

Figure 58. ^{1}H NMR spectrum of [Pd(PN^{H}P)(CH$_3$CN)](BF$_4$)$_2$ in CD$_3$CN (300 MHz).

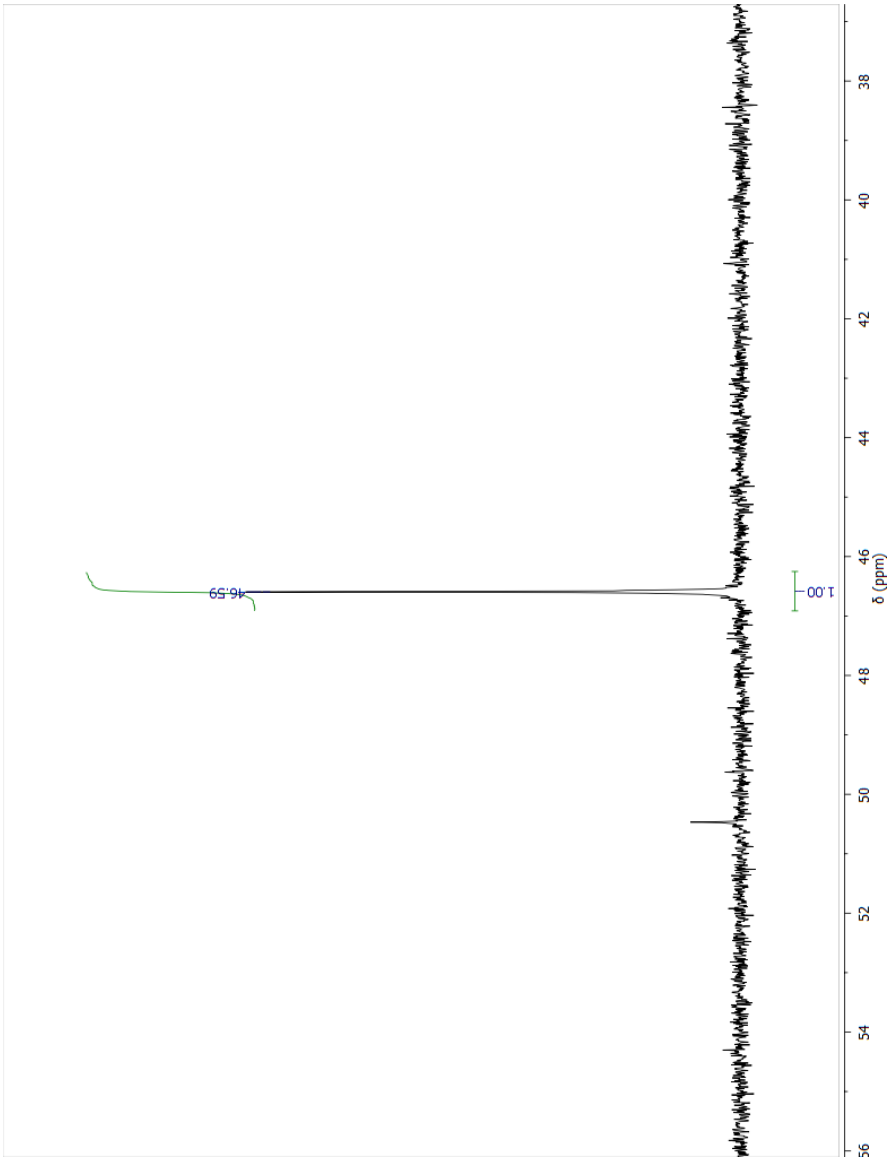

Figure 59. ^{31}P NMR spectrum of $[Pd(PN^{H}P)(CH_3CN)](BF_4)_2$ in CD_3CN (300 MHz).

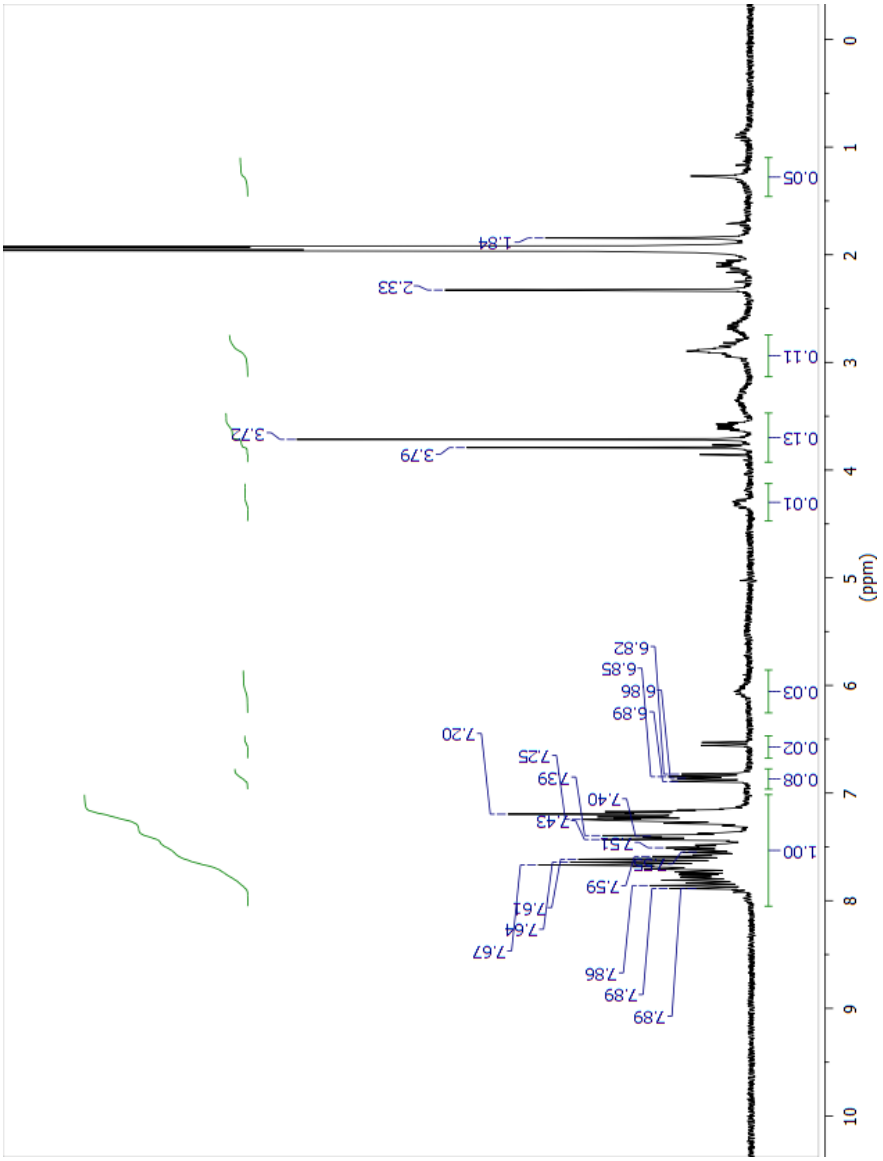

Figure 60. ^{1}H NMR spectrum of [Pd(PN^{H}P)(L$^{PhenBI+}$)](PF$_6$)(BF$_4$)$_2$ in CD$_3$CN (300 MHz).

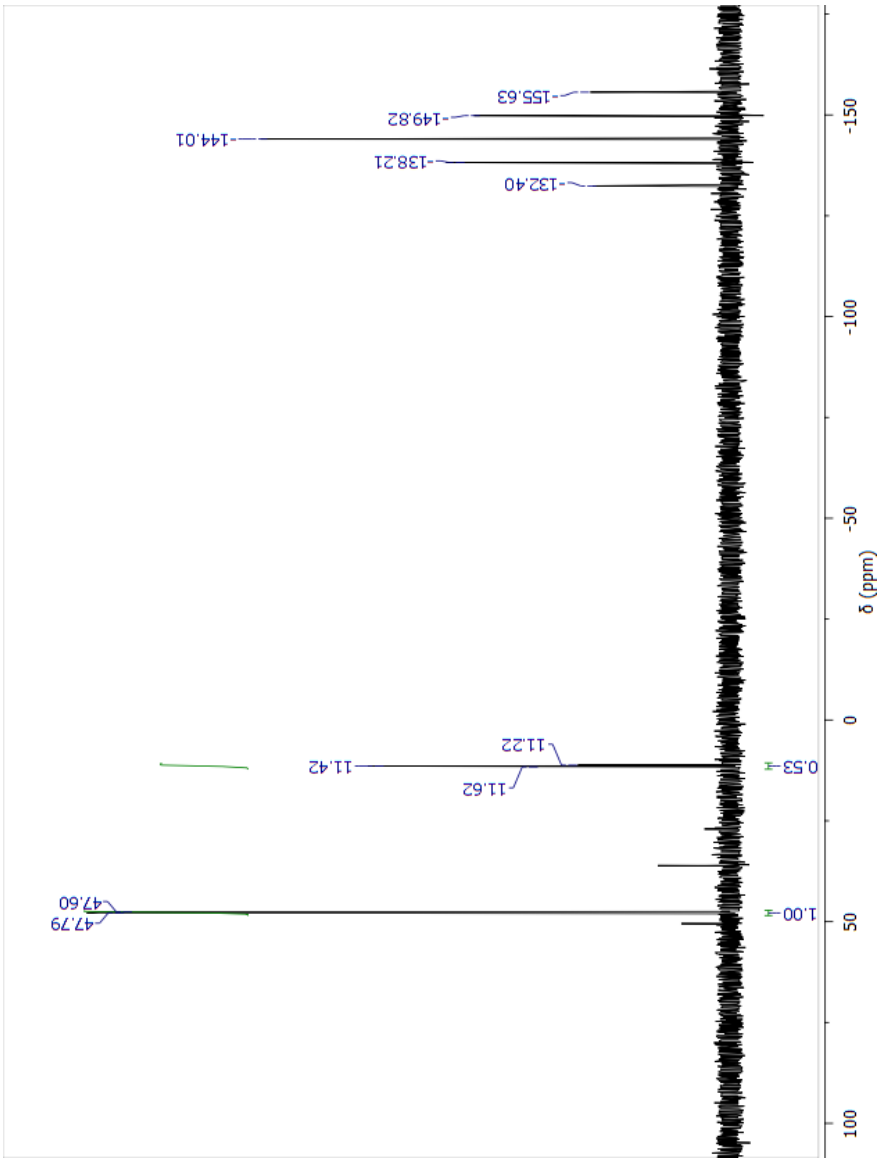

Figure 61. ^{31}P NMR spectrum of [Pd(PN^{H}P)(L$^{PhenBI+}$)](PF$_6$)(BF$_4$)$_2$ in CD$_3$CN (300 MHz).

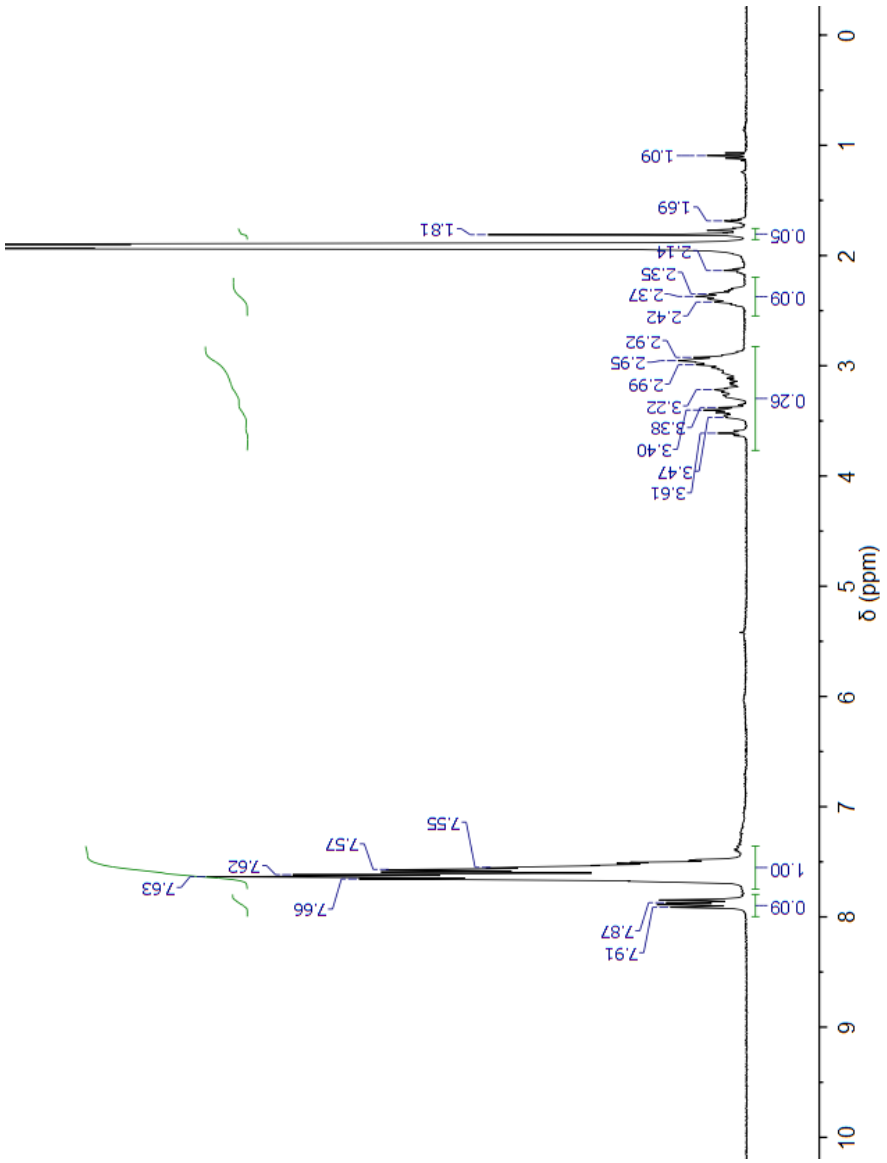

Figure 62. ^{1}H NMR spectrum of $[Pd(PP_2)(CH_3CN)](BF_4)_2$ in in CD_3CN (300 MHz).

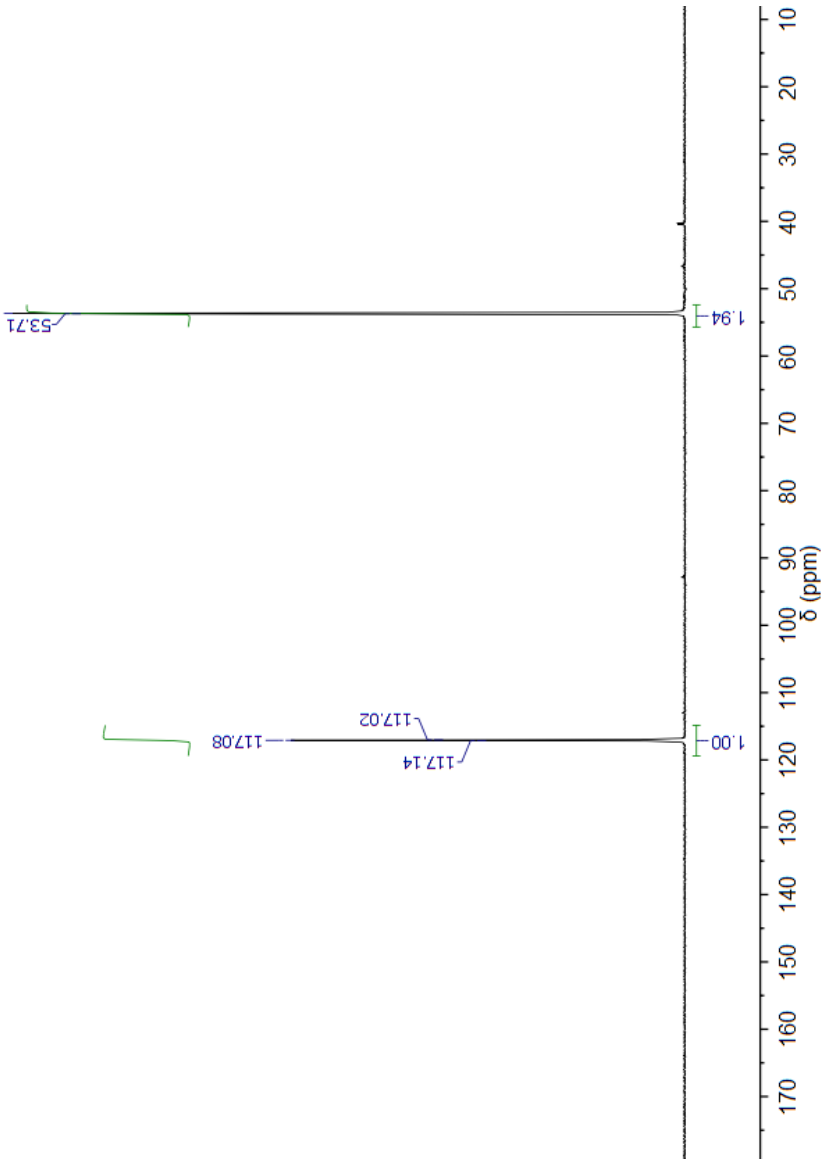

Figure 63. ^{31}P NMR spectrum of $[Pd(PP_2)(CH_3CN)](BF_4)_2$ in in CD_3CN (300 MHz).

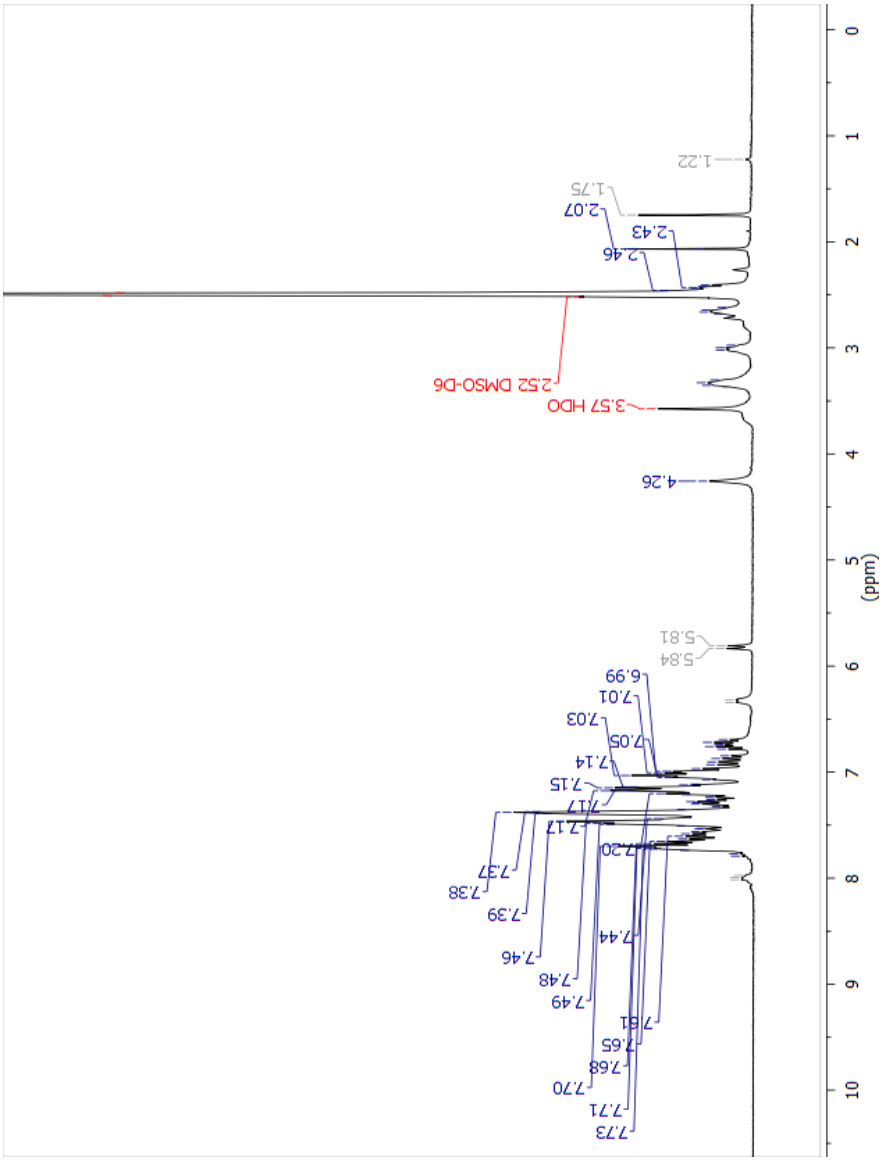

Figure 64. ^{1}H NMR spectrum of $[Pd(PP_2)(L^{PhenH})](BF_4)_2$ in in DMSO-d_6 (300 MHz).

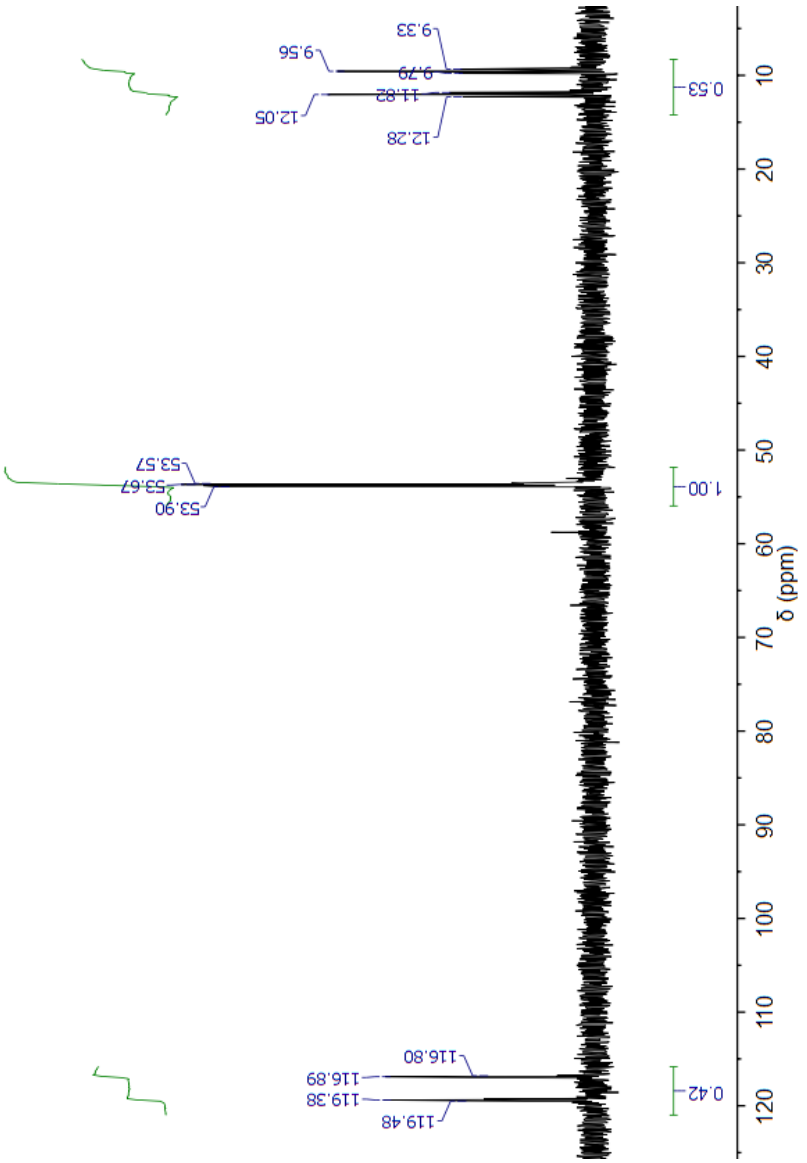

Figure 65. ^{31}P NMR spectrum of $[Pd(PP_2)(L^{PhenH})](BF_4)_2$ in DMSO-d_6 (300 MHz).

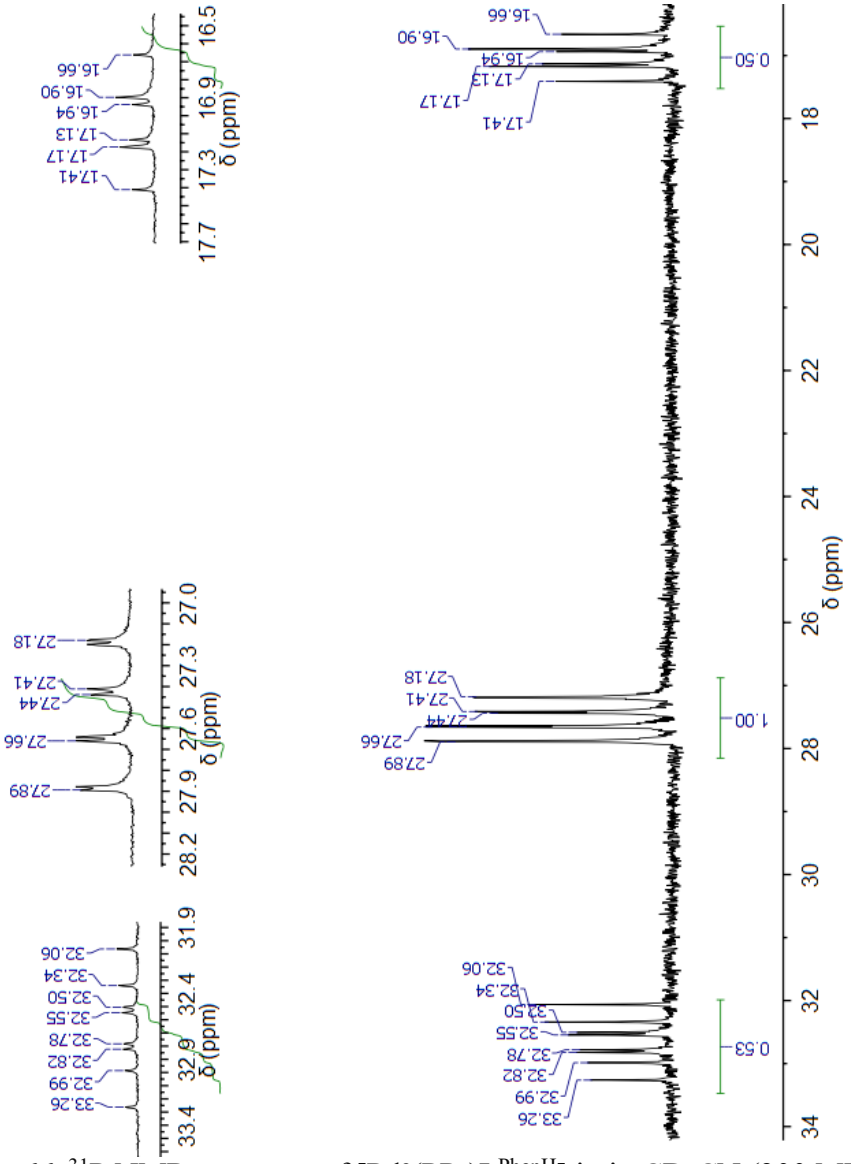

Figure 66. ^{31}P NMR spectrum of [Pd^{o}(PP$_2$)L^{PhenH}] in in CD_3CN (300 MHz).

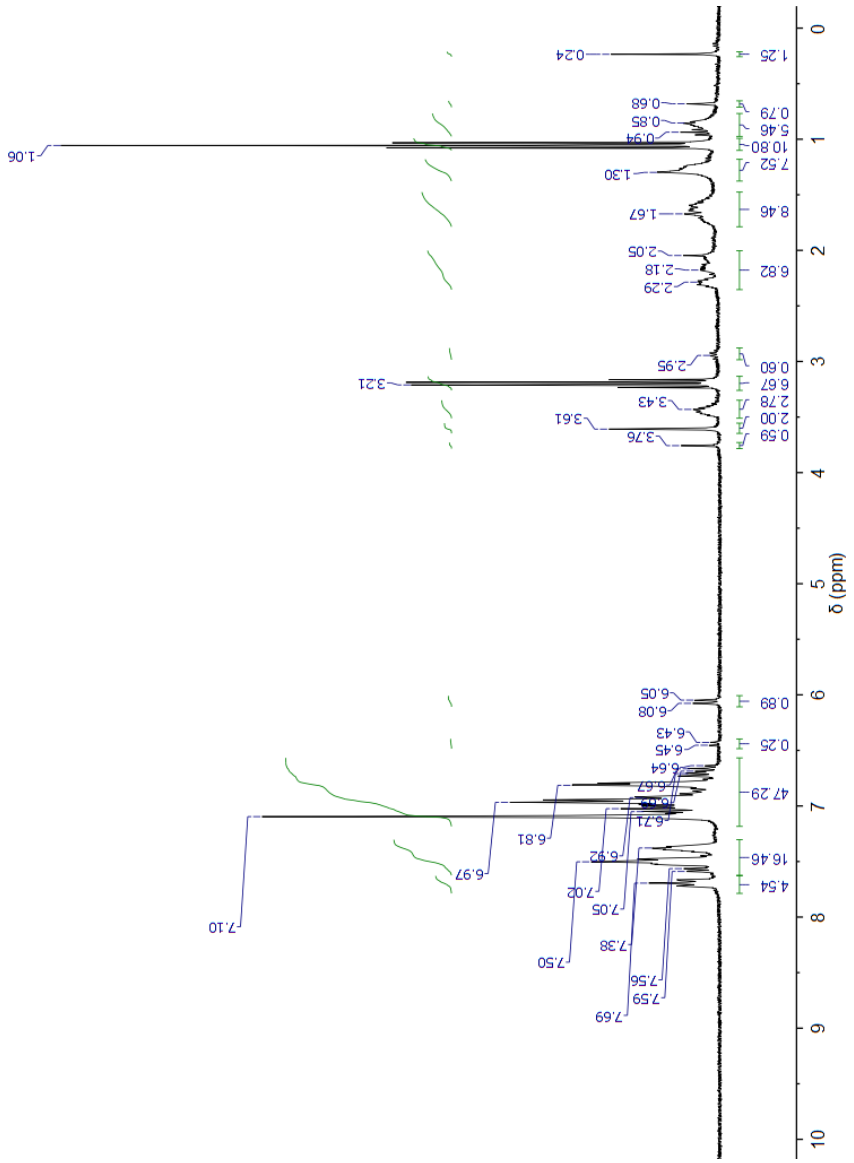

Figure 67. ^{1}H NMR spectrum of [Pd^{o}(PP$_2$)L^{PhenH}] in CD$_3$CN (300 MHz).

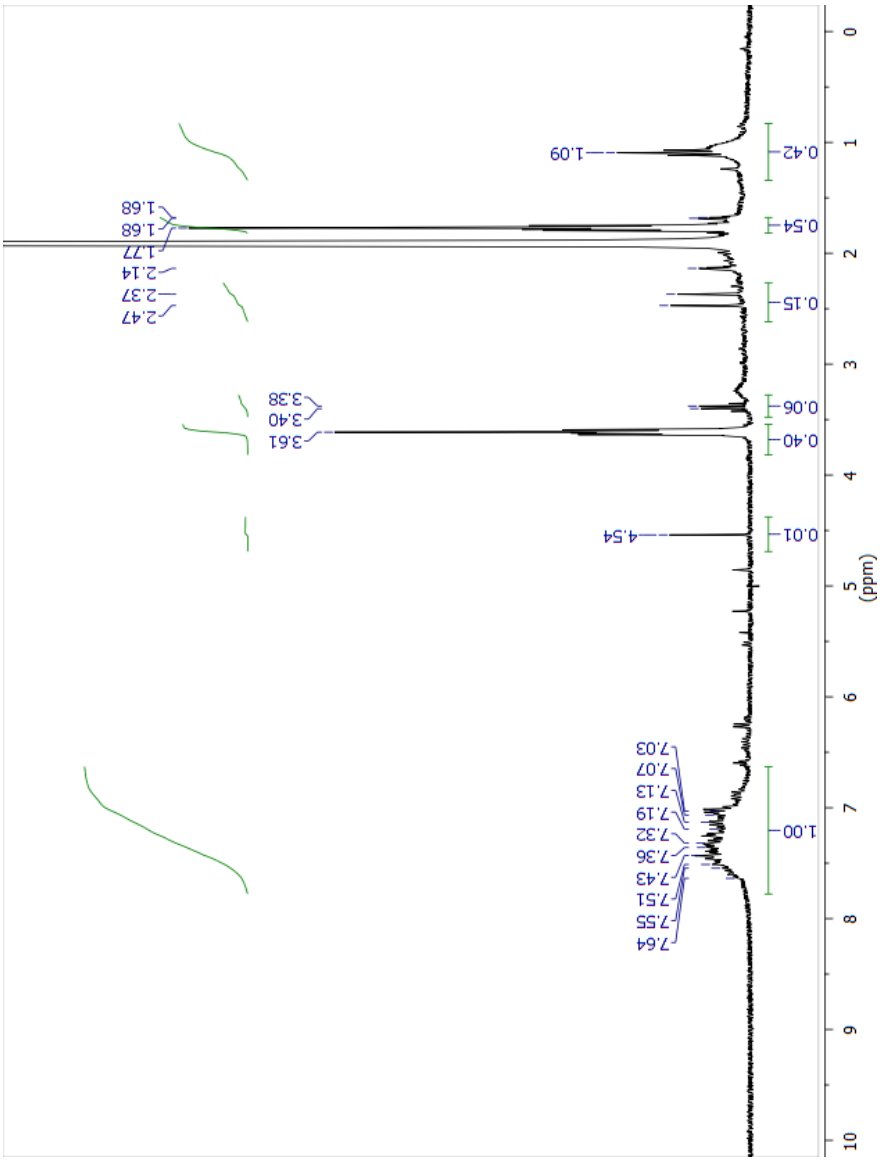

Figure 68. ^{1}H NMR spectrum of $[Pd^{o}(PP_2)L^{PhenBIH}](BF_4)$ in CD_3CN (300 MHz).

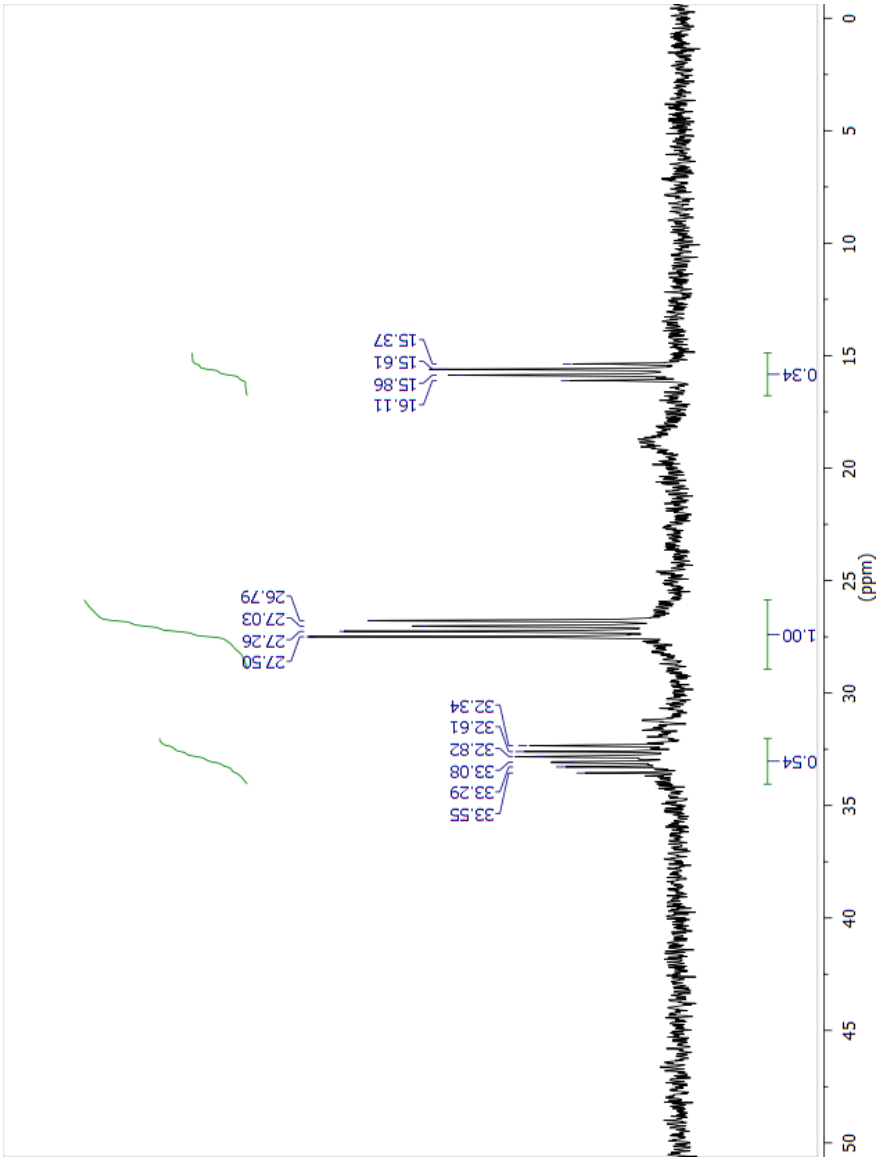

Figure 69. ^{31}P NMR spectrum of $[Pd^{o}(PP_2)L^{PhenBIH}](BF_4)$ in CD_3CN (300 MHz).

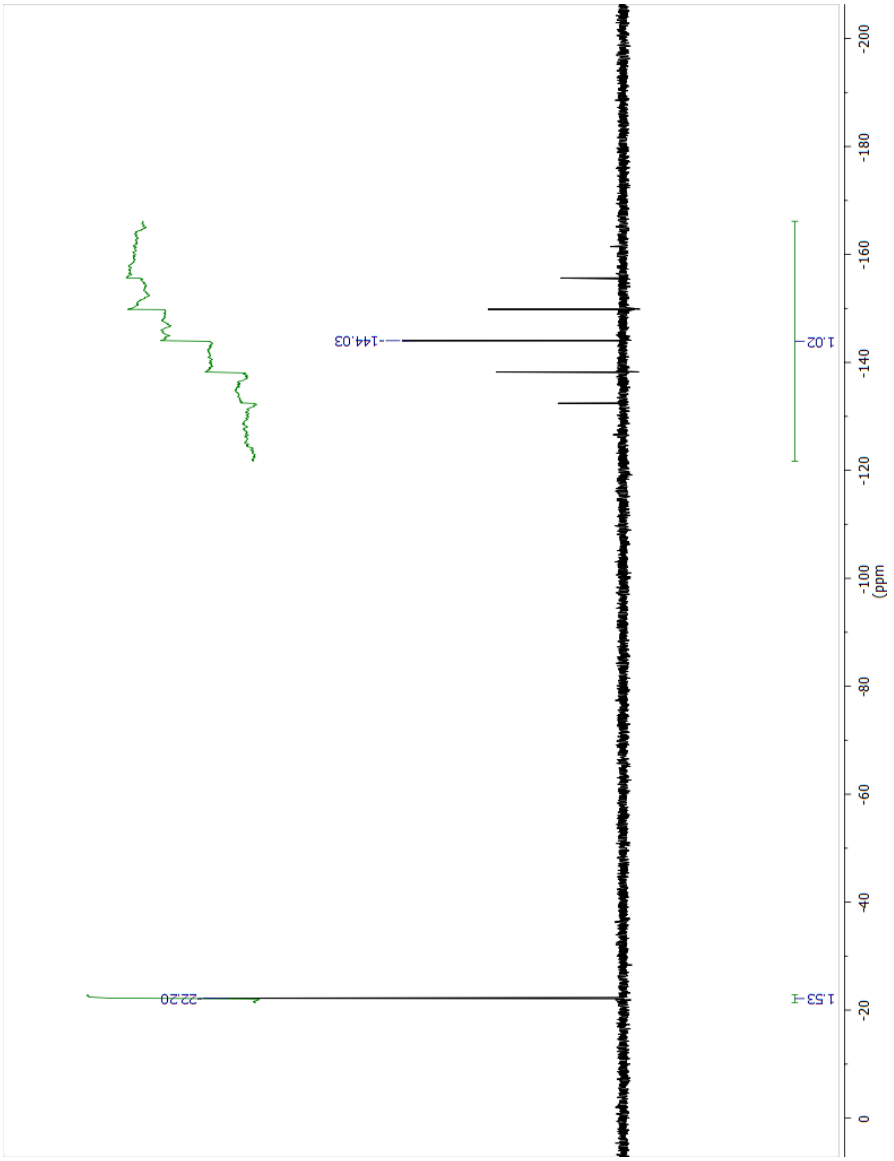

Figure 70. ^{31}P NMR spectrum of [$L^{PhenBI+}$][PF_6] in CD_3CN (300 MHz).

VITA

EDUCATION

Sam Houston State University, Texas, USA — August 2016-present
Master of Science (M.S.), Chemistry

Gauhati University, India — August 2015
Master of Science (M.Sc.), Organic Chemistry

Cotton College, India — July 2013
Bachelor of Science (B.Sc.), Chemistry

RESEARCH EXPERIENCE

Sam Houston State University, Huntsville, TX, USA — September 2016-present
M.S Research, Inorganic Chemistry
Advisor: Professor Christopher M. Zall

- Currently researching the synthesis of bifunctional catalysts for hydrogenation reactions that contain redox-active groups.
- Synthesis of phenanthridinium, benzimidazolium, phenylbenzimidazolium containing phosphine ligands.
- Synthesis of metal catalysts using transition metals like Ni, Pd and Ru.
- Characterized these complexes using multinuclear NMR spectroscopy, X-Ray diffraction.

Pacific Northwest National Laboratory, Richland, Washington, USA — June-Aug 2017
Alternate Sponsored Fellow (ASF)
Supervisor: Dr. John C. Linehan

- Studies of CO_2 hydrogenation using bifunctional catalysts with hydride relays using in operando NMR spectroscopy.
- Synthesized a Ru-cyclopentadienyl complex containing benzimidazolium ligand found to be catalytically active for CO2 hydrogenation at low temperature and pressure.

Gauhati University, Assam, India — Feb-July 2015
M.Sc. project, Organic Chemistry
Advisor: Professor Pranab Jyoti Das

- Worked in a project entitled “Synthesis of Quaternary Ammonium Bromates and their use as Oxidizing Agents”
- Synthesized tetrapropyl and tetraethyl ammonium bromates, two very mild, versatile and benign oxidizing agents towards the oxidation of aldehydes and secondary alcohols and the oxidation of formazans to the tetrazolium salts
- Characterized reagents by NMR and IR
- Characterized the formed oxidized products by NMR, IR and UV

Indian Institute of Technology (IIT), Guwahati June-July 2014
Summer Internship, Organic Synthesis
Advisor: Professor Bhisma Kumar Patel

- Worked on a project entitled "Regiospecific Benzoylation of Electron Deficient N-Heterocycles with Methylarenes via a Minisci type Reaction"
- Synthesized benzoylated N-heterocyclic products
- Characterized by ^{1}H NMR and IR

TEACHING EXPERIENCE

Graduate Teaching Assistant Fall 2016-Spring 2019
Sam Houston State University, TX, USA

- *General Chemistry I Lab* (Fall 2016-Spring 2017): assisted students with lab experiments, conducted quizzes, graded Lab work, and tutored Gen Chem I classroom courses
- *General Chemistry II Lab* (Fall 2016-Spring 2017): assisted students with lab experiments, conducted quizzes, graded Lab work, and tutored Gen Chem II classroom courses
- *Organic Chemistry I Lab* (Fall 2017-Fall 2018): assisted students with lab experiments on basic Organic Chemistry, graded Lab work, tutored Organic Chem I classroom courses, and helped students with spectral problems for MS, IR, ^{1}H NMR, ^{13}C NMR
- *Organic Chemistry II Lab* (Fall 2017-Spring 2019): assisted students with lab experiments on Organic Chemistry II, graded Lab work, tutored Organic Chem II classroom courses, and helped students with spectral problems for MS, IR, ^{1}H NMR, ^{13}C NMR
- *Intro to Organic and Biochemistry Lab* (Fall 2018): assisted students with lab experiments on basic Chemistry reactions, graded Lab work

Post Graduate Teacher (P.G.T), Chemistry April 2016-July 2016
St. Francis D'Assisi Senior Secondary School, Guwahati, Assam, India

- Taught chemistry in Classes 11 and 12
- Conducted unit tests and exams
- Guided Chemistry Labs for Classes 11 and 12

PRESENTATIONS

- N. Devi and C. M. Zall. "Synthesis, characterization and reactivity of bifunctional transition-metal complexes containing hydride-relay functionality" Presented at the American Chemical Society (ACS) National Meeting, Spring 2019 at Orlando, Florida, USA (Presented by N. Devi)
- N. Devi and C. M. Zall. "Development of Bifunctional Catalysts Containing Hydride-Relay Ligand for CO_2 Hydrogenation" Presented at the American Chemical Society (ACS) National Meeting, Spring 2018 at New Orleans, Louisiana, USA (Presented by N. Devi)
- C. M. Zall, N. Devi and W. Fernandez. "Incorporation of NADH-like Hydride Relays into Metal-Phosphine Catalysts for CO_2 hydrogenation" Presented at the

American Chemical Society (ACS) National Meeting, Spring 2018 at New Orleans, Louisiana, USA (Presented by C. M. Zall)

- N. Devi and C. M. Zall. "Hydrogenation of CO2 using Bifunctional Transition Metal Catalysts Containing Hydride-relay Ligands" Presented at the Texas Academy of Science (TAS) Conference, Spring 2018 at Midland, TX, USA (Presented by N. Devi)
- N. Devi and C. M. Zall. "Synthesis of Redox-Active Ligands with Hydride-Relays for Bifunctional Hydrogenation Catalysis" Presented at the South West Regional Meeting (SWRM) of the American Chemical Society (ACS), Fall 2017 at Lubbock, TX, USA (Presented by N. Devi)
- Attended the South West Regional Meeting (SWRM) of the American Chemical Society (ACS), Fall 2016 at Galveston, TX, USA
- Attended the National Seminar on Crystallography, 2015 at the Department of Chemistry, Gauhati University, Assam, India

MEMBERSHIP

- American Chemical Society: Graduate student member
- Texas Academy of Sciences: Graduate student member

TECHNICAL SKILLS

- NMR Spectroscopy: Actively handling JEOL 500MHz NMR Spectrometer, VARIAN 500 MHz Spectrometer and interpreting NMR spectra of Organic and Inorganic compounds
- Equipped to work on high/low pressure NMR reactions
- Air- free synthesis using Schlenk techniques: active synthesis of organic hydride and phosphine ligands
- Glove Box: Actively working on air sensitive reactions inside glove box
- Solvent System: Actively using in the lab to collect solvents like THF, Acetonitrile, DCM, Ether, Hexane, Toluene
- Single Crystal X-Ray Diffraction: Learner
- FT-IR Spectroscopy: Interpreted and carried out experiments on various Organic compounds in a Perkin-Elmer FT-IR Spectrometer using KBr pellet method
- UV Spectroscopy: Interpreted and carried out experiments in a Shimadzu 1800 UV vis Spectrometer of Formazan dyes and Tetrazolium salts
- Software experience with Gaussview 5.0, Mestrenova, ChemDraw

FELLOWSHIPS/AWARDS

- College of Science and Engineering Technology Graduate Achievement Scholarship, Sam Houston State University, Fall 2018 and Spring 2019
- Friends of Assam and Seven Sisters (FASS) Welcome Package, 2018
- Robert A. Welch Summer Fellowship, Summer 2018
- Graduate Travel Fund, Sam Houston State University, Fall 2017 and Spring 2018
- Alternate Sponsored Fellowship (ASF), Pacific Northwest National Laboratory, Richland, Washington, June 1-August 4, 2017
- Sam Houston State University Internal Chemistry Grant, Summer 2017